SYNTHESIS AND PHOTOPHYSICS OF ORGANOMETALLICS CONTAINING LIGAND-CENTERED AND CHARGE-TRANSFER EXCITED STATES

Irina E. Pomestchenko

A Dissertation

Submitted to the Graduate College of Bowling Green
State University in partial fulfillment of
the requirements for the degree of

DOCTOR OF PHILOSOPHY

May 2004

Committee:

Felix N. Castellano, Advisor

Margaret M. Yacobucci
Graduate Faculty Representative

Deanne L. Snavely

Pavel Anzenbacher

ABSTRACT

Felix N. Castellano, Advisor

The present thesis describes the synthesis and photophysics of a variety of organometallic Pt(II) and Re(I) diimine complexes containing ligand-centered and charge-transfer excited states. The photophysical properties have been investigated by electronic spectroscopy, steady-state and time-resolved photoluminescence (TRPL) at room temperature and 77 K, laser flash photolysis, and cyclic voltammetry measurements. In terms of the newly designed synthetically facile Pt(II) diimine bis(arylacetylide) complexes, either charge transfer emission or room temperature phosphorescence in fluid solution has been observed. In one particular instance, the excited state properties can be best described as possessing a combination of metal-to-ligand charge transfer (MLCT) and intraligand (IL) character, where the low-lying state dominates the behavior and solvent media allows transitioning between these two limits.

The synthesis and photophysical properties of two new Re(I) complexes are also reported: *fac*-Re(phen-C≡CH)$(CO)_3Cl$, phen-C≡CH is 5-ethynyl-1,10-phenanthroline, along with its Au(I)-acetylide analog *fac*-Re(phen-C≡C-$AuPPh_3$)$(CO)_3Cl$. In these two phen-C≡C-R containing molecules, the room temperature excited state decay is consistent with a MLCT assignment whereas at 77 K, the lowest excited state is clearly ^{3}IL, localized within the respective diimine ligand. The PL and time-resolved absorption data in *fac*-Re(phen-C≡C-$AuPPh_3$)$(CO)_3Cl$ indicate that in the charge-transfer excited

state, the electron is delocalized into the Au-acetylide fragment which aids in extending the lifetime of the excited state.

To my mother and husband with love and gratitude.

ACKNOWLEDGEMENTS

I wish to acknowledge all those people who provided significant help throughout my doctoral research.

I am deeply indebted to my advisor, Dr. Felix Castellano for years of guidance, encouragement and support. I would like to acknowledge my committee members: Dr. Pavel Anzenbacher, Dr. Deanne Snavely and Dr. Margaret Yacobucci for their criticism of this manuscript. I would like to thank Dr. Thomas Kinstle for constant support and having such unique personality. I thank Dr. Eugene Danilov for scientific collaborations, constructive discussions as well as assisting me with TA experiments. The nanosecond laser flash photolysis facilities were provided by the Ohio Laboratory for Kinetic Spectrometry at BGSU. I personally thank Dr. Kirk Schanze at the University of Florida for taking photoluminescence measurements on the Pt(dbbpy)(C≡C-Perylene)$_2$ complex. Dr. John Cable is greatly appreciated for performing all DFT calculations. I would like to acknowledge Dr. Raymond Ziessel and Muriel Hissler (ULP, Strasbourg, France) for providing the Pt(PBu$_3$)$_2$(C≡C-Pyrene)$_2$ model compound. I thank Dr. Jeffrey Moore (UIUC) for 3-ethynylperylene which was used for the synthesis of the Pt(dbbpy)(C≡C-Perylene)$_2$ complex. Dr. Radek Pohl is appreciated for sharing his knowledge and skills as well as the synthesis of 1-ethynylpyrene. Solen Kinayyigit also deserves special thanks for the synthesis of the Pt(PBu$_3$)$_2$Cl$_2$ precursor. Daniel Tyson and Charles Luman were extremely helpful through the years we shared at BGSU. Other members of the Castellano group are thanked for providing a great working environment and for their friendship. I also have to acknowledge Dr. J. Romanowicz and Dr. D.Y. Chen for assisting with mass spectrometry and ^{31}P NMR experiments, respectively.

I wish to thank my husband, Dmitry, whose love and support gave me the inspiration and strength to complete this dissertation. I also thank my family, especially my mother, whose passion for education has motivated me to strive for success.

TABLE OF CONTENTS

LIST OF FIGURES

LIST OF SCHEMES

LIST OF TABLES

CHAPTER I. INTRODUCTION

Towards Long-Lived Visible-Absorbing Luminescence Probes

The understanding of photophysical properties of transition metal complexes offers opportunities to use these materials as luminescence sensors and probes. Visible-absorbing luminescence probes that display long lifetimes are becoming increasingly important in biophysics, clinical chemistry, and lifetime-based chemical sensing. One particular class of compounds based on transition metal complexes displaying metal-to-ligand charge transfer (MLCT) excited states[1] have shown promise in such luminescence-based technologies.[2-5]

The photophysical properties of transition metal complexes displaying MLCT excited states are dominated by non-radiative decay process and can be predicted by the energy gap law.[6-8] Excited states lifetimes in such complexes are modulated through modification of the ligands and/or the central metal atom. Although this approach has been proven to be quite successful, complexes with very long lifetimes consequently possess large energy gaps, generally with MLCT absorption bands in UV. Alternatively, MLCT complexes containing ligands with large π-systems extend excited state lifetimes by imparting significant electronic delocalization into the charge transfer excited state.[9,10] Even though such complexes absorb in the visible, useful for analytical luminescence applications, their lifetimes are only slightly larger then that observed in the parent diimine system.

There have been several successful approaches taken towards the lifetime extension and at the same time maintaining visible absorbance features. For example, Ford and Rodgers[11] first noted that the luminescence lifetimes of Ru(II) polypyridine

complexes can be prolonged by the presence of coupled aromatic chromophores having their lowest-lying long-lived triplets at an energy proximate to the luminescent metal-based triplet level(s). In this case an appended chromophore acts as energy 'reservoir', whilst emission results exclusively from the ^{3}MLCT state. The relative energy differences between these two states dictate whether MLCT emission is controlled by thermal equilibrium or slow back energy transfer process.[12-21] It has been established by Castellano and co-workers[14-17] that the lifetime can be systematically varied as a function of the number of appended chromophores. Extended lifetimes have also been observed in Re(I) and Ru(II) systems where the excited states have been proposed to consist of mixed π-π^* and intraligand charge transfer (ILCT) character.[22]

In the present work it has been demonstrated that significantly extended lifetimes can be observed in the novel group of synthetically facile Pt(dbbpy)(C≡C-Aryl)$_2$ complexes if the appropriate chromophores are appended as arylacetylide ligands. This group of compounds incorporated a new approach and illustrates great potential towards the long-lived visible-absorption probes applications. The significantly extended lifetime of Re(I) d$\pi\rightarrow\pi^*$ diimine centered ^{3}MLCT excited state in newly synthesized bimetallic Re(phen-C≡C-AuPPh$_3$)(CO)$_3$Cl complex relative to the that of the parent Re(phen)(CO)$_3$Cl system is also reported in this thesis. The detailed understanding of the excited state decay in Re(I) complexes appended with Au-acetylide conjugated substituents serves as a platform for engineering of new polynuclear luminescent materials.

Introduction to Photophysical Processes

The interaction of light with matter can be conveniently described by means of a Jablonski diagram. If no external electromagnetic field is present all molecules are rested at their thermodynamic equilibrium point. This point usually corresponds to the electronic ground state. However, more than one vibrational level of the ground state is usually populated at temperatures different from absolute zero. Upon the interaction of the molecules with external electromagnetic radiation, transitions from the electronic ground to higher states may occur. Such transitions are called vertical (or Frank-Condon) because they are much faster than nuclear motion. Vertical transitions happen only within the same multiplicity manifold. Transitions between states of different multiplicity are spin-forbidden and the probability of those transitions is very low. After excitation, molecules are promoted into higher energy levels and then rapidly decay down to the lowest excited state. According to Kasha's rule, the rates of this *internal conversion* are higher than radiative rates. Thus the emission generally originates only from the lowest excited state. From the singlet excited state a molecule can give up its energy radiatively in form of *fluorescence* and return to the ground state. Alternatively, with sufficient spin-orbit coupling the molecule can change its multiplicity and reside in the triplet excited state. This phenomenon is known as *intersystem crossing*. From its triplet excited state a molecule can also radiatively decay to the ground state. Resulting *phosphorescence* is usually much weaker than fluorescence because vertical transitions of the different multiplicity are spin forbidden and non- radiative channel is more efficient in fluid media. Thus fluorescence and absorption spectroscopy are conventional methods to probe different exited states. The time resolved implementation of these spectroscopic methods

allows one to monitor the time evolution of the short lived states. The probing of triplet states by promoting electrons from lowest to higher levels of the triplet manifold is a convenient way to determine the triplet state lifetimes.

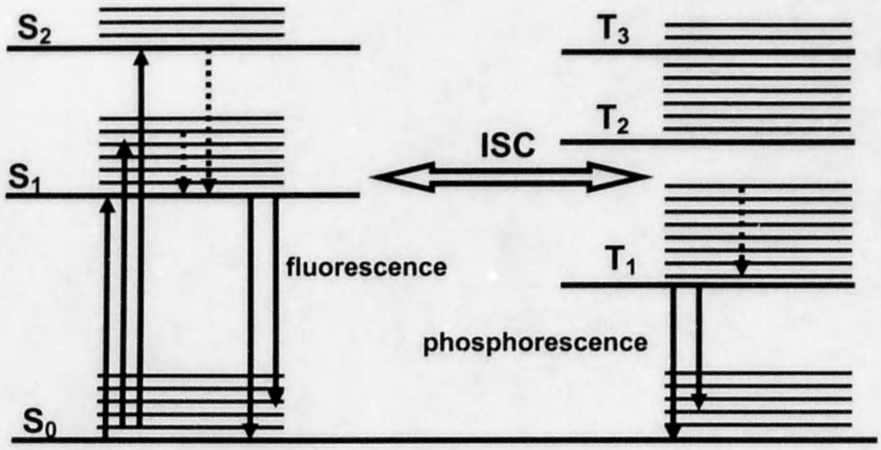

Figure.1.1. Jablonski diagram.

The fluorescence lifetime and quantum yield are important characteristics of the molecule.[3,23,24] The quantum yield is the measure of efficiency of photoinduced pathways and can be determined as a ratio of the number of emitted relative to the number of absorbed photons. The excited state decays to the ground state by radiative (k_r) and non-radiative (k_{nr}) pathways, therefore the quantum yield is given by

$$\Phi = \frac{k_r}{k_r + k_{nr}} \qquad (1.1)$$

The quantum yield can be close to unity if the rate of non-radiative decay is much smaller that the rate of radiative decay. The lifetime of the excited state is the average

time the molecule spends in the excited states prior to return to the ground state and can be determined from equation 1.2.

$$\tau = \frac{k_r}{k_r + k_{nr}} \qquad (1.2)$$

Luminescence quantum yield and lifetime can be determined experimentally by luminescence spectroscopic techniques. On the basis of experimentally measured quantum yield and lifetime the first order rate constants of radiative (k_r) and nonradiative (k_{nr}) decays can be calculated according to the equations:

$$k_r = \frac{\Phi}{\tau} \qquad (1.3)$$

$$k_{nr} = \frac{1-\Phi}{\tau} \qquad (1.4)$$

The techniques used for experimental measurements of Φ and τ are described in Chapter II.

MLCT Excited States

Charge-transfer (CT) states involve both the organic ligand and the metal. A charge transfer transition is defined by addition or removal of an electron from a partially filled shell of metal and a change in the oxidation state by +1 or -1.[23] There are two types of charge transfer transitions: MLCT (metal-to-ligand charge transfer) and LMCT (ligand to-metal charge transfer). The latter is not applicable to the content of the present thesis and won't be considered. MLCT involves promoting an electron from a metal orbital to a

ligand orbital. Both ^{1}MLCT (^1d-π^*) and ^{3}MLCT (^3d-π^*) states exist. The photophysical behavior of a particular MLCT compound depend on multiple factors, most important of which is electronic structure.

In coordination compounds, metals are surrounded by groups that are called ligands. The types of groups that may surround a metal atom or ion are greatly varied, but the may be broadly considered to be of two types: ligands that bond to metal atoms or ions through carbon atoms, and ligands that do not. Compounds in which the carbon atoms of organic groups are bounded to the metal atom are called organometallic.[25,26] The transition metal compounds can be characterized by the presence of partly filled *d* or *f* shells. It leads to unique experimental observations such as visible absorption spectra.[23] Electronic transitions in metal transition metal complexes can be understood through an examination of their structure and bonding. The effective approximation called crystal field theory provides a general approach for analyses of the bonding interactions between the metal and the ligands during the formation of the metal complex.[25-28] Pure crystal field theory postulates that that the metal and ligands interaction is only electrostatic or ionic in nature and ligands are considered as a negative point charges. Negative ligands repel the electrons located in *d*-orbitals of the metal which raises their energy with respect to the electrons remaining on the central core and electrons residing on the ligands. Electrons located on the d_z^2 and $d_{x^2-y^2}$ orbitals that have lobes directed towards the negative charges will be repelled stronger then d_{xy}, d_{yz} and d_{zx} orbitals that have lobes pointed between the charges. In the octahedral complex d_{xy}, d_{yz} and d_{zx} orbitals have entirely equivalent environments and therefore are equally favorable for the electron to reside. The d_z^2 and $d_{x^2-y^2}$ orbitals which are relatively unfavorable are also equivalent.

Therefore in an octahedral environment the metal ion has two kinds of *d*-orbitals. The three equivalent to each other are labeled t_{2g} and the other two are called e_g. The energetic difference Δ_0 (10 D*q*) is called crystal field splitting and D*q* is the crystal field parameter. Figure 1.2 presents the splitting of *d*-orbitals for the case of an octahedral ML_6 complex.[25,27]

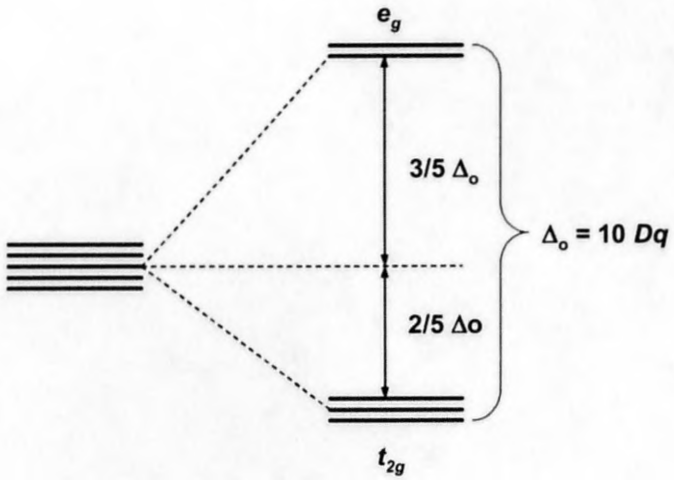

Figure 1.2. Splitting of the *d*-orbitals by an octahedral field.[25,27]

The crystal field splitting parameter Δ_0 is determined by the radius of the metal ion and its charge and the chemical nature of the ligands. The spectrochemical series list the ligands in order of increasing field strength. The bipyridine, phenanthroline (bidentate ligands), CO, and arylacetylide ligands used in the content of the present thesis are considered strong-field and cause large splitting of *d*-orbitals, therefore $\Delta_0 > P$, where P is the pairing energy. The $Re(I)L_6$ d^6 octahedral complexes with strong field ligands (L) will adopt a low spin configuration due to the higher crystal field stabilization energy. Crystal field stabilization energy is calculated from the equation:

$$CFSE = (0.4 \cdot x - 0.6 \cdot y)\Delta_0 - z \cdot P \qquad (1.5)$$

Where x is a number of electrons on t_{2g} orbitals, y is the number of electrons on e_g orbitals and z is the number of electron pairs. For strong field ligands $\Delta_0 > P$, therefore CFSE is greater and complex is more stable in a low spin configuration. For low field ligands $\Delta_0 < P$ and the high spin arrangement is more energetically favorable.

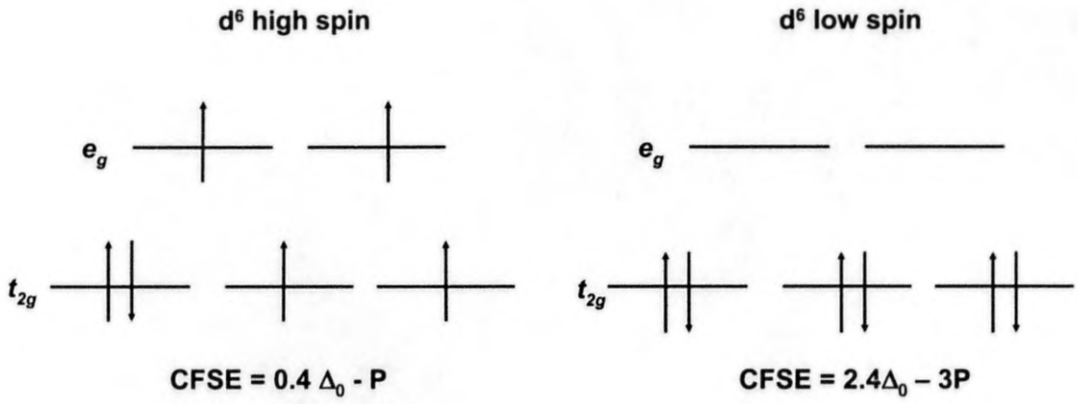

Figure 1.3. Diagrams showing two possibilities (high spin and low spin) for the ground state electron configuration of a d^6 ion in octahedral field.

If two *trans* ligands in an octahedral ML_6 complex are moved away from the metal ion the resulting complex becomes tetragonally distorted. The limiting case of tetragonal elongation results in a square-planar ML_4 (D_{4h} symmetry) complex. As a result, the e_g level splits into two levels, an upper b_{1g} ($d_{x^2-y^2}$) and lower a_{1g} (d_{z^2}) and the t_{2g} set splits into b_{2g} (d_{xy}) and a doubly degenerate e_g (d_{xz}, d_{yz}), Figure 1.4. The square planar geometry is favored by metal ions having a d^8 ground state configuration. All Pt(II) d^8 square planar complexes considered in the thesis have low spin configuration due to the large separation between highest ($d_{x^2-y^2}$) and second highest (d_{xy}) orbitals. This separation

prohibits the high-spin configuration in d^8 square planar complexes. The stronger the field of ligands, the higher $d_{x^2-y^2}$ orbital will be raised.[25-28]

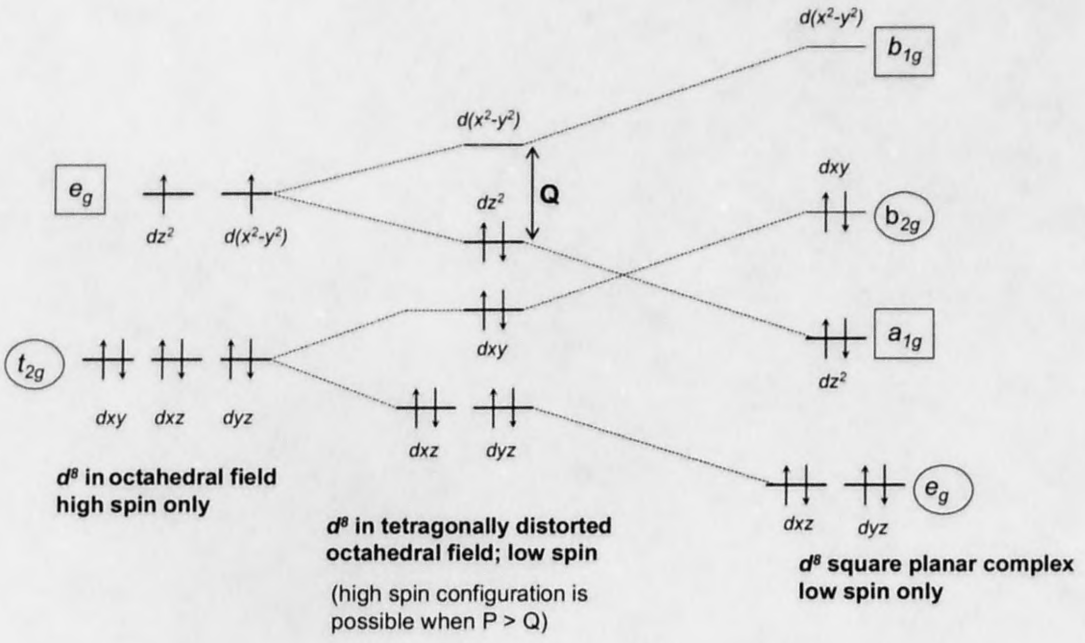

Figure 1.4. Energy level diagram showing an octahedral d^8 complex undergoing z axis elongation such that it becomes tetragonally distorted and finally reaches the square planar limit.

The molecular orbitals of a metal complex are formed through the mixing of nine valence orbitals of the metal (five nd orbitals, three (n+1)p orbitals and one (n+1)s orbital) and ligand group orbitals (LGOs) formed by σ-bonding ligands. Metal and ligand orbitals of any given symmetry then interact to give bonding and antibonding molecular orbitals.[29] The bond formation between a metal and a ligand is not solely governed by the σ-donating abilities of the ligand, but also by its π donating and accepting character. The π-acceptor interactions are very important in stabilizing the low formal oxidation states.

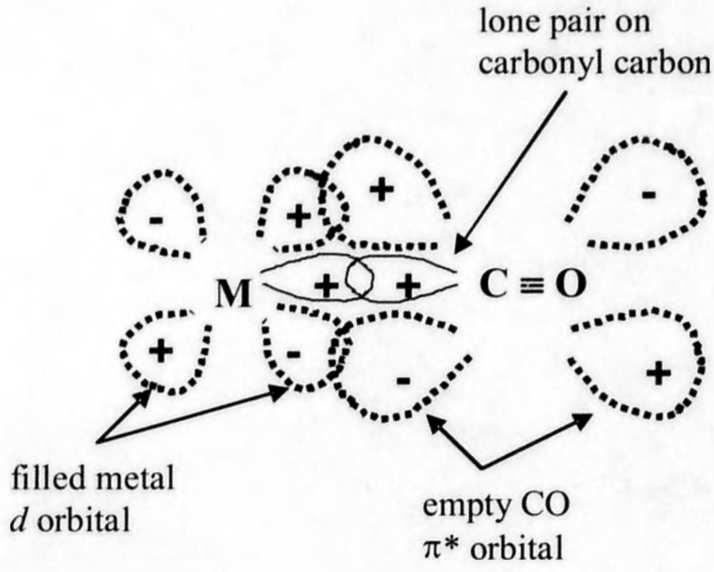

Figure 1.5. Metal-carbon bond in a metal carbonyl complex.

The carbon monoxide (CO) is one of the best known π-acceptor ligands. It has empty π* orbitals which interact with filled metal *d* orbitals, Figure 1.5. Resulting bonding MO of the metal complex gains some carbonyl character, which leads to delocalization of electron density from the metal to the carbonyl ligand. This delocalization, known as π-backbonding, decreases the C-O bond order and C-O distance due to promoting some electron density on the anti-bonding orbital of the CO ligand. The π-backbonding takes place in the Re(R-phen)$(CO)_3$Cl complexes in the content of the present thesis. The simplified diagram of molecular orbitals formed from an idealized metal *d*-orbital and antibonding π* orbital of carbonyl ligand is represented in Figure 1.6.

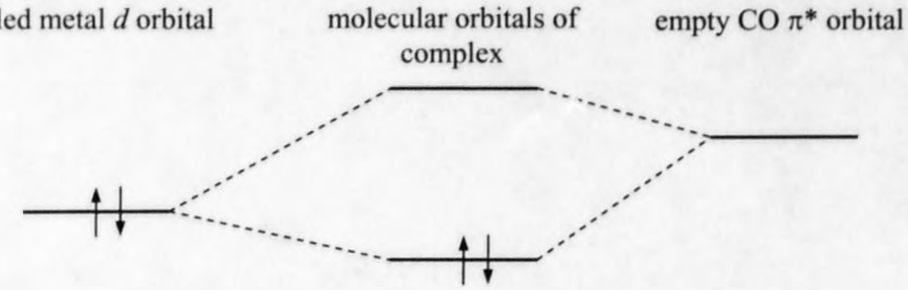

Figure 1.6. Molecular orbitals formed in a metal carbonyl complex.

The lowest excited states are derived from promoting an electron to one of the unoccupied orbitals. The state classification is determined by the original and final orbitals. There are three types of excited states being considered in this dissertation: metal-centered d-d states, ligand based π-π* states, and charge transfer states.

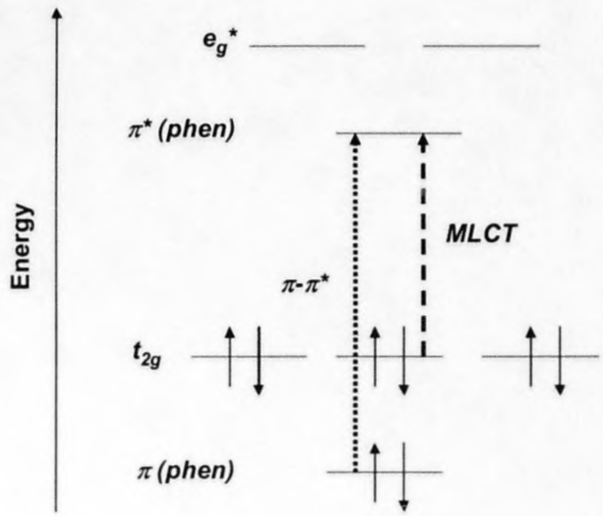

Figure 1.7. A simplified orbital diagram for $Re(phen)(CO)_3Cl$. Only the *d*-orbitals of Re(I) and π-orbitals of phenanthroline are shown. The transitions corresponding to the MLCT and π-π* are shown with the arrows.

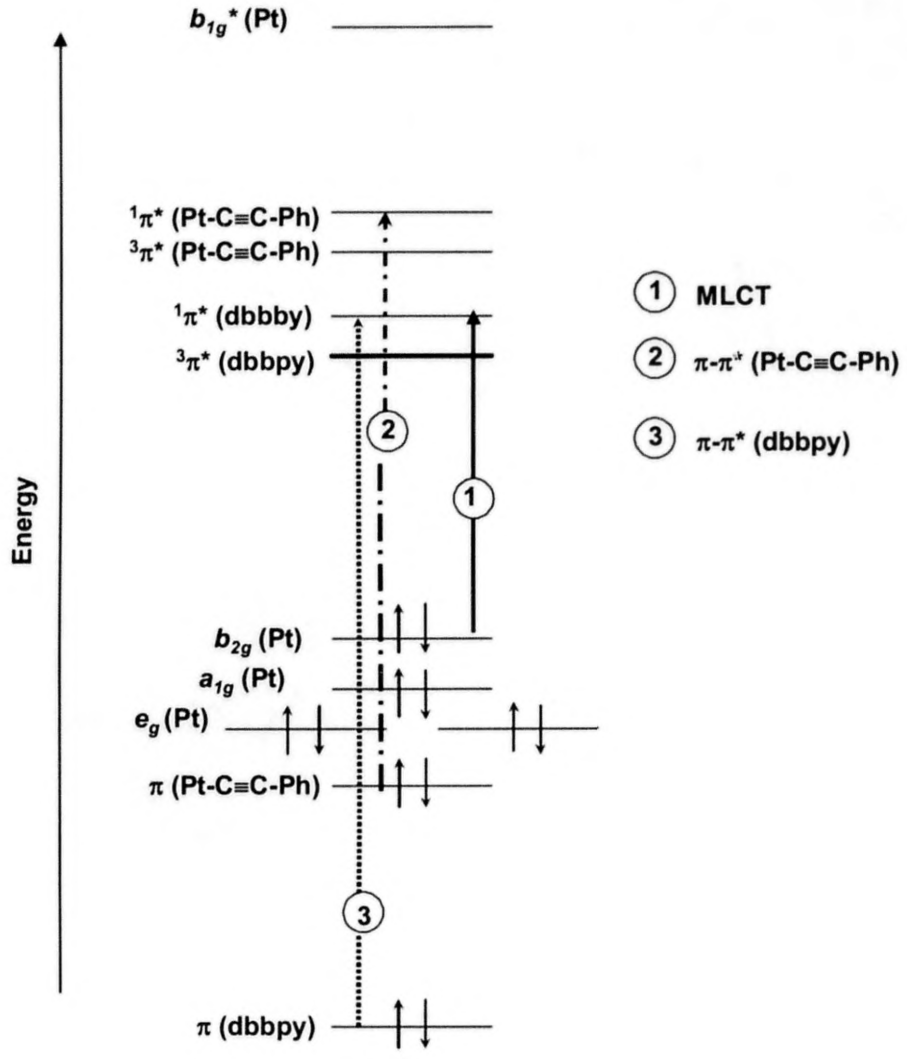

Figure 1.8. A simplified orbital diagram for Pt(dbbpy)(C≡C-Ph)$_2$ (Ph = C_6H_5) complex. The transitions corresponding to the MLCT (1) and π-π* (2 and 3) are shown with the arrows.

Generally, *d-d* singlet and triplet states could arise from promoting a metal-based bonding t_{2g} electron to an antibonding e^*_g level. Transitions to *d-d* states are formally forbidden, even for the spin-allowed singlet-singlet ones. Thus *d-d* emissions are characterized by long radiative lifetimes and high susceptibility to environmental

quenching. In the case of the Pt(dbbpy)(C≡C-Ph)$_2$ complex, the lowest lying *d-d* state b_{1g}* (e_g* in the case of Re(R-Phen)(CO)$_3$Cl) does not intercept the CT state due to the strong field nature of the ligands. The HOMO of Pt(dbbpy)(C≡C-Ph)$_2$ complex is predominately metal-based, with some π character due to interactions with close lying π bonding orbitals of the phenylacetylide and will be considered as of $d\pi$ character in the content of the present thesis. The LUMO in the molecules can be characterized as π^* and localized on the diimine ligand.

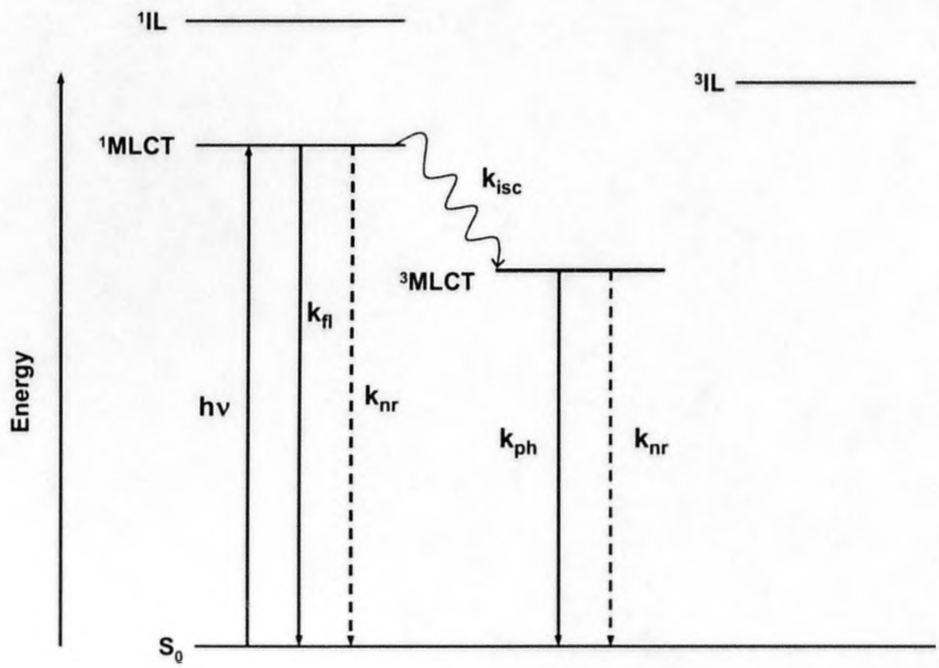

Figure 1.9. A Jablonski diagram for Pt(dbbpy)(C≡C-Ph)$_2$.

The Jablonski diagram for Pt(dbbpy)(C≡C-Ph)$_2$ is represented in Figure 1.9. Excitation in the visible into the MLCT absorption band results in population of the

singlet excited state. This process is followed by rapid non-radiative intersystem crossing to the triplet MLCT excited state. The triplet state decays to the ground state by radiative and non-radiative decay pathways. The MLCT absorption and emission spectra are usually broad and solvatochromic in nature due to the significant differences in the dipole moments of the ground and excited states.[30-32] In reality, the charge separation in the MLCT excited state is never complete, being somewhat diminished by the metal-ligand π-backbonding which mixes the donor and acceptor orbitals of the metal atom and the ligand, respectively, and by compensating effects of accompanying charges in the overall electron density distribution. MLCT transitions are strongly allowed. MLCT compounds including $Re(phen)(CO)_3Cl$ and $Pt(dbbpy)(C{\equiv}C\text{-}C_6H_5)_2$, both considered in this thesis have relatively long excited state lifetimes, which can be attributed to the highly efficient and fast transition to the ^{3}MLCT excited state. Transitions between electronic states involve changes in the orbital motion of electrons. The intrinsic angular momentum of the electron stays intact during this transition. Because the spin flip happens isoenergetically just due to the re-phasing of the spin angular momentum vector, the minor perturbation in the magnetic field of the atom or molecule can induce a transition between two states of different multiplicity (e.g. ^{1}MLCT$\rightarrow{}^3$MLCT). Such perturbations usually occur due to the interaction between spin angular momentum and orbital angular momentum known also as *spin-orbit coupling*.[28,33] One consequence of the spin-orbit coupling is to smear the distinction between different spin multiplicity. If the coupling is strong, states of separate identity may become mixed. However, for practical purposes, it is still possible to use singlet and triplet states configuration labels, especially for MLCT excited states. The magnitude of spin-orbit coupling is proportional to the atomic number

of the atoms present in the system and is called the *heavy atom effect.* The influence of an element on the spin-orbit interaction can be measured quantitatively and represented in form of the spin-orbit coupling constant ξ_l. The coupling constants for light atoms are relatively small (e.g. for carbon $\xi_l = 32$ cm^{-1}, for hydrogen atom $\xi_l = 0.24$ cm^{-1}) compared with heavy atoms (e.g. ξ_l(Pt) = 4481 cm^{-1}, ξ_l(Re) = 2903 cm^{-1}, ξ_l(Au) = 5104 cm^{-1}).[34,35]

Another important factor determining the decay lifetimes of MLCT compounds is the *energy gap law.*[36-38] This law states that as the energy gap or emission energy decreases, the non-radiative decay rate increases exponentially. The radiationless process become more efficient as the emitting state approaches the ground state, due to the higher efficiency of overlap between wavefunctions of vibronic levels of the ground state and wavefunctions of vibrationless levels of the emitting state. The energy gap law can be used only within a very similar series of complexes and doesn't work well for comparing different types of complexes.[3,24]

The quantum yield of the MLCT luminescence is high, often exceeding 10%. Also, the molar extinction coefficients of the spin-allowed transitions are large, which makes these CT states easy to pump optically. The energy of the MLCT state correlates with the reduction potential of the ligand involved in MLCT transition and the oxidation potential of the metal in the complex.[23] Low-temperature (77 K) spectra of MLCT transitions show vibrational structure and possess a significant value of thermally induced Stokes shifts ($\Delta E_s = E_{00}$(77 K) - E_{00}(298 K)). It is due to the fact, that in rigid media (glasses, frozen solutions, plastics, solids, etc.) MLCT emission occurs at higher energy than in solution, a phenomenon termed "*luminescence rigidochromism*" by Wrighton et al.[39] This phenomenon occurs because the dipole orientational part of the solvent

polarization (λ_{00}) is frozen in rigid media. According to Marcus, the reorganization energy (λ_0) is partitioned into two parts λ_{00} and λ_i, where λ_{00} is the orientational part and λ_i is the translational part. In rigid media λ_{00} becomes a part of energy gap, Figure 1.10.

$$\lambda_0 = \lambda_{00} - \lambda_{0i} \qquad E_{em}(\text{rigid}) - E_{em}(\text{fluid}) \approx 2\lambda_{00} \qquad (1.6)$$

According to eq. 1.6 the difference between the emission maxima in rigid media and in solution is a function of λ_{00} which varies as a change in dipole moments between ground and excited states.[40]

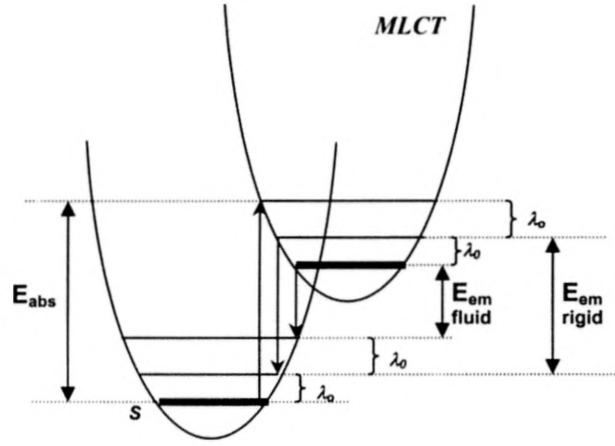

Figure 1.10. Energy diagram demonstrating luminescence rigidochromism.

In the case if the lowest excited state in the metal complex is ligand-centered (intraligand) a significant extension of lifetime compared to the MLCT excited states can be achieved.[41-43] In the present work the photophysical properties of several molecules

will be governed by the low-lying ^{3}IL states centered on the arylacetylide moieties of several Pt(II) complexes. Therefore, the basic photophysical properties of IL excited states need to be mentioned. The emission originating from ligand-centered (intraligand) excited states is generally more structured then from the MLCT excited state. It is possible to distinguish IL and MLCT-based emissions by energy and lifetime criteria. The ^{3}IL state emission of the complexes theoretically should resemble the shape, energy and vibronic spacing of the $^3\pi$-π^* emission of uncoordinated ligand under the same conditions.[23] Due to the spin forbidden nature of $^3\pi$-π^* transitions, the addition of ethyliodide incorporates an external heavy atom effect and low temperature (77 K) can be used to observe the ^{3}IL phosphorescence from the uncoordinated ligand. Another approach, successfully used in the present work in order to unambiguously distinguish between ^{3}MLCT and ^{3}IL arylacetylide-centered emissions is to prepare the structural model lacking the MLCT excited states but incorporating the same ligand fragments attached to the metal center. The emission energy of the IL excited states does not exhibit solvatochromism and rigidochromism because of its non-polar nature.[40] The ^{3}IL phosphorescence can rarely be observed in fluid solution at room temperature due to the fast thermally activated decay processes. This obstacle has been effectively overcome in the present work for the group of new complexes by careful structural and excited state engineering. ^{3}IL arylacetylide-based phosphorescence was sensitized from the ^{3}MLCT excited state via undefined intramolecular energy migration processes.

The different kinds of energy transfer mechanisms can be readily distinguished. Radiative energy transfer occurs because the emission from the donor is simply reabsorbed by the acceptor. Non-radiative energy transfer processes can occur by two

mechanisms: the Förster type mechanism,[44] based on Coulombic interactions, and the Dexter type mechanism,[45] based on exchange interactions.[3,24] Efficient non-radiative energy transfer requires that the energy level excited in B is not higher that that of A*.

$$*A\sim B \rightarrow A\sim B^*$$

The Dexter-type mechanism is a short range mechanism, *i.e.* the energy-transfer process is strongly distance dependent and the transfer rate diminishes rapidly at distances larger than 5Å. Therefore, this kind of energy transfer mechanism requires that A* and B are located sufficiently close to each other to allow overlap of the electron orbitals involved. The electron from A* physically transfers into the lowest unoccupied molecular orbital of B with a simultaneous transfer of an electron from the highest occupied molecular orbital of B to the corresponding orbital of A. The schematic representation of the Dexter mechanism is depicted below.

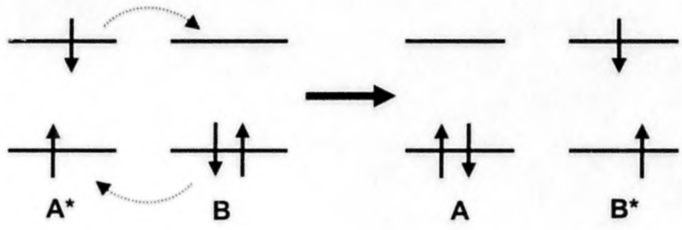

Figure 1.11. Schematic representation of the Dexter electron-exchange mechanism.

Dexter derived the following relationship[24] between the distance and the energy transfer rate:

$$K_{et} \sim e^{-2r/L} \qquad (1.7)$$

Where r is the distance between the donor and acceptor, and the L is the sum of the Van der Waals radii of the donor and acceptor.[24] The energy transfer rate is also dependent on of the overlap of the emission spectrum of A* and the absorption spectrum of B, but it is largely insignificant.[46,47] The probability of energy transfer is dictated by the Wigner rule of spin conservation. The possible combinations of the spins for products and reactants of energy transfer by the Dexter mechanism are:

$$^1A^* + {}^1B \rightarrow {}^1A + {}^1B^* \qquad {}^3A^* + {}^1B \rightarrow {}^1A + {}^3B^*$$

$$^1A^* + {}^1B \rightarrow {}^1A + {}^3B^* \qquad {}^3A^* + {}^1B \rightarrow {}^1A + {}^1B^*$$

$$^3A^* + {}^3B \rightarrow {}^1A + {}^1B^*$$

The Förster type mechanism[44] is a long range mechanism. Its rate falls of as $1/r^6$, where r is the separation distance between donor and acceptor. This mechanism doesn't involve any emission and reabsorption of photons and is quite efficient in the range of 20-60 Å, therefore can occur inter- and intramolecularly. The concept is based on considering a fluorophore as an oscillating dipole, which exchanges energy with another dipole with a similar resonance frequency. As a result of this interaction, A* become de-excited and returns to its ground state concurrent with the excitation of B.[24] The schematic representation of the Förster mechanism is depicted below.

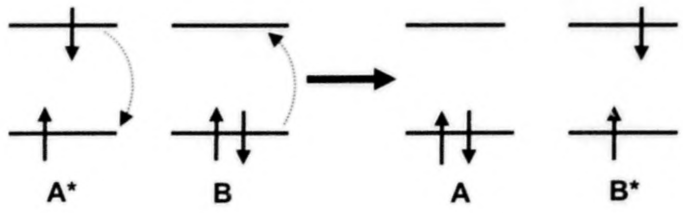

Figure 1.12. Schematic representation of the Förster energy transfer mechanism.

The rate of energy transfer according to the Förster mechanism can be calculated on the basis of spectroscopic quantities by the following equation.[48]

$$K_{et} = 5.87 \cdot 10^{-25}(\Phi_A / n^4 \tau_A r^6) \int_0^\infty F_A(\bar{\nu}) \varepsilon_B(\bar{\nu}) d\bar{\nu} / \bar{\nu}^4 \qquad (1.8)$$

Here, Φ_A and τ_A are the luminescence efficiency and lifetime of the donor excited state, and the integral is related to the spectral overlap between donor emission and acceptor absorption. The possible combinations of the spins for products and reactants of energy transfer by the Förster mechanism are:

$$^1A^* + {}^1B \rightarrow {}^1A + {}^1B^* \qquad\qquad {}^1A^* + {}^3B \rightarrow {}^1A + {}^3B^*$$

Where ^3B represents the first electronically excited triplet state T_1 and $^3B^*$ is a higher triplet state T_2.

Mechanisms involved in the intramolecular energy migration in the metal complexes considered in the present study haven't been investigated but are believed to proceed by the Dexter type pathway judging from relatively small distance (~3 Å) between arylacetylide and bipyridine chromophores, in addition to their intimate electronic connection.

In addition to the photophysical behavior ascribed to the "pure" excited states it is also possible to observe the excited properties attributed to the equilibrated or

configuration mixed excited states.[49-57] For example, the close proximity of the MLCT and π-π* excited states for the new Pt(dbbpy)(C≡C-Napthalene)$_2$ compound considered in the present thesis resulted in a wide array of configuration mixed or equilibrated excited states composed of varying degrees of ^{3}MLCT and ^{3}π-π* character. The highly solvatochromic nature of MLCT excited states have been used to fine-adjust the ^{3}MLCT level relative the ^{3}π-π* state. State mixing is frequently desirable because, when properly done, the best attributes of both states are incorporated. In the case of Pt(dbbpy)(C≡C-Napthalene)$_2$, the MLCT state introduces environmental sensitivity due to its solvatochromic nature. At the same time the ^{3}π-π* IL character confers longer radiative lifetimes.

Introduction to Pt(II) Diimine Complexes

Since Pt(II) diimine complexes are employed in this thesis (Chapter III) it is worthwhile to introduce the photophysical properties of the known analogous. For more than a decade platinum (II) diimine complexes, of the general formula Pt(diimine)X_2 , where X = halide, cyanide, thiolate, isonitrile, and acetylide have been known to be luminescent in fluid solution.[43,58-62] Such an extensive interest to this group of complexes has been inspired by the fact that the directional nature of charge-transfer excited states in square planar Pt(II) diimine complexes is ideal for electron-hole creation and separation, therefore these systems merit consideration for use in molecular photochemical devices. The coordinative unsaturation of square planar complexes also renders them of interest for sensor applications.[63] At the same time transition metal complexes and polymers containing acetylide fragments have been found to be valuable due to their potential

applications in many fields of material chemistry, including nonlinear optics, liquid crystals, conducting polymers and luminescent materials.[64-66]

It has been established that the energy and nature of the emitting state in Pt(II) complexes depends on the anionic ligand.[42,43,58-62,67-72] Table 1.1 contains some representative examples illustrating how the nature of the ligands affect the origin of the emitting state and therefore its lifetime.

Table 1.1. Some representative examples of Pt(II) diimine compounds.

Complex	Emitting state	Lifetime
Pt(diimine)Cl_2[58,59]	^{3}*d-d* or ^{3}MLCT (solid or frozen)	20 ns - 30 μs
Pt(diimine)$(CN)_2$[43,60]	$^3\pi$-π^*	100 ns – 3 μs
Pt(diimine)(S_2R)[61,70-72]	MMLLCT[a]	3.4 ns - 2 μs
Pt(4'-Aryl-trpy)Cl^+[42,69]	^{3}MLCT/^{3}ILCT/π-π^*	85 ns – 64 μs

[a]mixed metal/ligand (dithiolate)-to-ligand(diimine) charge-transfer.[72]

In 1994, Che and co-workers published a brief account of a different luminescent platinum compounds in one of which X = phenylacetylide.[73] The complex Pt(phen)(C≡C-$C_6H_5)_2$ was observed to be highly emissive with an excited state energy between those of the di(cyanide) and the dithiolate, and was proposed to originate from a ^{3}MLCT excited state (τ = 0.3 - 2.1 μs). The bright luminescence and the change in the excited state from those of di(cyanide) and the dithiolate complexes made this system and its derivatives interesting for further study.

In 2000, the photophysical properties of a wide variety of complexes with the general formula Pt(diimine)(C≡C-Ar)$_2$ have been investigated by Eisenberg et al.[31] The nature of the excited states in these compounds has been probed by systematic ligand variation and its influence on excited state properties has been studied. In this context, two series of complexes were synthesized and studied, one having the formula Pt(R-phen)(C≡C-C_6H_5)$_2$ where R-phen was 1,10-phenanthroline substituted in the 5-position with R = H, Me, Cl, Br, NO_2 or C≡C-C_6H_5, while the second had formula Pt(dbbpy)(C≡C-$C_6H_4X_2$) where dbbpy = 4,4'-di(*tert*-butyl)bipyridine and X = H, Me, F or NO_2. The complexes appeared to be brightly emissive in fluid solution (λ_{max} = 570-640 nm) with relative emission quantum yields ranging from $3 \cdot 10^{-3}$ to 10^{-1}. All the complexes exhibited an absorption band around 400 nm that corresponds to a Pt d $\rightarrow \pi^*$ diimine charge transfer transition. Through this investigation the emitting state was confirmed to be a Pt-to-diimine charge transfer in accord with that originally proposed by Che.[73] This assignment was consistent with observation that variation of the diimine ligand affects the energy of the lowest unoccupied molecular orbital, and that variation of the arylacetylide leads to only minor changes in the Pt-based HOMO. Luminescence decay measurements revealed excited-state lifetimes between 0.01 - 5.6 μs.[31] These complexes were found to undergo electron-transfer quenching and excited state reduction potentials were estimated. Also, it was established that studied Pt(diimine)(C≡C-Ar)$_2$ complexes undergo self-quenching in solution with increasing of concentration of the metal complex. As a consequence of this observation a separate investigation of self-quenching by platinum diimine complexes in general was conducted.[72]

In 2001, as a consequence of the original study[73] Che and co-workers published an extensive study of a wide variety of highly photoluminescent bis(phenylacetylide) platinum(II) complexes with alkyl- and phenyl-substituted bipyridine and phenanthroline ligands coordinated to the platinum center.[74] In accordance with Eisenberg's work discussed above,[31] all bis(phenylacetylide) derivatives exhibited intense triplet MLCT photoluminescence in the solid state and in fluid solutions at room temperature. It was demonstrated, that it was possible to fine-tune the energy of the emissive state (^{3}MLCT) by changing substituents on the diimine ligands, which is consistent with behavior observed by Eisenberg for structurally related complexes.[31] A significant observation was made regarding the nature of lowest-energy excited state for a bis(butadiynyl) complex, Pt(4,4'-dtbpy)(C≡C-C≡C-C_6H_5)$_2$ (dtbpy = 4,4'-di-*tert*-butyl-2,2'-bipyridine). At room temperature in fluid solution emission from this complex was found to be similar to bis(phenylacetylide) analog and was assigned to a ^{3}MLCT excited state. The 77 K solid state and glassy photoluminescence was proposed to originate from a metal-perturbed $^3[\pi\pi^*$(C≡C-C≡C-C_6H_5)] excited state. Che and co-workers attributed the difference between the emissive states to the influence of solvent molecules. It was suggested that the energy levels of the two excited states were comparable and solvent binding to the coordinatively unsaturated platinum center stabilized the [5d Pt→π^* dtbpy] MLCT state in solution. However, in solid or glassy media at low temperature, the MLCT state occurred at higher energy and the $\pi\pi^*$ intraligand emission dominated.[74]

At the same time a comprehensive photophysical investigation was carried out on a series of another eight complexes of the type Pt(diimine)(C≡C_6H_5X)$_2$ by Schanze and co-workers, where the diimine was a series of 2,2'-bipyridine (bpy) ligands and –C≡C-

C_6H_5X was a series of substituted phenylacetylide ligands.[32] In the first series of complexes, the energy of the Pt → bpy MLCT excited states was varied by changing the substituents on the 4,4'- and/or the 5,5'-positions of bpy ligand and X = CH_3. In a second series of complexes the electronic demand on the phenylacetylide ligand was varied by changing the para substituent (X) on the phenyl ring, where X = CF_3, CH_3, OCH_3, $N(CH_3)_2$. The results of this study revealed that for the first series of complexes the photophysical properties were dominated by the energetically low lying Pt → bpy ^{3}MLCT excited state, with decay lifetimes from 20 to 1300 ns, which is strongly consistent with the Che and Eisenberg observations.[31,73,74] The photophysical properties of the second series of complexes which featured a fixed diimine acceptor ligand (4,4'-bis-*tert*-butyl-2,2'-bipyridine) along with a series of substituted phenylacetylide ligands were found to be more complicated. The most obvious exception from the series was the -NO_2 substituted complex, which possessed a RT lifetime of 3.6 μs. The lack of a significant value of Stokes shift for the -NO_2 and -$N(CH_3)_2$ substituted complexes suggests that emission does not emanate from a ^{3}MLCT manifold. It was suggested that IL $^3\pi\pi^*$ and ^{3}MLCT states were very close in energy and PL originated from the state having IL $^3\pi\pi^*$ character. The observed RT photoluminescence was very weak and its intensity dramatically increased in a glassy matrix. The involvement of the IL $^3\pi\pi^*$ state in the photophysics of some of the complexes also was supported by unusual features in the transient absorption, time-resolved infrared, photoluminescence spectra and excited-state decay kinetics.[32] The detailed study completed by Schanze and co-workers demonstrated that the ^{3}IL states of the acetylide ligands can markedly influence excited state decay in this class of complexes.

The detailed review presented above reveals that in most studies, the Pt (II) diimine bis(arylacetylides) possess relatively long-lived excited states with photophysical properties consistent with a dπ Pt → π* (diimine) MLCT assignment. However, there are numerous examples where the photophysical behavior of certain complexes is inconsistent with the MLCT assignment and a low lying intraligand π-π* (^{3}IL) state is believed to contribute to the excited state decay. Extremely rarely, however, has pure ^{3}IL based emission, in RT fluid solutions been observed.[75]

On the other hand, platinum-acetylide based π-conjugated oligomers and polymers have been studied extensively by multiple groups. Schanze and co-workers established that compounds with general formula C_6H_5-[C≡C-Pt(PBu_3)$_2$-C≡C-C_6H_4-]$_n$-H (n = 2 – 7) exhibited long-lived (18 - 24μs) ^{3}π-π* phosphorescence, while ^{1}π -π* fluorescence has also been observed but phosphorescence dominated.[41] Davy also reported similar observations in the Pt(PBu_3)$_2$(C≡C-C_6H_4-C≡C-C_6H_5)$_2$ compound.[47] The photophysical characterization of a series of platinum(II)-containing phenyl-ethynyl oligomers has been also reported by Rogers and McLean.[46] The photophysical properties of the investigated phenyl-ethynyl oligomers was about entirely dominated by phosphorescence at room temperature from the appended phenyl-ethynyl moieties exhibiting lifetimes up to 86 μs.

The latter observation of extraordinary long lived ^{3}π-π* phosphorescence observed in a fluid solution from the platinum-acetylide oligomers and visible absorption features of the Pt(diimine)(C≡C-C_6H_5-R) group of MLCT complexes inspired the challenging idea of combining those two features useful for analytical luminescence applications. In essence generating single multichromophoric structures yielding new Pt(dbbpy)(C≡C-Aryl)$_2$ complexes possessing diverse photophysical properties.

Design of New Synthetically Facile Pt(dbbpy)(C≡C-Aryl)$_2$ Complexes

In the present work we postulated that one could potentially observe significantly extended lifetimes in synthetically facile Pt(II) systems if the appropriate chromophores are appended as acetylide ligands. It the present study we believed that proper selection of ligand in Pt(dbbpy)(C≡C-Aryl)$_2$ (dbbpy = 4,4'-di(*tert*-butyl)-2,2'-bipyridine) complexes or solvent media may be able to produce either "pure" ^{3}MLCT or $^3\pi$-π^* (^{3}IL) excited states in addition to equilibrated or configuration mixed excited states composed of varying degrees of ^{3}MLCT and $^3\pi$-π^* character. The wide range of Pt(dbbpy)(C≡C-Aryl)$_2$ complexes has been carefully designed, where C≡C-Aryl are different polyaromatic ligands with energies of their triplet excited states strategically positioned above or below the expected Pt d$\pi \rightarrow \pi^*$ (dbbpy) ^{3}MLCT state. According to the design, it is expected that in case of Aryl = C_6H_5 or biphenyl, the emission properties of the complexes will be dominated by the ^{3}MLCT excited state, due to the fact that their ^{3}IL states lie above the ^{3}MLCT manifold. In the case of Aryl = pyrene, anthracene or perylene, "pure" intraligand-based phosphorescence is expected. The triplet state of the C≡C-Naphthalene ligand is almost isoenergetic to the ^{3}MLCT excited state. Therefore, due to the highly polar ground state it should be possible change ^{3}MLCT energy by the solvents of different polarities in the way that mixed excited states composed of varying degrees of ^{3}MLCT and $^3\pi$-π^* character will result. There is also an interesting consequence to using a square planar geometry[63] in that the lowest expected ^{3}MLCT (dπ Pt $\rightarrow \pi^*$ diimine) and ^{3}IL (acetylide π-π^*) excited states are located on the opposite ends of the molecule. Table 1.2 represents the triplet energies of free aromatic compounds

which were used for the rough estimate of the relative triplet energies of C≡C-Aryl ligands.

Table 1.2. Triplet state energies of some aromatic compounds.[34]

Aromatic ligand	**E_T, kJ/mol**
Benzene	353
Biphenyl	274
Naphthalene	253
Pyrene	203
Anthracene	178
Perylene	148

It was assumed, that even though the real energies of the ^{3}IL states in the designed complexes will be different by some magnitude the relative differences in energies will likely be unperturbed.

The qualitative Jablonski diagram presented below illustrates the proposed photophysical behavior of the designed compounds, Figure 1.13.

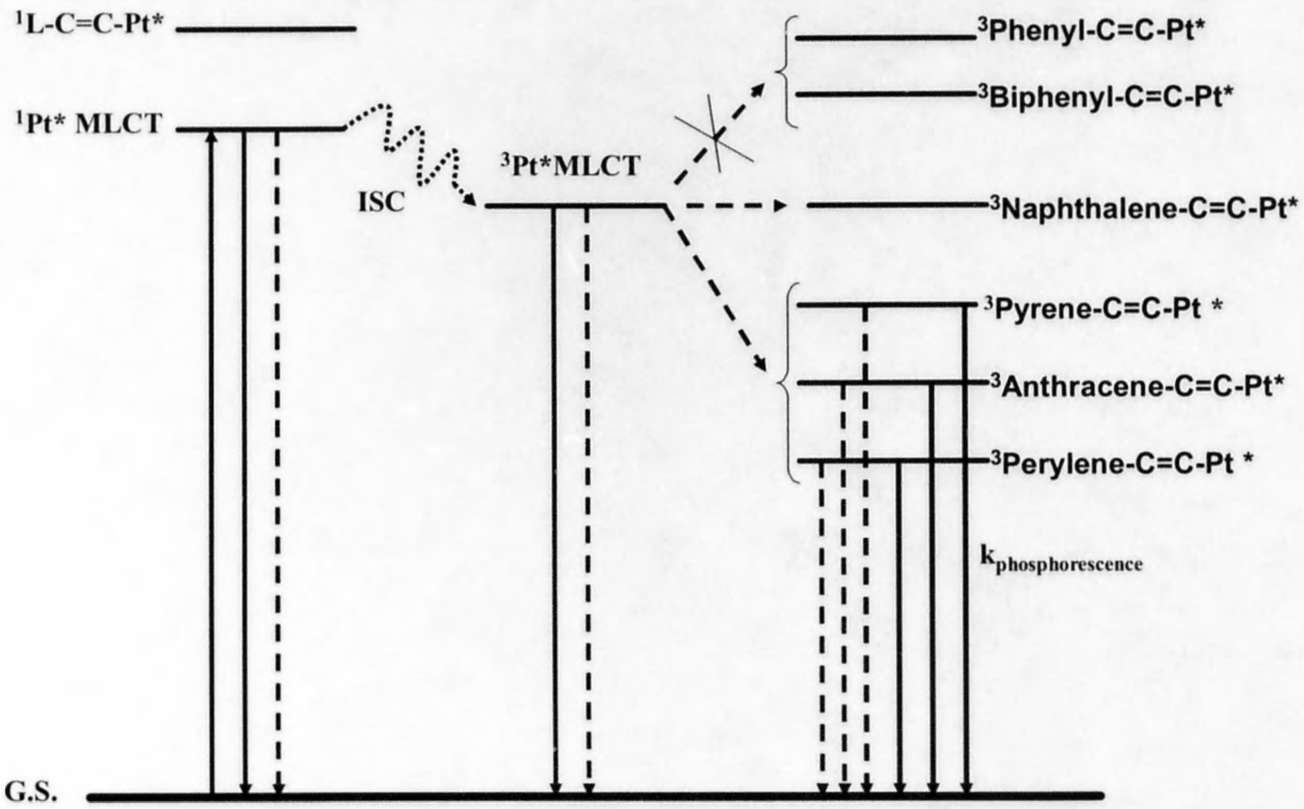

Figure 1.13. Qualitative Jablonski diagram of the generic Pt(dbbpy)(C≡C-R)$_2$ system, where R = C_6H_5, Biphenyl, Naphthalene, Pyrene, Anthracene, Perylene. Dashed lines – non radiative transitions, solid lines – radiative transition.

Introduction to the Re(I) Diimine Complexes

Since some Re(I) diimine complexes are engaged in this thesis (Chapter 4) it is worthwhile to briefly highlight some photophysical patterns ruling the photophysics of this group of complexes. The unique photophysical properties of the Re(diimine)$(CO)_3$X chromophore, where X is an anionic ligand, have been discovered by Wrighton at al. in 1974. In a study of a series of substituted 1,10-phenanthroline complexes they observed moderately long-lived (300 - 600 ns) luminescence in a fluid solution which was assigned to a dπ Re → π* (phenanthroline) MLCT excited state.[76] Since that time the photophysics of a wide variety of Re(I) d^6 complexes have been reported in respect to the studies involving photochemical electron and energy transfers, studying medium effects and exploring the fundamental photophysics of MLCT excited states.[77-99] However, there are several reports where the photophysical properties of Re(I) compounds are not governed by MLCT excited states and can vary upon introducing the appropriate substituent to the diimine ligand.

In 1991 Schmehl and co-workers reported weak structured ^{3}π-π phosphorescence at room temperature in the $[(CO)_3(CH_3CN)Re(dstyb)Re(CO)_3(CH_3CN)](PF_6)_2$ bimetallic complex emanating from the stilbene-like chromophore dstyb appended to the diimine ligand (dstyb = 1,4-bis[2-(4'-methyl-2,2'-bipyridyl-4-yl)ethenyl]benzene).[100] The same research group also reported long-lived excited states in the Re(I) diimine complex where the pyrene chromophore was covalently attached to the diimine ligand. The emission origin was believed to be of pyrene (π) to bpy (π*) ^{3}ILCT origin or ^{3}ILCT with significant pyrene triplet character.[22] Perturbation of the luminescence properties through the structural variation of the organic-based substituents in the Re(diimine)$(CO)_3$(C≡C-R)

complexes has also been achieved.[101-104] The introduction of the stronger field acetylide ligands into the d^6 metal diimine system had the added advantage of raising the energy of *d-d* states, thus rendering the metal center more electron rich, improving the MLCT state population. The ^{3}MLCT energy was highly tunable upon variation of the σ-donating ability of acetylide ligands.

The luminescent Re(I)-based carbon wires incorporating these structures have been constructed.[101-104] A comprehensive study of a new class of π-conjugated metal-organic oligomers and polymers containing $Re(bpy)(CO)_3Cl$ chromophores has been reported by Schanze and co-workers.[105-108] The metal oligomers featured a weak, relatively long-lived red photoluminescence that was assigned to both the $^3\pi$-π^* manifold of the π-conjugated system and the dπ Re → π* bpy-olygomer ^{3}MLCT excited state. The dual origin of the photoluminescence was ascribed to the fact that oligomer based $^3\pi$-π^* and ^{3}MLCT states were in close energetic proximity and some configurational interaction could occur.[107] The experimental results described above illustrated that placing ethynylene-containing substituents within the diimine framework promotes interesting electronic effects in Re(I) diimine group of complexes. In the context of the present research the photophysics of a new Re(I) complex bearing the electron donating C≡C-$AuPPh_3$ substituent on the diimine framework has been studied. The gold-acetylide moiety incorporates a near-visible absorbing chromophore with its triplet state lying above in a close proximity to the MLCT state. It has been reported previously that introducing the electron donating substituents into the diimine framework in the some MLCT complexes shifts the emission maximum to the higher energy,[31,32] therefore some lifetime extension can be predicted upon the structural design for new Re(phen-C≡C-

$AuPPh_3)(CO)_3Cl$ molecule relative to the parent $Re(pnen)(CO)_3Cl$ system. Also, in accord with results reported by Schanze,[107] some interesting contributing factors to the photophysical properties of the new $Re(phen\text{-}C{\equiv}C\text{-}AuPPh_3)(CO)_3Cl$ complex associated with electron delocalization into the Au-acetylide fragment are proposed.

References

(1) Juris, A.; Balzani, V.; Barigelletti, F.; Campagna, S.; Belser, P.; von Zelewsky, A. *Coord. Chem. Rev.* **1988**, *84*, 85-277.

(2) Guo, X.-Q.; Castellano, F. N.; Li, L.; Lakowicz, J. R. *Anal. Chem.* **1998**, *70*, 632-643.

(3) Lakowicz, J. R. *Principles of Fluorescence Spectroscopy*; Kluver Academic/Plenum Publishers: New York, 1999.

(4) Terpetschnig, E.; Szmacinski, H.; Malak, H.; Lakowicz, J. R. *Biophys. J.* **1995**, *68*, 342-350.

(5) *Topics in Fluorescence Spectroscopy*; Plenum Press: New York, 1994; Vol. 4.

(6) Caspar, J. V.; Kober, E. M.; Sullivan, B. P.; Meyer, T. J. *J. Am. Chem. Soc.* **1982**, *104*, 630-637.

(7) Kober, E. M.; Marshall, J. L.; Dressick, W. J.; Sullivan, B. P.; Caspar, J. V.; Meyer, T. J. *Inorg. Chem.* **1985**, *24*, 2755-2763.

(8) Kober, E. M.; Caspar, J. V.; Lumpkin, R. S.; Meyer, T. J. *J. Phys. Chem.* **1986**, *90*, 3722-3734.

(9) Boyde, S.; Strouse, G. F.; Jones, W. E.; Meyer, T. J. *J. Am. Chem. Soc.* **1990**, *112*, 7395-7396.

(10) Strouse, G. F.; Schoonover, J. R.; Duesing, R.; Boyde, S.; Jones, W. E.; Meyer, T. J. *Inorg. Chem.* **1995**, *34*, 473-487.

(11) Ford, W. E.; Rodgers, M. A. J. *J. Phys. Chem.* **1992**, *96*, 2917-2920.

(12) Simon, J. A.; Curry, S. L.; Schmehl, R. H.; Schatz, T. R.; Piotrowiak, P.; Jin, X. Q.; Thummel, R. P. *J. Am. Chem. Soc.* **1997**, *119*, 11012-11022.

(13) Wilson, G. J.; Launikonis, A.; Sasse, W. H. F.; Mau, A. W.-H. *J. Phys. Chem. A* **1997**, *101*, 4860-4866.

(14) Tyson, D. S.; Gryczynski, I.; Castellano, F. N. *J. Phys. Chem. A* **2000**, *104*, 2919-2924.

(15) Tyson, D. S.; Henbest, K. B.; Bialecki, J.; Castellano, F. N. *J. Phys. Chem. A* **2001**, *105*, 8154-8161.

(16) Tyson, D. S.; Luman, C. R.; Zhou, X.; Castellano, F. N. *Inorg. Chem.* **2001**, *40*, 4063-4071.

(17) Tyson, D. S.; Castellano, F. N. *J. Phys. Chem. A* **1999**, *103*, 10955-10960.

(18) Hissler, M.; Harriman, A.; Khatyr, A.; Ziessel, R. *Chem. Eur. J.* **1999**, *11*, 3366-3381.

(19) Harriman, A.; Hissler, M.; Khatyr, A.; Ziessel, R. *Chem. Commun.* **1999**, 735-736.

(20) Thornton, N. B.; Schanze, K. S. *New. J. Chem.* **1996**, *20*, 791-800.

(21) McClenaghan, N. D.; Barigelletti, F.; Maubert, B.; Campagna, S. *Chem. Commun.* **2002**, 602-603.

(22) Guerzo, A. D.; Leroy, S.; Fages, F.; Schmehl, R. H. *Inorg. Chem.* **2002**, *41*, 359-366.

(23) Kalyanasundaram, K. *Photochemistry of Polypyridine and Porphyrin complexes*; Academic Press INC.: San Diego, 1992.

(24) Gilbert, A.; Baggott, J. *Essentials of Molecular Photochemistry*; Blackwell Science Ltd.: Cambridge, 1991.

(25) Cotton, F. A.; Wilkinson, G.; Gaus, P. L. *Basic Inorganic Chemistry* New York, 1995.

(26) Cotton, F. A.; Wilkinson, G. *Advanced Inorganic Chemistry*; John Wiley and Sons: New York, 1980.

(27) Huheey, J. E.; Keiter, E. A.; Keiter, R. L. *Inorganic Chemistry. Principles of Structure and Reactivity*, 1993.

(28) Kettle, F. A. *Physical Inorganic Chemistry*; Oxford University Press, 1998.

(29) Collman, J. P.; Hegedus, L. S.; Norton, J. R.; Finke, R. G. *Principles and Applications of Organotransition Metal Chemistry*; University Science Books: Mill Valley, 1987.

(30) Reichardt, C. *Chem. Rev.* **1994**, *94*, 2319-2358.

(31) Hissler, M.; Connick, W. B.; Geiger, D. K.; McGarrah, J. E.; Lipa, D.; Lachicotte, R. J.; Eisenberg, R. *Inorg. Chem.* **2000**, *39*, 447-457.

(32) Whittle, C. E.; Weinstein, J. A.; George, M. W.; Schanze, K. S. *Inorg. Chem.* **2001**, *40*, 4053-4062.

(33) Turro, N. J. *Molecular Photochemistry*; W. A. Benjamin, Inc.: New York, 1965.

(34) Murov, S. L.; Carmichael, I.; Hug, G. L. *Handbook of Photochemistry*; Marcel Dekker, INC.: New York, 1993.

(35) Jensen, P.; Bunker, P. R. *Computational Molecular Spectroscopy*; John Wiley and Sons: New York, 2000.

(36) Englman, R.; Jortner, J. *Mol. Phys.* **1970**, *18*, 145.

(37) Bixon, M.; Jortner, J. *J. Chem. Phys.* **1968**, *48*, 715.

(38) Freed, K. F.; Jortner, J. *J. Chem. Phys.* **1970**, *52*, 6272.

(39) Wrighton, M.; Morse, D. L. *J. Am. Chem. Soc.* **1974**, *96*, 998-1003.

(40) Chen, P.; Meyer, T. J. *Chem. Rev.* **1998**, *98*, 1439-1477.

(41) Liu, Y.; Jiang, S.; Glusac, K.; Powell, D. H.; Anderson, D. F.; Schanze, K. S. *J. Am. Chem. Soc.* **2002**, *124*, 12421-12413.

(42) Michalec, J. F.; Bejune, S. A.; Cuttell, D. G.; Summerton, G. C.; Gertenbach, J. A.; Field, J. S.; Haines, R. J.; McMillin, D. R. *Inorg. Chem.* **2001**, *40*, 2193-2200.

(43) Wan, K.-T.; Che, C.-M.; Cho, K.-C. *J. Chem. Soc. Dalton Trans.* **1991**, 1077-1080.

(44) Forster, T. H. *Discuss. Faradey Soc.* **1959**, *27*, 7-17.

(45) Dexter, D. L. *J. Chem. Phys.* **1953**, *21*, 836-850.

(46) Rogers, J. E.; Cooper, T. M.; Fleitz, P. A.; Glass, D. J.; McLean, D. G. *J. Phys. Chem. A* **2002**, *106*, 10108-10115.

(47) McKay, T. J.; Bolger, J. A.; Staromlynska, J.; Davy, J. R. *J. Chem. Phys.* **1998**, *108*, 5537-5541.

(48) Balzani, V.; Juris, A.; Venturi, M.; Campagna, S.; Serroni, S. *Chem. Rev.* **1996**, *96*, 759-834.

(49) Crosby, G. A. *Acc. Chem. Res.* **1975**, *8*, 231-238.

(50) Demas, J. N.; Crosby, G. A. *J. Mol. Spectrosc.* **1968**, *26*, 72-77.

(51) Demas, J. N.; Crosby, G. A. *J. Phys. Chem.* **1971**, *75*, 991-1024.

(52) Hager, G. D.; Crosby, G. A. *J. Am. Chem. Soc.* **1975**, *97*, 7031-7037.

(53) Hager, G. D.; Watts, R. J.; Crosby, G. A. *J. Am. Chem. Soc.* **1975**, *97*, 7037-7042.

(54) Hipps, K. W.; Crosby, G. A. *J. Am. Chem. Soc.* **1975**, *97*, 7042-7048.

(55) Watts, R. J.; Crosby, G. A. *J. Am. Chem. Soc.* **1971**, *93*, 3184-3188.

(56) Watts, R. J.; Crosby, G. A.; Sansregret, J. L. *Inorg. Chem.* **1972**, *11*, 1474-1483.

(57) Watts, R. J.; Crosby, G. A. *Chem. Phys. Lett.* **1972**, *13*, 619-621.

(58) Miskowski, V. M.; Houlding, V. H. *Inorg. Chem.* **1989**, *28*, 1529-1533.

(59) Miskowski, V. M.; Houlding, V. H.; Che, C.-M.; Wang, Y. *Inorg. Chem.* **1993**, *32*, 2518-2524.

(60) Kunkely, H.; Vogler, A. *J. Am. Chem. Soc.* **1990**, *112*, 5625-5627.

(61) Zuleta, J. A.; Chesta, C. A.; Eisenberg, R. *J. Am. Chem. Soc.* **1989**, *111*, 8916-8917.

(62) Zuleta, J. A.; Bevilacqua, J. M.; Proserpio, D. M.; Harvey, P. D.; Eisenberg, R. *Inorg. Chem.* **1992**, *31*, 2396-2404.

(63) Kunugi, Y.; Mann, K. R.; Miller, L. L.; Exstrom, C. L. *J. Am. Chem. Soc.* **1998**, *120*, 589-590.

(64) Manna, J.; John, K. D.; Hopkins, M. D. *Adv. Organomet. Chem.* **1995**, *38*, 79-154.

(65) Manna, J.; Kuehl, C. J.; Whiteford, J. A.; Stang, P. J.; Muddiman, D. C.; Hofstadler, S. A.; Smith, R. D. *J. Am. Chem. Soc.* **1997**, *119*, 11611-11619.

(66) Nguyen, P.; Gomez-Elipe, P.; Manners, I. *Chem. Rev.* **1999**, *99*, 1515-1522.

(67) Zuleta, J. A.; Bevilacqua, J. M.; Rehm, J. M.; Eisenberg, R. *Inorg. Chem.* **1992**, *31*, 1332-1337.

(68) Bevilacqua, J. M.; Zuleta, J. A.; Eisenberg, R. *Inorg. Chem.* **1994**, *33*, 258-266.

(69) Michalec, J. F.; Bejune, S. A.; McMillin, D. R. *Inorg. Chem.* **2000**, *39*, 2708-2709.

(70) Cummings, S. D.; Eisenberg, R. *J. Am. Chem. Soc.* **1996**, *118*, 1949-1960.

(71) Huertas, S.; Hissler, M.; McGarrah, J. E.; Lachicotte, R. J.; Eisenberg, R. *Inorg. Chem.* **2001**, *40*, 1183-1188.

(72) Connick, W. B.; Geiger, D.; Eisenberg, R. *Inorg. Chem.* **1999**, *38*, 3264-3265.

(73) Chan, C.-W.; Cheng, L.-K.; Che, C.-M. *Coord. Chem. Rev.* **1994**, *132*, 87-97.

(74) Chan, S.-C.; Chan, M. C. W.; Wang, Y.; Che, C.-M.; Cheung, K.-K.; Zhu, N. *Chem. Eur. J.* **2001**, *7*, 4180-4190.

(75) Pomestchenko, I. E.; Luman, C. R.; Hissler, M.; Ziessel, R.; Castellano, F. N. *Inorg. Chem.* **2003**, *42*, 1394-1396.

(76) Wrighton, M. S.; Morse, D. L. *J. Am. Chem. Soc.* **1974**, *96*, 998-1003.

(77) Caspar, J. V.; Meyer, T. J. *J. Phys. Chem.* **1983**, *87*, 952-957.

(78) Worl, L. A.; Duesing, R.; Chen, P.; Della Ciana, L.; Meyer, T. J. *J. Chem. Soc. Dalton Trans.* **1991**, 849-858.

(79) Luong, J. C.; Nadjo, L.; Wrighton, M. S. *J. Am. Chem. Soc.* **1978**, *100*, 5790-5795.

(80) Giordano, P. J.; Wrighton, M. S. *J. Am. Chem. Soc.* **1979**, *101*, 2888-2897.

(81) Fredericks, S. M.; Luong, J. C.; Wrighton, M. S. *J. Am. Chem. Soc.* **1979**, *101*, 7415-7417.

(82) Smothers, W. K.; Wrighton, M. S. *J. Am. Chem. Soc.* **1983**, *105*, 1067-1069.

(83) Chen, P.; Westmoreland, T. D.; Danielson, E.; Schanze, K. S.; Anthon, D.; Neveux Jr., P. E.; Meyer, T. J. *Inorg. Chem.* **1987**, *26*, 1116-1126.

(84) Mabrouk, P. A.; Wrighton, M. S. *Inorg. Chem.* **1986**, *25*, 526-531.

(85) Kalyanasundaram, K. *J. Chem. Soc. Faraday Trans. 2* **1986**, 2401-2415.

(86) Juris, A.; Campagna, S.; Bidd, I.; Lehn, J.-M.; Ziessel, R. *Inorg. Chem.* **1988**, *27*, 4007-4011.

(87) Sacksteder, L.; Zipp, A. P.; Brown, E. A.; Streich, J.; Demas, J. N.; DeGraff, B. A. *Inorg. Chem.* **1990**, *29*, 4335-4340.

(88) Perkins, T. A.; Hauser, B. T.; Eyler, J. R.; Schanze, K. S. *J. Phys. Chem.* **1990**, *94*, 8745-8748.

(89) Shaw, J. R.; Schmehl, R. H. *J. Am. Chem. Soc.* **1991**, *113*, 389-394.

(90) Leasure, R. M.; Sacksteder, L.; Nesselrodt, D.; Reitz, G. A.; Demas, J. N.; DeGraff, B. A. *Inorg. Chem.* **1991**, *30*, 3722-3728.

(91) MacQueen, D. B.; Eyler, J. R.; Schanze, K. S. *J. Am. Chem. Soc.* **1992**, *114*, 1897-1898.

(92) Kotch, T. G.; Lees, A. J.; Fuerniss, S. J.; Papathomas, K. I. *Chem. Mater.* **1992**, *4*, 675-683.

(93) Sacksteder, L.; Lee, M.; Demas, J. N.; DeGraff, B. A. *J. Am. Chem. Soc.* **1993**, *115*, 8230-8232.

(94) Wang, Y.; Schanze, K. S. *Inorg. Chem.* **1994**, *33*, 1354-1362.

(95) Striplin, D. R.; Crosby, G. A. *Chem. Phys. Lett.* **1994**, *221*, 426-430.

(96) Paolucci, F.; Marcaccio, M.; Paradisi, C.; Roffia, S.; Bignozzi, C. A.; Amatore, C. *J. Phys. Chem. B* **1998**, *102*, 4759-4769.

(97) Schanze, K. S.; Lucia, L. A.; Cooper, M.; Walters, K. A.; Ji, H.-F.; Sabina, O. *J. Phys. Chem. A* **1998**, *102*, 5577-5584.

(98) Yam, V. W.-W.; Lau, V. C.-Y.; Wu, L.-X. *J. Chem. Soc. Dalton Trans.* **1998**, 1461-1468.

(99) Guo, X.-Q.; Castellano, F. N.; Li, L.; Lakowicz, J. R. *Anal. Chem.* **1998**, *70*, 632-637.

(100) Schmehl, R. H.; Shaw, J. R. *J. Am. Chem. Soc.* **1991**, *113*, 389-394.

(101) Yam, V. W.-W.; Lau, V. C.-Y.; Cheung, K.-K. *Organometallics* **1995**, *14*, 2749-2753.

(102) Yam, V. W.-W.; Lau, V. C.-Y.; Cheung, K.-K. *Organometallics* **1996**, *15*, 1740-1744.

(103) Yam, V. W.-W.; Chong, S. H.-F.; Cheung, K.-K. *Chem. Commun.* **1998**, 2121-2122.

(104) Yam, V. W.-W. *Chem. Commun.* **2001**, 789-796.

(105) Ley, K. D.; Schanze, K. S. *Coord. Chem. Rev.* **1998**, *171*, 287-307.

(106) Ley, K. D.; Li, Y.; Johnson, J. V.; Powell, D. H.; Schanze, K. S. *Chem. Commun.* **1999**, 1749-1750.

(107) Walters, K. A.; Ley, K. D.; Cavalaheiro, C. S. P.; Miller, S. E.; Gosztola, D.; Wasielewski, M. R.; Bussandri, A. P.; van Willigen, H.; Schanze, K. S. *J. Am. Chem. Soc.* **2001**, *123*, 8329-8342.

(108) Walters, K. A.; Dattelbaum, D. M.; Ley, K. D.; Schoonover, J. R.; Meyer, T. J.; Schanze, K. S. *Chem. Commun.* **2001**, 1834-1835.

CHAPTER II. EXPERIMENTAL METHODS

UV-VIS spectra were measured with a Hewlett Packard 8453 diode array spectrophotometer, accurate to ± 2 nm. Steady state photoluminescence spectra were obtained with a single photon counting spectrofluorimeter from Edinburgh Analytical Instruments (FL/FS 900). The excitation was performed with a 450W Xe lamp optically coupled to a monochromator (± 2 nm) and the emission was gathered at 90^0 and passed through a second monochromator (± 2 nm). The luminescence was measured with a Peltier-cooled (-30^0C), R955 red sensitive photomultiplier tube (PMT). Excitation spectra were corrected with a photodiode mounted inside the fluorimeter that continuously measures the Xe lamp output. All photophysical experiments used optically dilute solutions (OD = 0.09 - 0.11) prepared in spectroscopic grade solvents unless otherwise stated. All luminescence samples in 1 cm^2 anaerobic quartz cells (Starna Cells) were deoxygenated with solvent-saturated argon for at least 30 minutes prior to measurement.

Low temperature 77 K frozen glass emission samples were prepared by inserting a 5 mm inner diameter NMR tube containing a 10^{-5} M solution of the appropriate compound into a quartz-tipped finger dewar containing liquid nitrogen. Solvents typically used for the 77 K experiment were butyronitrile, 2-methyltetrahydrofurane, 3-methylpentane or a mixture of ethanol/methanol in a 4 to 1 ratio. In some cases, 10% ethyliodide was added to induce phosphorescence.

Radiative quantum yields (Φ_r) of each metal complex were measured relative to $[Ru(bpy)_3]ClO_4$ (Φ_r = 0.062 in CH_3CN)[1] for the Pt complexes (Chapter III); and relative to $Re(bpy)(CO)_3Cl$ (Φ_r = 0.005 in CH_2Cl_2)[2] for Re(phen-C≡C-H)$(CO)_3$Cl and Re[phen-

C≡C-Au(PPh)$_3$](CO)$_3$Cl (Chapter IV). Radiative quantum yields[3] (Φ_r) were calculated according to the equation:

$$\Phi_x = \Phi_s \left(\frac{I_x}{A_x} \right) \left(\frac{A_s}{I_s} \right) \left(\frac{\eta_x}{\eta_s} \right)^2 \qquad (2.1)$$

where Φ_x is the radiative quantum yield of the sample, Φ_s is the radiative quantum yield of the standard, I_x and I_s are the integrated emission intensities of the sample and standard, respectively, A_x and A_s are the absorbances of the sample and standard, respectively, at the excitation wavelength, and η_x and η_s are the indexes of refraction of solvents used for the sample and standard solutions, respectively.

Emission lifetimes were measured by means of a nitrogen-pumped broadband dye laser (2-3 nm fwhm) from PTI (GL-3300 N_2 laser, GL-301 dye laser). BPBD (360-395 nm), Coumarin 460 (440-480 nm) laser dyes were used to tune the excitation. Pulse energies were typically attenuated to ~50 μJ/pulse, measured with a Molectron Joulemeter (J4-05). The luminescence was collected at 90^0 through a long pass optical filter (>550 nm or >450 nm when necessary), focused through a lens system and passed through a monochromator (± 4 nm). The emission was detected with a Hamamatsu R928 PMT wired for fast response. The PMT signal was terminated through a 50 ohm resistor to a Tektronix TDS 300 digital oscilloscope (400 MHz). The data from the oscilloscope represented an average of 128 laser shots collected at 2-3Hz, was transferred to a computer and processed by Origin 6.1 software.

The nanosecond laser flash photolysis instrumentation included a Q-switched Nd:YAG laser (Surelite I, Continuum) operating at 5 or 10 Hz. Transient absorption spectra and decay kinetics were obtained using the unfocused second or third harmonic

532 or 355 nm, respectively (5-7 ns fwhm). Alternatively, the third harmonic was used to pump an in-house constructed high-pressure Raman shifter filled with H_2 gas (400 psi) and the first Stokes line isolated (λ_{ex} = 416 nm, 3 mJ/pulse). The kinetic spectrophotometer is described elsewhere[4,5] and a brief description with recent modifications are as follows. The transient absorption was monitored at a right angle using white light (probe) from a 150 W xenon CW arc lamp (Oriel Corporation). The probe beam was focused through the sample and re-imaged on the entrance slit of a Spex 1681 (0.22 m) monochromator. The monochromatic light was detected with Hamamatsu R928 PMT using 5 instead of the typical 9 stage dynode amplifier negatively biased with a Keithley 247 high voltage supply. The resulting signal was routed through a DC-coupled back-off circuit that stored and displayed digital readouts for I_o. A fast shutter (Uniblitz VMM-D1) was used to minimize the exposure of the sample to probe light. The real time signal from the PMT was then sent to the oscilloscope which averaged the signal over a pre-determined number of shots (typically 16-32). The counter/timer board (National Instruments NI-TIO) synchronized the Nd:YAG laser, fast shutter driver and oscilloscope. The data were collected using an in-house software routine written in LabVIEW (National Instruments), which generated the absorption difference spectra. The kinetic profiles were collected in the same manner, at one particular wavelength and averaging over 32 shots. Appropriate filters were used to suppress the scattered light from laser beam. All samples were thoroughly degassed prior to measurements with high purity argon and kept under an argon atmosphere throughout the experiment. Typical excitation energies were maintained at 2-5 mJ/pulse. All flash photolysis measurements

were conducted at the ambient temperature 22 ± 2 ^{0}C. The data analyses were performed in Origin 6.1.

Cyclic voltammetry was performed in a one-compartment cell using a three-electrode arrangement including a Pt disk working electrode, a Pt wire auxiliary electrode, and Ag/AgCl (3M KCl) reference electrode. All electrochemistry was performed on a BAS Epsilon system. A scan rate of 200 mV/s was typically used.

References

(1) Caspar, J. V.; Meyer, T. J. *J. Am. Chem. Soc.* **1983**, *105*, 5583-5590.

(2) Caspar, J. V.; Meyer, T. J. *J. Phys. Chem.* **1983**, *87*, 952-957.

(3) Demas, J. N.; Crosby, G. A. *J. Phys. Chem.* **1971**, *75*, 991-1024.

(4) Tyson, D. S.; Castellano, F. N. *J. Phys. Chem. A* **1999**, *103*, 10955-10960.

(5) Tyson, D. S.; Henbest, K. B.; Bialecki, J.; Castellano, F. N. *J. Phys. Chem. A* **2001**, *105*, 8154-8161.

CHAPTER III. PHOTOPHYSICAL PROCESSES IN Pt(II) DIIMINE BIS(ARYLACETYLIDE) COMPLEXES

Introduction

The coupling of transition metals or transition metal complexes with selected organic chromophores has generated new molecules and materials that exhibit a wide range of fundamentally interesting and potentially useful excited state properties.[1-22] A significant amount of experimental work in this area has largely focused on d^6 metal polypyridine complexes of Ru(II), Os(II), and Re(I) which display metal-to-ligand charge transfer (MLCT) excited states. The general motivation for using these molecules as the "metal-containing" fragment in more complex systems lies in the widespread experience and knowledge gained in the field over the past 45 years.[23-42] In more recent history, MLCT chromophores have become appealing for a variety of technologies, including photovoltaics,[43] optical data storage,[5,7] luminescence sensors,[44,45] and electroluminescence displays.[46-49]

Over the past 15 years there has been increasing interest in the properties of d^8 Pt(II) complexes of the general formulation Pt(diimine)L_2, where L is a monodentate ligand such as halide, nitrile, thiolate, or acetylide.[50-64] Several recent papers have appeared describing structure-photophysical property relationships in systems containing a diimine ligand such as 2,2'-bipyridine or 1,10-phenanthroline (and structurally related derivatives), where L is typically a substituted phenylacetylide.[54,57,58,63,64] In most cases, these molecules possess long-lived excited states with photophysical properties consistent with a $d\pi$ Pt $\rightarrow \pi^*$ diimine MLCT assignment. However, there are numerous examples

within the work from several laboratories where the photophysical behavior of certain Pt(diimine)($C\equiv CR)_2$ molecules is inconsistent with the MLCT assignment, which has indeed been recognized in several instances.[54,58] In those cases, it is believed that a low lying intraligand $^3\pi$-π^* (^{3}IL) excited state based within the diimine or acetylide ligand(s) contributes to the excited state decay. Our group has recently recognized that the ^{3}MLCT excited state can be used to internally sensitize the formation of a low-lying ^{3}IL excited state on an appended pyrenylacetylide ligand, leading to the observation of extremely long-lived room temperature phosphorescence in the red.[17] This work will be described in chapter 3.4. Clearly, the photophysical processes available in Pt(diimine)($C\equiv CR)_2$ complexes warrant their further investigation. We postulate that proper selection of ligands and/or solvent medium in Pt(diimine)($C\equiv CR)_2$ complexes may be able to produce either "pure" ^{3}MLCT or $^3\pi$-π^* excited states in addition to equilibrated or configuration mixed excited states composed of varying degrees of ^{3}MLCT and $^3\pi$-π^* character. This suite of accessible photophysical behavior can be expected to yield a wide range of excited state absorptions, emissions, and associated dynamics. In related work it has been shown that energy flow in $[Ru(Pyr_nbpy)(CN)_4]^{2-}$ (n = 1,2, Pyr = pyrene) is readily modulated with solvent, yielding a variety of excited state decay behavior.[19]

CHAPTER III.I. SYNTHESIS OF Pt(II) DIIMINE BIS(ARYLACETYLIDE) COMPLEXES

Materials and Methods

All reagents not specifically listed below were obtained from commercial sources and used as received. Anhydrous dichloromethane was purchased from Aldrich and used as received or distilled over CaH_2. Various amines (different suppliers) were dried and distilled according to standard procedures prior to use.[65] Potassium carbonate (Aldrich) was dried in an oven (140 ^{0}C) at least 12 h before use. Water was deionized by means of Barnstead E-Pure system. All synthetic manipulations were performed under an inert and dry argon atmosphere using standard Schlenk techniques. ^{1}H NMR spectra were recorded on Varian Gemini 200 (200 MHz) or Varian Unity + (400 MHz) spectrometer. ^{31}P $\{^1$H$\}$ NMR spectra were recorded Varian Unity + (162 MHz) spectrometer. All chemical shifts are referenced to residual solvent signals previously referenced to TMS and splitting patterns are designated as s (singlet), d (doublet), t (triplet), q (quartet), m (multiplet), and br (broad). Electrospray ionization (ESI) and atmospheric pressure chemical ionization (APCI) mass spectra were measured at the University of Toledo using an Esquire-LC spectrometer. Fast atom bombardment (FAB) mass spectra were measured at the School of Chemical Sciences, University of Illinois, Urbana, IL. Elemental analyses were obtained at Atlantic Microlab, Inc. GC and DIP mass spectra were measured in-house using a Shimadzu QP5050A spectrometer. MALDI mass spectra were measured in-house using a Bruker-Daltonics Omniflex spectrometer.

Reaction Schemes.

The synthetic procedures used in the work are summarized in Schemes 3.1.1 – 3.1.7. Details on the syntheses of each Pt(II) complex are located in the synthesis section of this chapter.

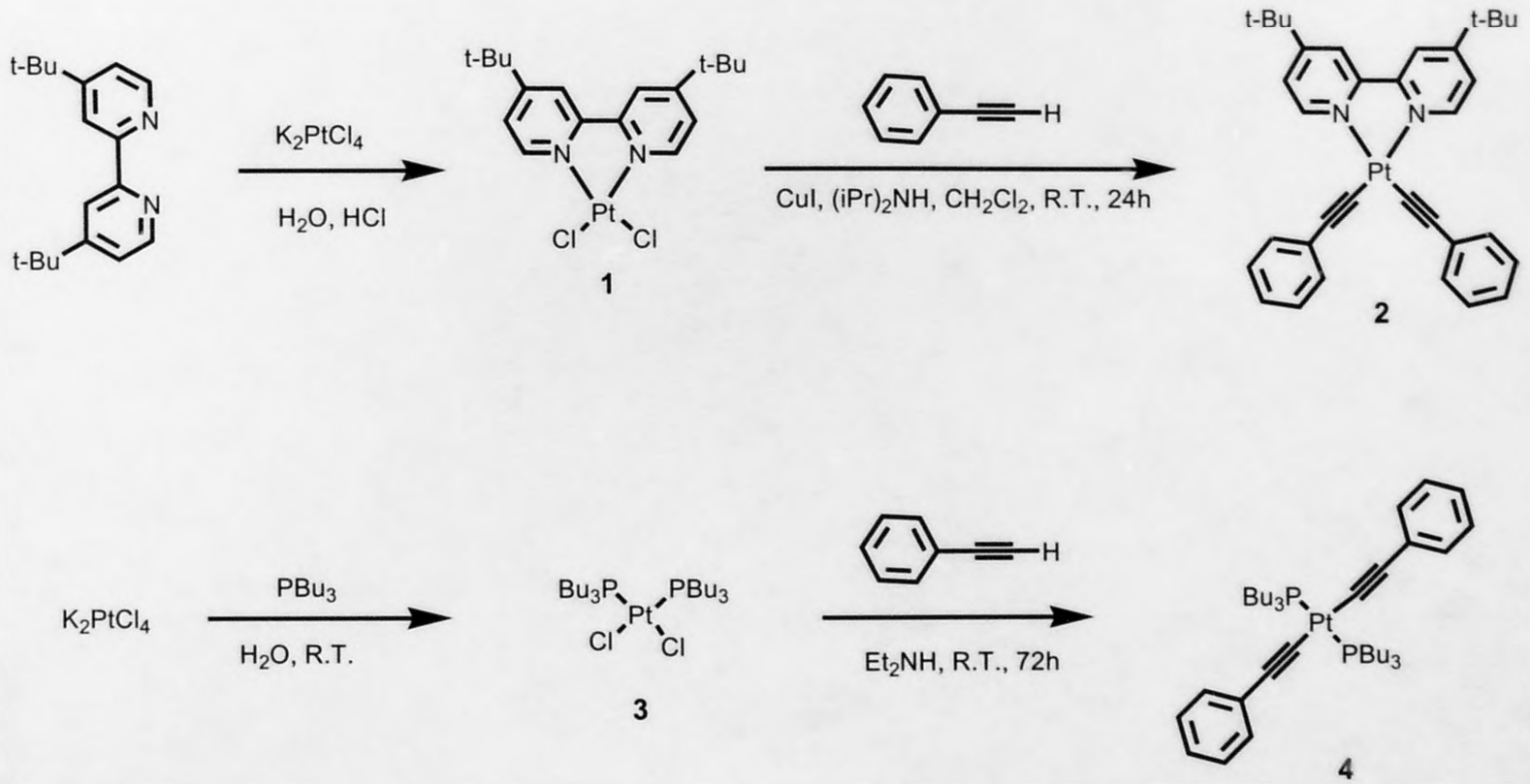

Scheme 3.1.1. Synthesis of $Pt(dbbpy)Cl_2$ (**1**), $Pt(dbbpy)(C{\equiv}C\text{-}C_6H_5)_2$ (**2**), *cis*-$Pt(PBu_3)_2Cl_2$ (**3**) and *trans*-$Pt(PBu_3)_2(C{\equiv}C\text{-}C_6H_5)_2$ (**4**).

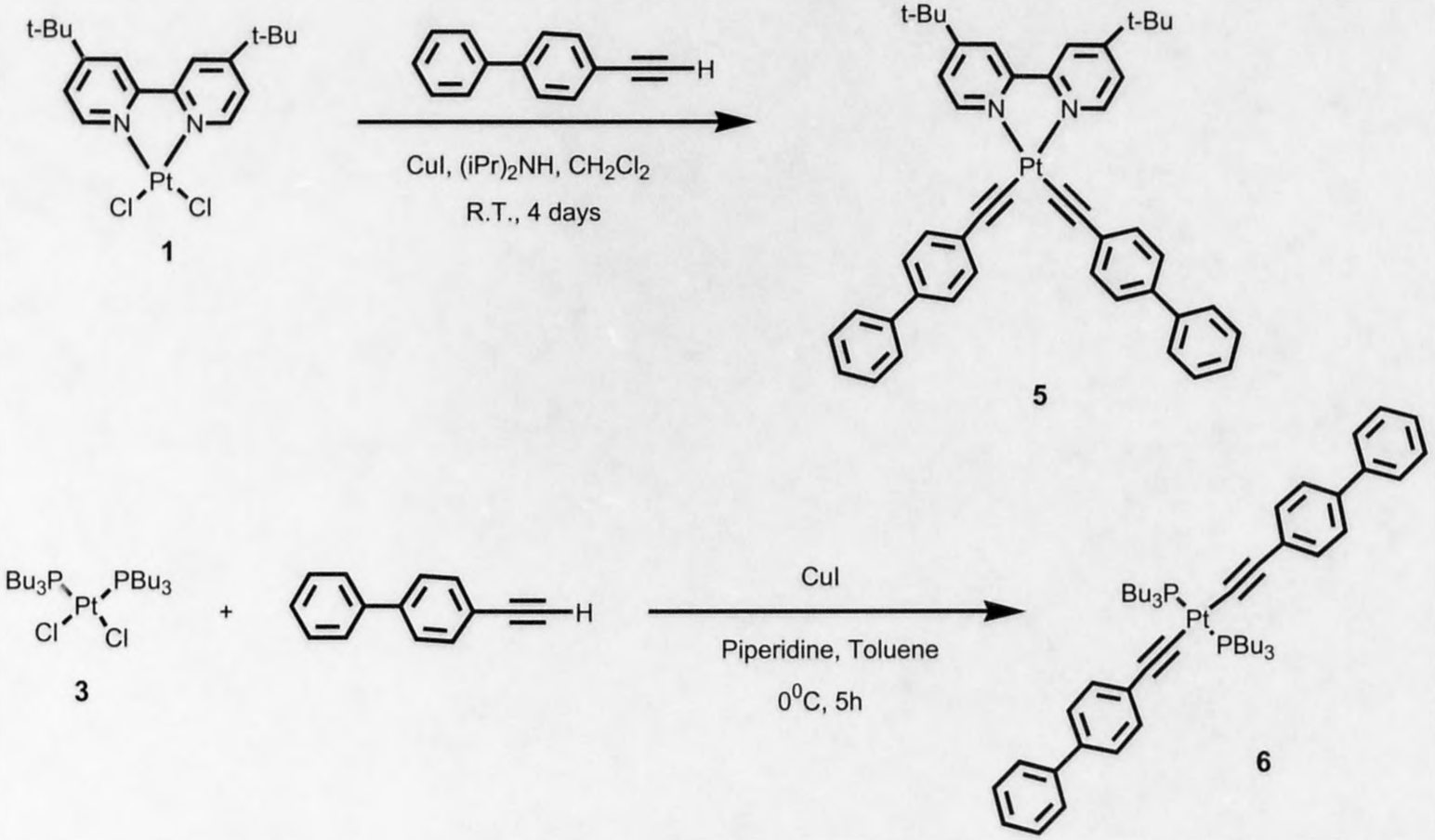

Scheme 3.1.2. Syntheses of Pt(dbbpy)(C≡C-Biphenyl)$_2$ (**5**) and *trans*-Pt(PBu$_3$)$_2$(C≡C-Biphenyl)$_2$ (**6**).

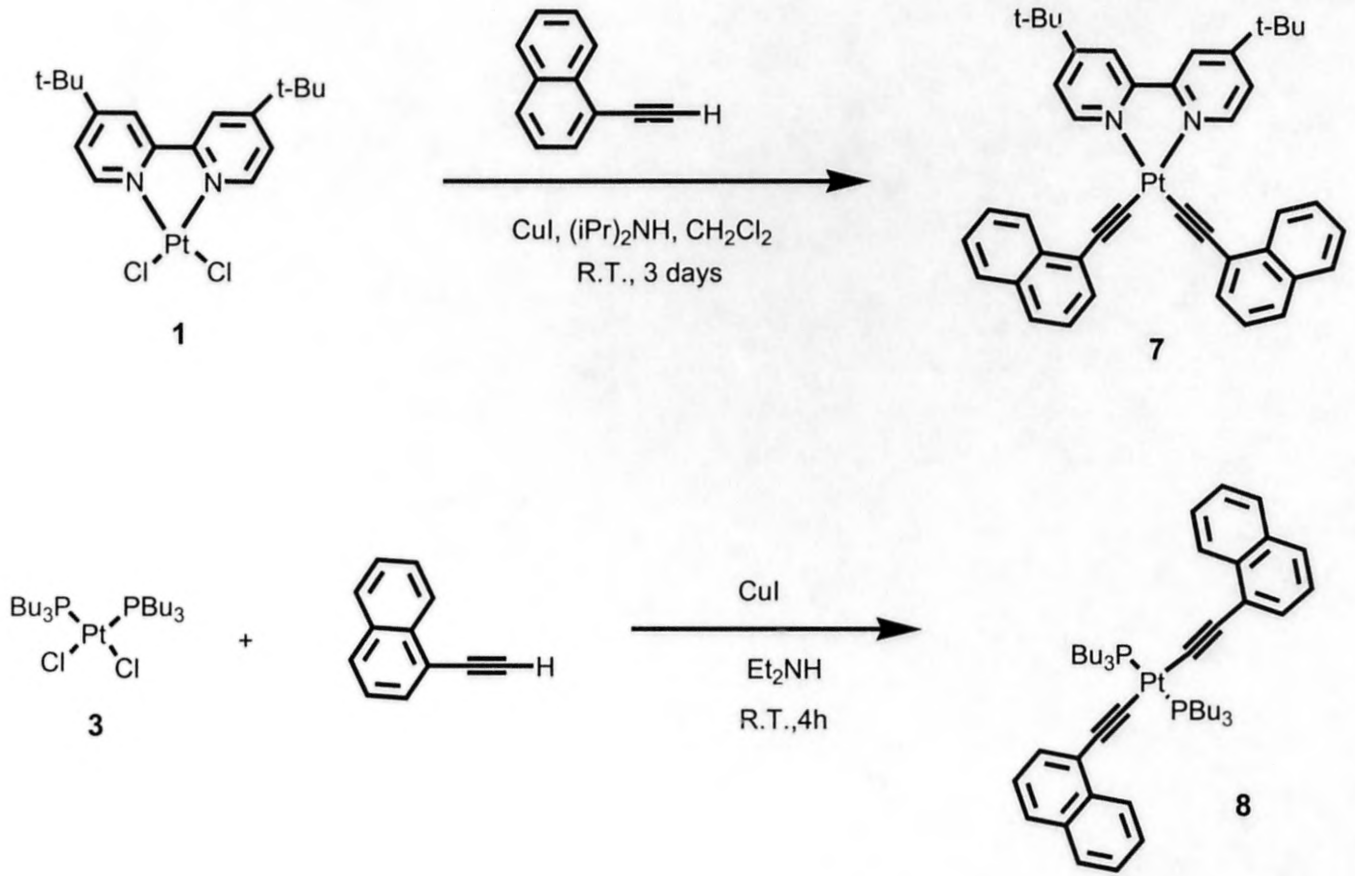

Scheme 3.1.3. Syntheses of Pt(dbbpy)(C≡C-Naphthalene)$_2$ (**7**) and *trans*-Pt(PBu$_3$)$_2$(C≡C-Naphthalene)$_2$ (**8**).

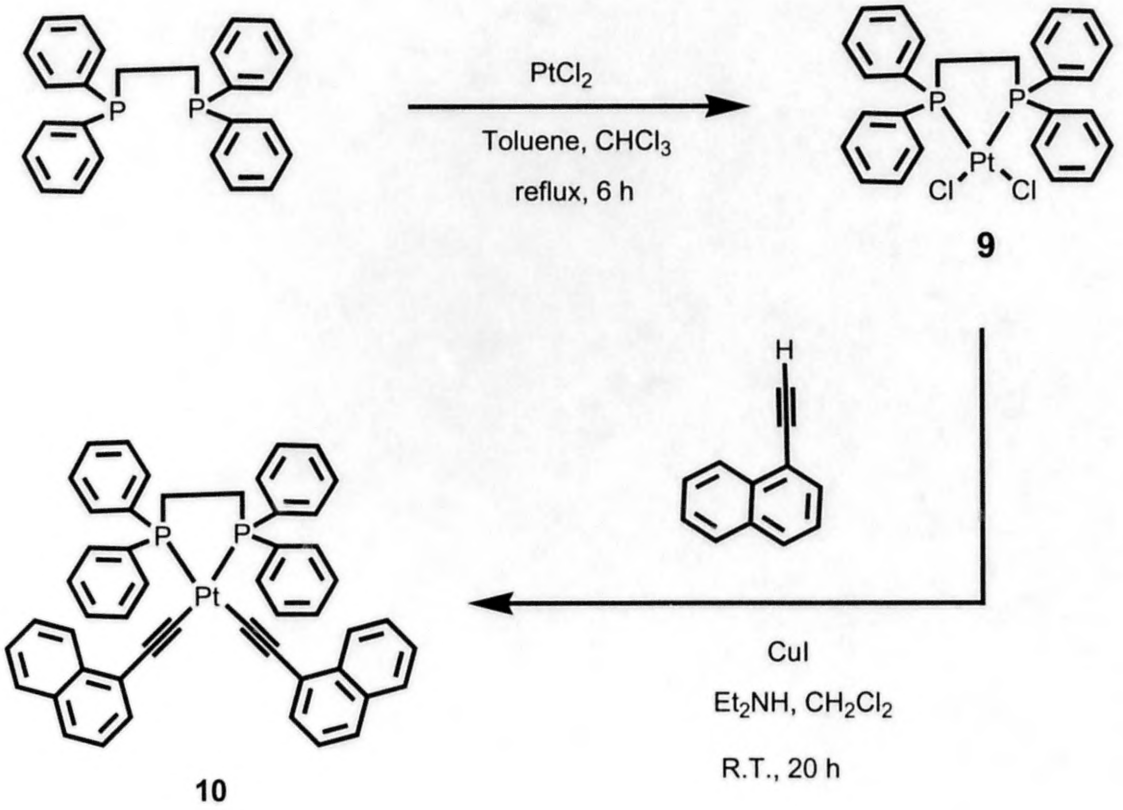

Scheme 3.1.4. Syntheses of Pt(dppe)Cl_2 (**9**) and Pt(dppe)(C≡C-Naphthalene)$_2$ (**10**)

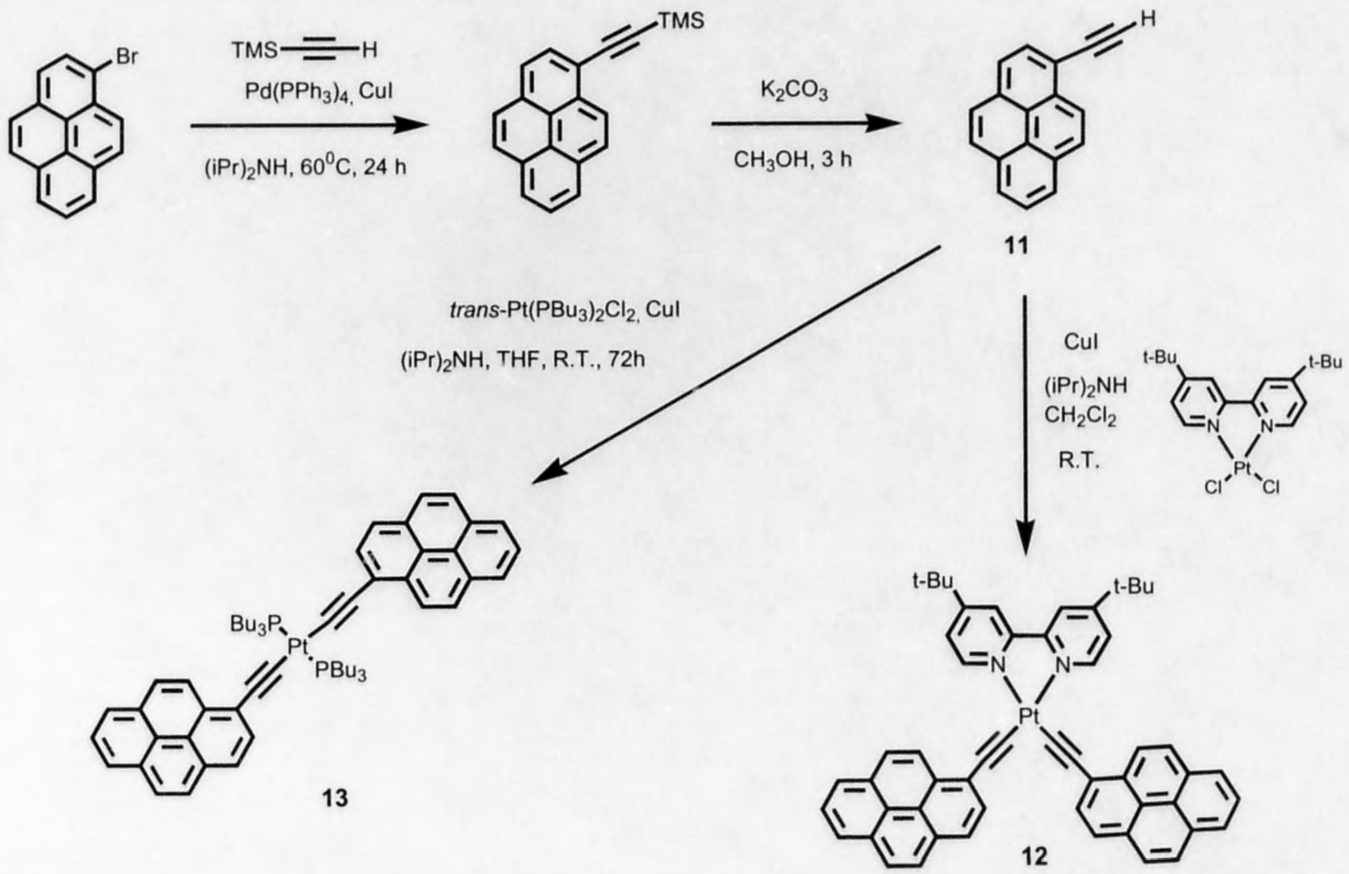

Scheme 3.1.5. Syntheses of Pt(dbbpy)(C≡C-Pyrene)$_2$ (**12**) and *trans*-Pt(PBu$_3$)$_2$(C≡C-Pyrene)$_2$ (**13**).

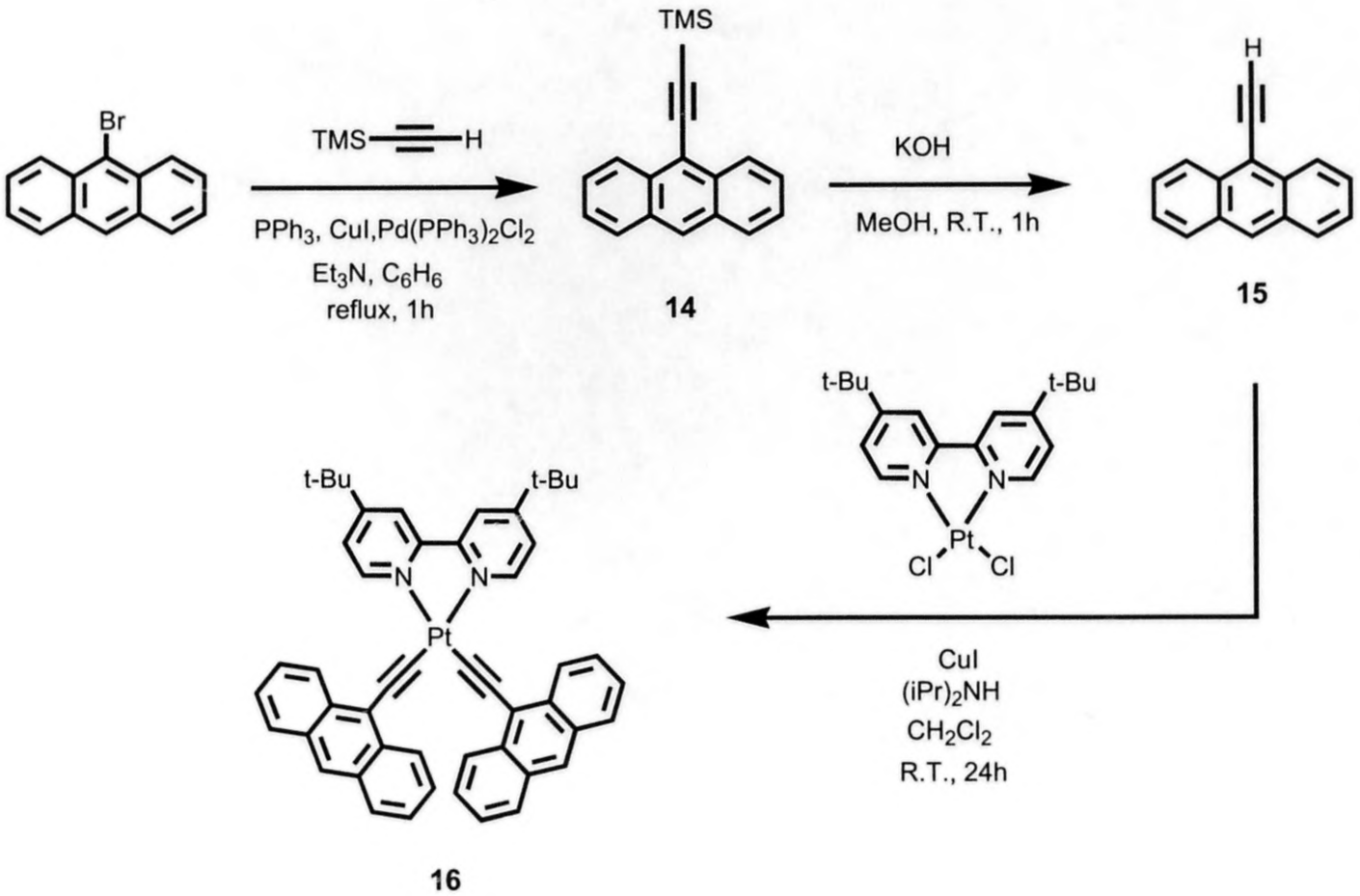

Scheme 3.1.6. Syntheses of 9-Anthracenyl-trimethylsilylacetylene (**14**), 9-Ethynylanthracene (**15**) and Pt(dbbpy)(C≡C-Anthracene)$_2$ (**16**).

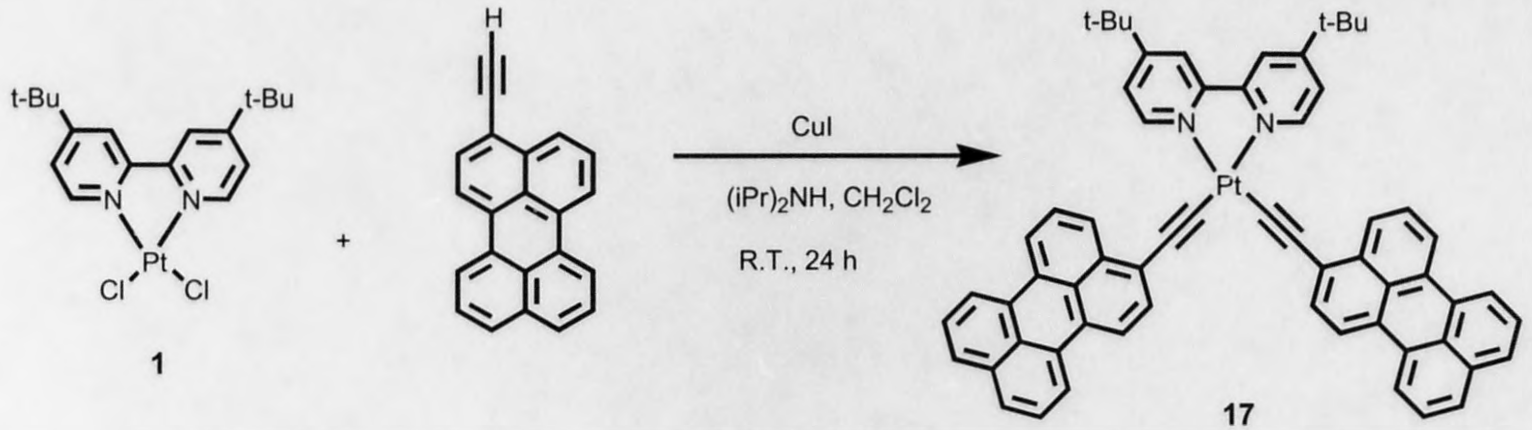

Scheme 3.1.7. Synthesis of Pt(dbbpy)(C≡C-Perylene)$_2$ (**17**).

Synthesis

The synthesis and analysis of each compound presented in this thesis are described below. Previously published procedures have been referenced where appropriate and all compounds (unless specifically noted) were satisfactory characterized by a combination of proton and phosphorous nuclear magnetic resonance spectrometry (^{1}H and ^{31}P NMR), elemental analysis (El. Anal.), and mass spectrometry.

$Pt(dbbpy)Cl_2$ (**1**),[66] $Pt(dbbpy)(C{\equiv}C\text{-}C_6H_5)_2$ (**2**),[57,59] *trans*-$Pt(PBu_3)_2(C{\equiv}C\text{-}C_6H_5)_2$ (**4**),[21] *trans*-$Pt(PBu_3)_2(C{\equiv}C\text{-}Biphenyl)_2$ (**6**),[67] $Pt(dppe)Cl_2$ (**9**),[68] 9-anthracenyl-trimethylsilylacetylene (**14**),[69] 9-ethynylanthracene (**15**),[69] were prepared according to literature procedures and yielded satisfactory mass and ^{1}H NMR spectra. The syntheses of some compounds depicted above are included for completeness. I would like to thank Dr. Radek Pohl for synthesis of 1-ethynylpyrene (**11**),[13] Sölen Kinayyigit for synthesis of *cis*-$Pt(PBu_3)_2Cl_2$ (**3**),[70] Prof. Jeffrey Moore (UIUC) for providing 3-ethynylperylene, and the group of Dr. Raymond Ziessel (ULP, Strasburg, FR) for the synthesis of the *trans*-$Pt(PBu_3)_2(C{\equiv}C\text{-}Pyrene)_2$ (**13**)[13] model compound.

Bis(diphenylphosphino)ethane (dppe), ethynylnaphthalene, phenylacetylene, copper (I) iodide, 4-ethynylbiphenyl and 4,4'-di-*tert*-butyl-2,2'-dipyridyl (dbbpy) were purchased from Aldrich and used as received. Potassium tetrachloroplatinate (K_2PtCl_4) was purchased from Alfa Aesar and used as received.

2) $Pt(dbbpy)(C{\equiv}C\text{-}C_6H_5)_2$

Compound **2** was synthesized according a modified literature procedure.[57,59] A 724 mg (1.35 mmol) sample of $Pt(dbbpy)Cl_2$ was placed in a sealable reaction vessel. A

mixture of 70 ml of CH_2Cl_2 and 33 ml $(iPr)_2NH$ was degassed in a separate flask for 15 min and transferred into reaction vessel via canula under Ar. A solution of ethynylbenzene (1.38 g, 13.5 mmol) in 30 ml of CH_2Cl_2 was degassed separately and transferred to the reaction vessel. CuI (25.7 mg, 0.135 mmol) was added and the reaction vessel was sealed under Ar with a Teflon screw-cap fitted with an o-ring, and stirred at room temperature for 24 hrs. The solvent was removed under vacuum and the residue was chromatographed on silica gel using 100% dichloromethane as eluent. Evaporation of the solvent yielded **2** as a bright yellow solid. $R_f = 0.33$ (100% dichloromethane, silica gel). DIP-MS m/z 665. ^1H NMR ($CDCl_3$): δ 9.74 (d, 2H); 7.94 (d, 2H); 7.52-7.58 (m, 6H); 7.21-7.26 (t, 4H); 7.12 (t, 2H); 1.44 (s, 18 H).

4) ***trans*-$Pt(PBu_3)_2(C{\equiv}C\text{-}C_6H_5)_2$**

Compound **4** was synthesized according to a literature procedure.[21] *cis*-Dichlorobis(tri-n-butylphosphine)platinum(II) (180 mg, 0.268 mmol) was dissolved in freshly distilled diethylamine (30 ml). Phenylacetylene (0.11 g, 1.08 mmol) was added and solution was degassed for 15 min. Then copper iodide (6 mg, 0.031 mmol) was added to the reaction mixture. The solution was stirred for 3 h at room temperature. The solvent was removed under reduced pressure and the residue was redissolved in a small amount of dichloromethane. The solution was added dropwise into hexane. The precipitate solid was filtered off as a side product. The filtrate was collected and the solvents were removed under reduced pressure. The remaining solid was purified by column chromatography (silica gel) using 10 vol% acetone in hexane as eluent. The product **4** was obtained in 68% yield (146 mg) as a white crystalline solid. $R_f = 0.39$ (10

vol% acetone in hexane). DIP-MS m/z 802. ^{1}H NMR ($CDCl_3$): δ 0.93 (t, 18H, J = 7.2 Hz), 1.43 (m, 12H, J = 7.2 Hz), 1.53 (m, 12H), 2.01 (m, 12H), 7.09 (t, 2H, J = 7.6 Hz), 7.18 (t, 4H, J = 7.6 Hz), 7.4 (d, 4H, J = 8.4 Hz).

5) Pt(dbbpy)(C≡C-Biphenyl)$_2$

Pt(dbbpy)Cl_2 (0.25 g, 0.46 mmol) and CuI (8.8 mg, 0.046 mmol) were placed in a sealable reaction vessel. A solution of dichloromethane and diisopropylamine (3:1) (150 ml) was degassed for 15 min and added to the flask. 4-Ethynylbiphenyl (0.249 g, 1.4 mmol) was added to the reaction mixture, the reaction vessel was sealed under Ar with a Teflon screw-cap fitted with an o-ring, and stirred at room temperature for 4 days. The solvent was removed under vacuum and the residue was chromatographed on silica gel using dichloromethane as eluent. Evaporation of the solvent yielded **5** as a bright yellow solid (0.183g, 48%). R_f = 0.56 (dichloromethane, silica gel). DIP-MS: m/z 817. APCI-MS ($CHCl_3$/MeOH): m/z 817. ^{1}H NMR ($CDCl_3$): δ 9.77 (d, 2H), 7.96 (d, 2H), 7.61 (m, 10H), 7.51 (d, 4H), 7.42 (t, 4H), 7.31 (d, 2H), 1.45 (s, 18H).

6) *trans*-Pt(PBu_3)$_2$(C≡C-Biphenyl)$_2$

Compound **6** was synthesized according to a literature procedure.[67] *cis*-Dichlorobis(tri-n-butylphosphine) platinum(II) (200 mg, 0.298 mmol) and 4-ethynylbiphenyl (0.282 g, 1.588 mmol) were dissolved in mixture of piperidine and toluene (1 : 3, 12 ml) at 0^{0}C under Ar. Then copper iodide (10 mg) was added to the reaction mixture. The solution was stirred for 5 h at 0^{0}C. The volatiles were then removed under reduced pressure. The residue was redissolved in hexane and filtered which

removed the dimer (C_6H_5-C_6H_4-C≡C-C_6H_4-C_6H_5). The filtrate was concentrated under reduced pressure and ran through the short frit packed with neutral alumina using hexane as eluent. The second yellow-colored fraction was collected. Evaporation of the solvent yielded **6** as yellow oil which spontaneously crystallized upon cooling. R_f = 0.30 (10 vol% acetone in hexane). DIP-MS m/z 954. ^{1}H NMR ($CDCl_3$): δ 0.94 (t, 18H), 1.44 (m, 12H), 1.56 (m, 12H), 2.05 (m, 12H), 7.26-7.49(br m, 16H), 7.58 (d, 4H).

7) Pt(dbbpy)(C≡C-Naphthalene)$_2$

Pt(dbbpy)Cl_2 (0.25 g, 0.46 mmol) and CuI (8.8 mg, 0.046 mmol) were placed in a sealable reaction vessel. A solution of dichloromethane and diisopropylamine (3:1) (200 ml) was degassed for 15 min and added to the flask. 1-Ethynynaphthalene (0.213 g, 1.39 mmol) was dissolved in a small volume of dichloromethane (10 ml), degassed for 15 min and then added to the reaction mixture. The reaction vessel was sealed under Ar with a Teflon screw-cap fitted with an o-ring, and stirred at room temperature for 3 days. The solvent was removed under vacuum and the residue was chromatographed on silica gel using dichloromethane as eluent. Evaporation of the solvent yielded **7** as an orange solid (0.194 g, 54 %). R_f = 0.52 (dichloromethane, silica gel). DIP-MS: m/z 766. APCI-MS ($CHCl_3$/MeOH): m/z 766. ^{1}H NMR ($CDCl_3$): δ 9.86 (d, 2H), 8.92 (d, 2H), 7.98 (d, 2H), 7.73-7.80 (m, 4H), 7.66 (d, 2H), 7.59 (m, 2H), 7.34-7.44 (br m, 6H), 1.46 (s, 18H).

8) *trans*-Pt(PBu$_3$)$_2$(C≡C-Naphtnalene)$_2$

cis-Dichlorobis(tri-n-butylphosphine)platinum(II) (200 mg, 0.298 mmol) was dissolved in freshly distilled diethylamine (40 ml). Ethynylnaphthalene (0.181 g, 1.192

mmol) was added and solution was degassed for 15 min. Then copper iodide (6.7 mg, 0.035 mmol) was added to the reaction mixture. The solution was stirred for 4 h at room temperature. The reaction mixture was filtered. The filtrate was collected and solvent was removed under reduced pressure. The residue was redissolved in a small amount of dichloromethane. The solution was added dropwise in hexane. The formed solid was filtered off as a side product. The filtrate was collected and solvents were removed under reduced pressure. The remaining material was purified by column chromatography (silica gel) using 10 vol% acetone in hexane as eluent. The desired product **8** was obtained in 53% yield (142 mg) as a white solid. R_f = 0.32 (10 vol% acetone in hexane). DIP-MS m/z 902. ^{1}H NMR ($CDCl_3$): δ 0.94 (t, 18H, J = 7.2 Hz), 1.45 (m, 12H, J = 7.2 Hz), 1.58 (m, 12H), 2.5 (m, 12H), 7.12 (m, 2H), 7.32 (m, 4H), 7.6 (m, 4H), 7.7 (d, 2H, J = 7.6 Hz), 8.8 (d, 2H, J = 8.4 Hz).

10) Pt(dppe)(C≡C-Naphthalene)$_2$

Pt(dppe)Cl_2 (**9**) (1 g, 1.505 mmol) was placed in a sealable reaction vessel. A solution of freshly distilled diethylamine (300 ml) and dichloromethane (250 ml) was degassed for 15 min and added to the flask. 1-Ethynylnaphthalene (0.473 g, 3.311 mmol) was dissolved in diethylamine (10 ml) in a separate flask, degassed and then transferred to the reaction vessel. Copper iodide (15 mg, 0.150 mmol) was added and the reaction vessel was sealed under Ar with a Teflon screw-cap fitted with an o-ring, and stirred at room temperature for 20 hrs. The reaction mixture was filtered to remove undissolved *cis*-dichlorobis(tri-n-butylphosphine)platinum(II) and solvents were removed under reduced pressure. Crude product was purified by column chromatography (silica gel)

using 25 vol% hexane in dichloromethane as eluent. Evaporation of the solvents yielded **10** as yellow crystalline solid (0.153 g, 11%). R_f = 0.65 (25 vol% hexane in dichloromethane). MALDI-MS: Calculated for $C_{50}H_{38}P_2Pt$ 895.96; found 896.60. $^{31}P\{^1H\}$ NMR (162 MHz, $CDCl_3$, ppm): δ 41.826 (J = 2286.5 Hz). ^1H NMR ($CDCl_3$): δ 2.46 (m, 4H), 7.09 (m, 2H), 7.30 (m, 4H), 7.35-7.48 (br m, 14H), 7.57 (d, 2H), 7.69 (d, 2H), 7.98-8.07 (br m, 8H), 8.31 (d, 2H).

12) Pt(dbbpy)(C≡C-Pyrene)$_2$

$Pt(dbbpy)Cl_2$ (34.4 mg, 0.073 mmol) and CuI (1.39 mg, 0.0073 mmol) were placed in a sealable reaction vessel. A solution of dichloromethane and diisopropylamine (3:1) (40 ml) was degassed for 15 min and added to the flask. 1-Ethynylpyrene (50 mg, 0.22 mmol) was added to the reaction mixture, the reaction vessel was sealed under Ar with a Teflon screw-cap fitted with an o-ring, and stirred at room temperature for 24 hrs. The solvent was removed under vacuum and the residue was chromatographed on silica gel using hexane / dichloromethane (1:3) as eluent. Evaporation of the solvent yielded **12** as a bright orange solid (31 mg, 45%). R_f = 0.54 (25 vol % hexane in dichloromethane, silica gel). ^1H NMR ($CDCl_3$): δ 9.98 (d, 2H, J = 5.56 Hz), 9.21 (d, 2H, J = 9.6 Hz), 8.30 (d, 2H, J = 7.2 Hz), 8.1–7.9 (br m, 16H), 7.65 (d, 2H, J = 6Hz), 1.48 (s, 18H). ESI-MS ($CHCl_3$/ MeOH): m/z 936 $[M+Na]^+$. APCI-MS ($CHCl_3$/MeOH): m/z 915. Anal. Calcd. for $C_{54}H_{42}N_2Pt \cdot 0.5CH_2Cl_2$: C, 68.63; N, 2.91; H, 4.50. Found: C, 68.73; N, 3.01; H, 4.55. The CH_2Cl_2 used in the elemental analysis fit was observed by NMR.

14) 9-Anthracenyltrimethylsilylacetylene

Compound **14** was synthesized according to a modified literature procedure.[69] A solution of 9-bromoanthracene (6.75 g, 26.25 mmol), triphenylphosphine (0.69 g, 2.63 mmol), copper iodide (0.25 g, 1.31 mmol) and bis(triphenylphosphine)palladium dichloride (0.37 g, 0.53 mmol) was degassed in for 15 min in a 1:1 mixture of triethylamine / benzene (175 ml) and trimethylsilylacetylene (5.57 ml, 39.37 mmol) was added. The solution was heated at reflux for 1h. The cooled solution was diluted with ethyl ether (100 ml) and filtered. The filtrate was washed with H_2O and dried over Na_2SO_4 and filtered. Solvents were removed under reduced pressure to yield the crude product as an orange-red oil. After refrigerating some side products crystallized out as a fluffy white solid. The mixture was diluted with some hexane and this solid was removed by filtration. The filtrate was concentrated down and chromatographed (SiO_2) using hexane as an eluent. The product was eluted as second band with a characteristic orange color and blue luminescence. After evaporation of the solvent and cooling **14** spontaneously crystallized as dark red crystals (3.75g, 52%). R_f = 0.28 (hexane / silica gel). GC-MS (hexane): m/z 274. ^1H NMR ($CDCl_3$): δ 8.59 (d, 2H, J = 8.4 Hz), 8.41(s, 1H), 7.99 (d, 2H, J = 8.4 Hz), 7.6 (t, 2H, 8.8 Hz), 7.51 (t, 2H, J = 8.8 Hz), 0.46 (s, 9H).

15) 9-Ethynylanthracene

Compound **15** was synthesized according to a modified literature procedure.[69] 9-anthracenyl-trimethylsilylacetylene (**14**) (1g, 3.6 mmol) was dissolved in methanol (100 ml) and 3.5M KOH (aq.) (2 ml, 7.2 mmol) was added and stirred for 1h. The conversion was followed by GC-MS. The reaction was quenched with water (150 ml) and the

product was extracted with diethyl ether. The combined organic layers were washed with water, dried over Na_2SO_4 and filtered. Evaporation of the solvent yielded **15** as a red solid (700 mg, 96%). R_f = 0.28 (hexane, silica gel). GC-MS (ethyl ether): m/z 202, single pick. The procedures described above for compounds **14** and **15** represent a drastic modification of the published synthesis.[69] Attempts precisely to follow the published procedure resulted in very low yield of 9-ethynylanthracene.

16) Pt(dbbpy)(C≡C-Anthracene)$_2$

Pt(dbbpy)Cl_2 (3.02 g, 0.56 mmol) and CuI (10.7 mg, 0.056 mmol) were placed in a sealable reaction vessel. A solution of dichloromethane (162 ml) and diisopropylamine (70 ml) was degassed for 15 min and added to the flask. 9-Ethynylanthracene (0.404 g, 1.99 mmol) was dissolved in dichloromethane (70 ml) in a separate flask, degassed for 15 min and added to the reaction mixture. The reaction vessel was sealed under Ar with a Teflon screw-cap fitted with an o-ring, and stirred at room temperature for 24 hrs. The solvent was removed under vacuum. The product was purified by three subsequent columns; two on silica gel using hexane / dichloromethane (1:3) and one using hexane / chloroform (1:9) as eluents under low light conditions. Evaporation of the solvent yielded **16** as a dark red solid. R_f = 0.53 (25 vol % hexane in dichloromethane, silica gel). It was not possible to obtain good ^{1}H NMR spectra of the product due to rapid decomposition of the sample in the presence of light and oxygen, but satisfactory mass spectra were obtained which clearly shows Pt(dbbpy)(C≡C-Anthracene)$_2$ present in the analyzed sample. ESI-MS ($CHCl_3$/ MeOH): m/z 866. FAB$^+$ m/z 866 $[M+H]^+$.

17) Pt(dbbpy)(C≡C-Perylene)$_2$

Pt(dbbpy)Cl_2 (32 mg, 0.060 mmol) and CuI (1.1 mg, 0.0060 mmol) were placed in a sealable reaction vessel. A solution of dichloromethane and diisopropylamine (3:1) (80 ml) was degassed for 15 min and added to the flask. 1-ethynylperylene (50 mg, 0.18 mmol) was added to the reaction mixture, the reaction vessel was sealed under Ar with a Teflon screw-cap fitted with an o-ring, and stirred at room temperature for 24 hrs. The solvent was removed under vacuum. Product was separated by two subsequent columns; first – a flash column on silica gel using dichloromethane as eluent, second - conventional chromatography with 25 vol% hexane in dichloromethane as eluent on silica gel. Evaporation of the solvent yielded **17** as a dark red solid (31 mg, 45%). R_f = 0.29 (25 vol % hexane in dichloromethane, silica gel). FAB^+ m/z 1015 $[M+H]^+$. ^1H NMR ($CDCl_3$): δ 9.85 (d, 2H); 8.82 (d, 2H); 8.11-8.21 (m, 10H); 8.0 (d, 2H); 7.76 (d, 2H); 7.60-7.68 (m, 8H); 7.35-7.50 (m, 6H); 1.48 (s, 18H).

CHAPTER III.II. COMPLEXES WITH MLCT-BASED EMISSION

Structures

Complexes **2**, **5** and **6** have been synthesized according to standard procedures (Chapter III.I), purified by column chromatography and structurally characterized. The photophysical properties of **2** have been extensively investigated in the literature.[57,59] Therefore, **2** is a good model system for the photophysical studies in this chapter of the thesis. Based upon the structural design, the C≡C-R based (R = C_6H_5, biphenyl) ^{3}IL states of **2** and **5** are located significantly higher in energy than the corresponding ^{3}MLCT state, therefore the photophysical properties of **2** and **5** are expected be governed solely by Pt $d\pi \rightarrow \pi^*$ (dbbpy) MLCT excited states. Compound **6** served as a model for compound **5**, since it doesn't possess any low energy MLCT excited states but contains the Pt(II) center in order to impart the internal heavy atom effect. It is well established that photophysical properties of **2** are attributed to MLCT parentage,[57,59] therefore it will be used in the present study as a model representing $d\pi$ Pt $\rightarrow \pi^*$ (dbbpy) MLCT excited state.

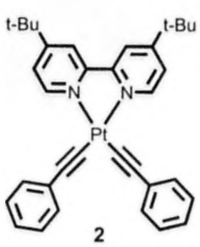

2

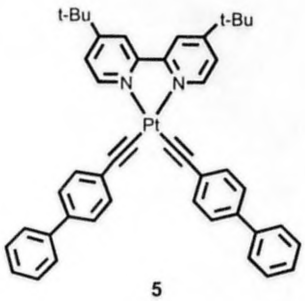

5

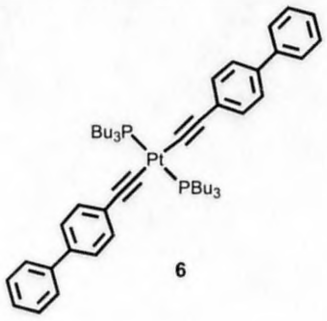

6

Absorption Properties

The absorption spectra of **5**, **6** and biphenyl-C≡C-H compounds in BuCN are displayed in Figure 3.2.1. The biphenylacetylide chromophores in **5** and **6** are responsible for the $\pi \rightarrow \pi^*$ transitions between 250 - 350 nm. These absorptions are significantly red-shifted relative to those of the free biphenyl-C≡C-H species due to the large sigma donation of C≡C-biphenyl electron density to the Pt(II) center. Figure 3.2.2 presents the absorption spectra of **5** in two solvents of different polarity, CH_2Cl_2 and BuCN. It can be noticed that the absorption band between 350 – 450 nm exhibit some solvatochromism confirming the charge transfer character of this transition. The molar extinction coefficient (ε) measured for **5** in CH_2Cl_2 at the MLCT absorption band maximum (402 nm) was found to be 10,706 $M^{-1}cm^{-1}$ which is slightly higher than that of **2** (7,900 $M^{-1}cm^{-1}$ at 450 nm).

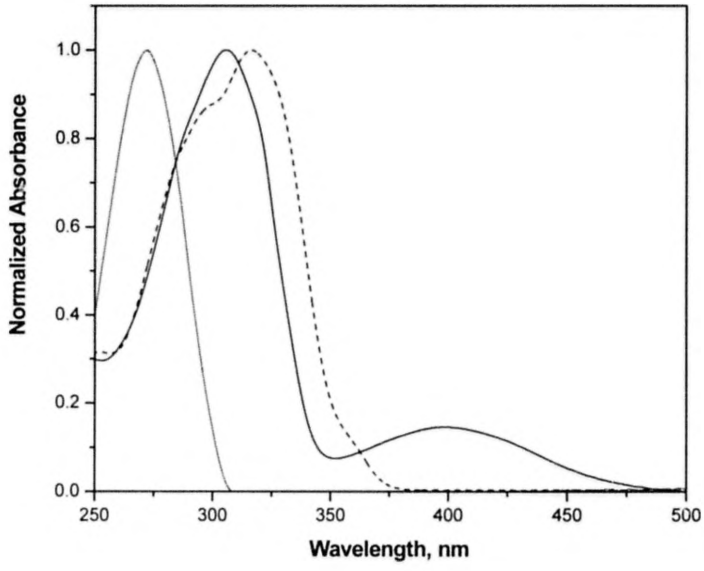

Figure 3.2.1. UV-Vis spectra of **5** (solid line), **6** (dashed line) and Biphenyl-C≡C-H (dotted line) in BuCN.

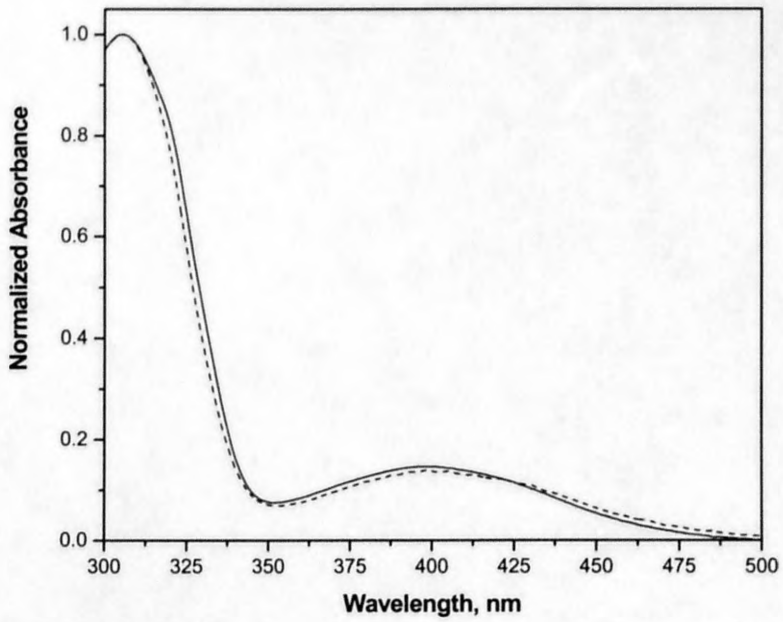

Figure 3.2.2. Normalized absorption spectra of **5** in BuCN (solid line) and CH_2Cl_2 (dotted line).

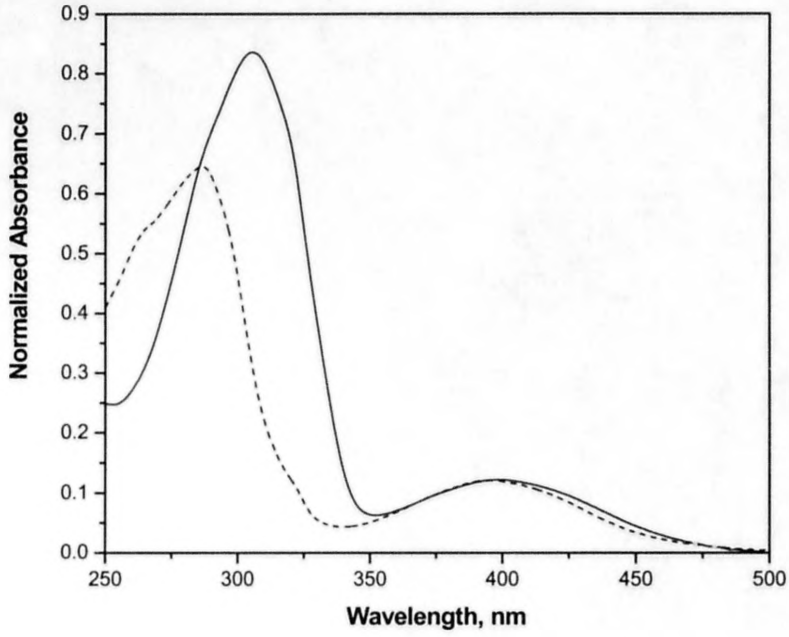

Figure 3.2.3. UV-Vis spectra of **5** (solid line) and **2** (dashed line) in BuCN normalized at 400 nm.

In general, the absorption features of **5** and **2** are quite similar (Figure 3.2.3) and in accord with those reported previously for Pt(diimine)(C≡C-X)$_2$ complexes, where X is a substituted or non-substituted phenylacetylide.[53,57,58] The slight red shift of the ^{1}MLCT energy in **5** compared to **2** is consistent with the larger sigma donation of C≡C-biphenyl electron density to the Pt(II) center.

Photoluminescence Properties

Figure 3.2.4. presents the room temperature emission spectra of **5** in aerated and deaerated dichloromethane. Upon the excitation into MLCT absorption band at 400 nm compound **5** exhibits a broad, structureless emission centered at 570 nm which is substantially quenched by oxygen.

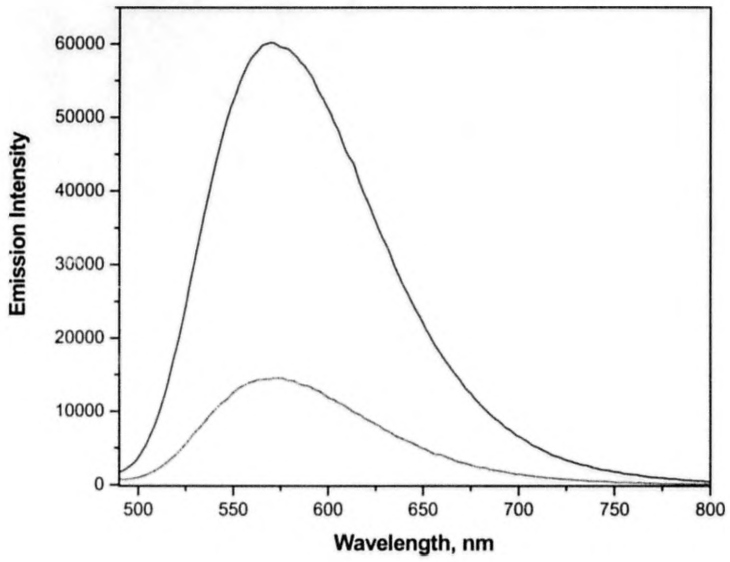

Figure 3.2.4. Emission spectra of **5** in argon saturated (solid line) and air saturated CH_2Cl_2 (dotted line).

The luminescence spectra of **5** also exhibit some negative solvatochromism, i.e. the energy of the emitting state increases with increasing solvent polarity Figure 3.2.5. The luminescence spectra of **5, 2** and **6** in deaerated BuCN are compared in Figure 3.2.6. Model compound **6** exhibits structured ^{3}IL C≡C-biphenyl centered photoluminescence centered at 510 nm with pronounced vibronic transition (1259 cm^{-1}) whereas the emission of **5** is completely structureless. At the same time, the emission profiles of **2** and **5** look very similar. It has been established previously[57,59] that the luminescence of **2** originates from the MLCT manifold, therefore the same nature of the lowest excited state in complexes **2** and **5** can be proposed. The minor red shift in the emission maximum in **5** relative to **2** is attributed to the larger σ-donation of the C≡C-biphenyl electron density to the Pt(II)-based HOMO, lowering the ^{3}MLCT energy.

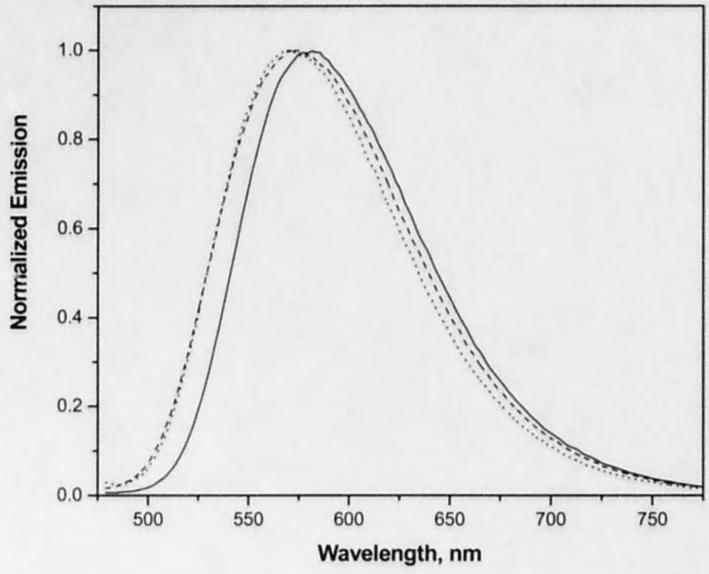

Figure 3.2.5. Emission spectra of **5** in MTHF (solid line), BuCN (dashed line) and CH_2Cl_2 (dotted line).

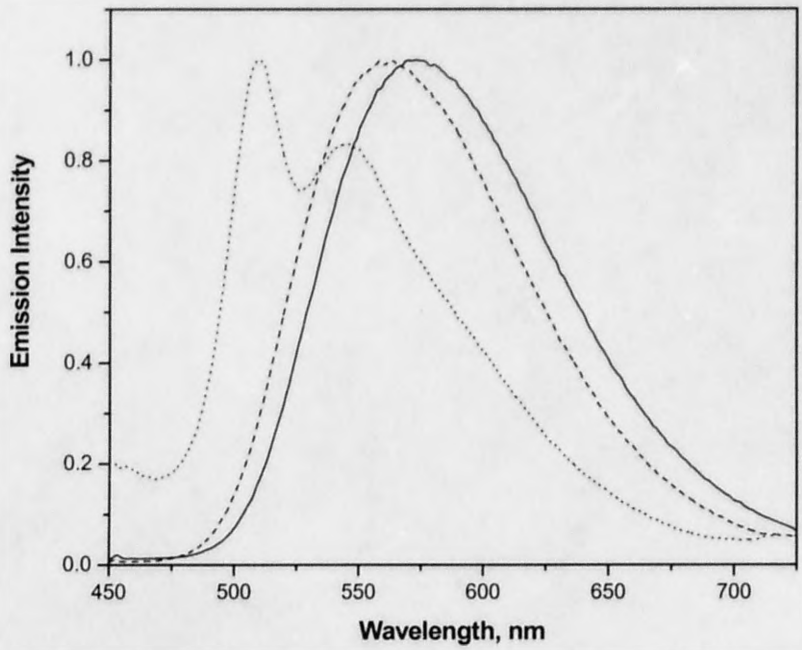

Figure 3.2.6. Emission spectra of **5** (solid line), **2** (dashed line) and **6** (dotted line) in deaerated BuCN at room temperature.

Red shifts in the emission energy bands upon increasing the electron density of the arylacetylide ligands and the electron withdrawing ability of substituents on diimine have already been observed for multiple structurally related complexes.[57,58] Both changes are consistent with a mainly metal-based HOMO and π^* (diimine) LUMO.

Photoluminescence Dynamics

The room temperature luminescence lifetimes of **5, 2** and **6** measured in deaerated solutions of BuCN with N_2-pumped dye laser (383 ± 2 nm, 500 ps fwhm) are presented in Figures 3.2.7 - 3.2.8 respectively. In all cases the emission intensity decays were well modeled by single-exponential kinetics.

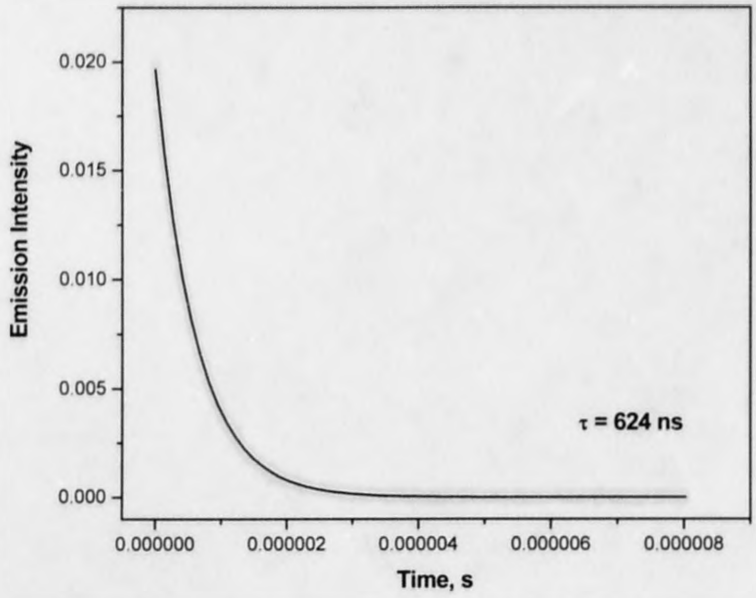

Figure 3.2.7. Emission decay of **5** in deaerated BuCN at room temperature following by 383 ± 2 nm excitation. Solid line – single exponential fit (624 ns).

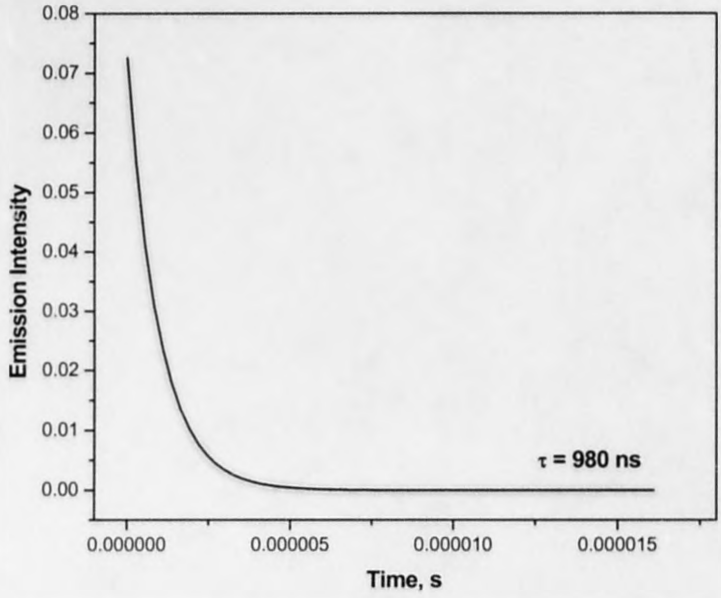

Figure 3.2.8. Emission decay of **2** in deaerated BuCN at room temperature following by 383 ± 2 nm excitation. Solid line – single exponential fit (980 ns).

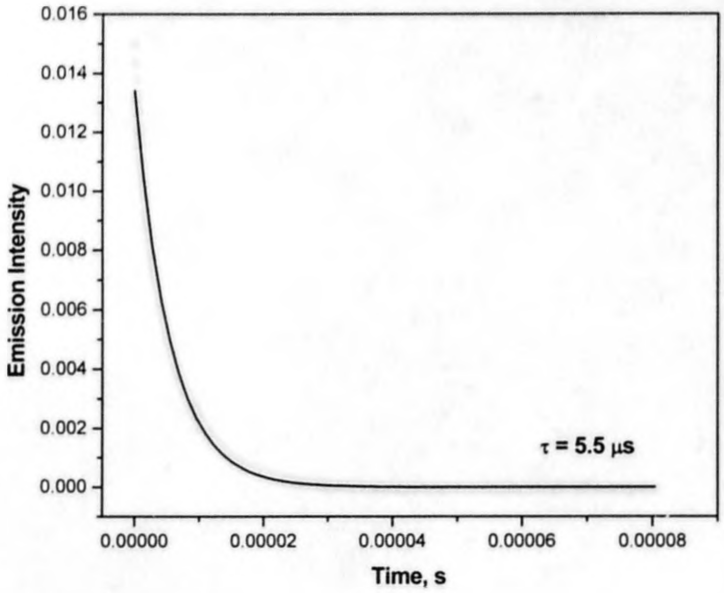

Figure 3.2.9. Emission decay of **6** in deaerated BuCN at room temperature following by 383 ± 2 nm excitation. Solid line – single exponential fit (5.5 μs).

Since Pt(II) chromophores of this type are known to undergo excited state self-quenching reactions[52,56-58,62] all luminescence measurements were performed in optically dilute solutions (10^{-6}–10^{-5} M), where the measured lifetimes were invariant to concentration. Compound **5** exhibits a lifetime of 624 ns in BuCN which is of the same magnitude with the lifetime of **2** (980 ns) providing additional evidence towards the MLCT nature of photoluminescence. The lifetime of **6** is strikingly different (5.5 μs) due to the ^{3}IL C≡C-biphenyl-based origin of phosphorescence.

Transient Absorption

Additional support to the MLCT nature of the lowest excited state in **5** comes from the TA measurements. All nanosecond laser flash photolysis experiments were

carried out in thoroughly degassed solutions and kept under argon atmosphere during the entire experiment. The concentrations used in flash photolysis were slightly different than in the luminescence experiments, and some variations in excited state lifetime were observed (865 ns for **2**, 618 ns for **5**, and 13.8 μs for **6**). The excitation wavelengths for **5** and **2** were chosen to predominantly pump the low energy MLCT transitions. Compound **2** in BuCN believed to possess a low energy MLCT excited state, features excited state absorptions at ~355 nm and ~470 nm which are attributed to the reduced dbbpy ligand, Figure 3.2.10. This data is consistent with the TA spectra measured for the structurally related Pt(II) complexes.[58] Flash photolysis performed on **5** in BuCN generated positive transients in the region of 320 – 480 nm (Figure 3.2.11). The ground state bleaching of the C≡C-biphenyl units in **5** is ~30 nm red shifted relative to the bleaching of C≡C-C_6H_5 in **2**, which is consistent with differences in their relative absorption band positions (Figure 3.2.3). Transient absorption experiments on **5** (λ_{exc} = 416 nm) have also been performed in CH_3CN (some DCE was added for solubility purposes) and MTHF and revealed some variations in the shape of the spectra with the nature of the solvent, Figures 3.2.13 and 3.2.14. The excited state absorption difference spectrum obtained for **6** in BuCN (λ_{exc} = 355 nm) exhibit a strong absorption transient near 550 nm along with a strong ground state bleaching below 375 nm, Figure 3.2.12. The absorption at 530 nm is assigned to the triplet-to-triplet absorption of the C≡C-biphenyl chromophore, as no other absorption transients are expected for this model system. Therefore, the TA data obtained in **5** are more consistent with a charge-transfer assignment and no formation of biphenylacetylide-based triplet is observed in any solvent.

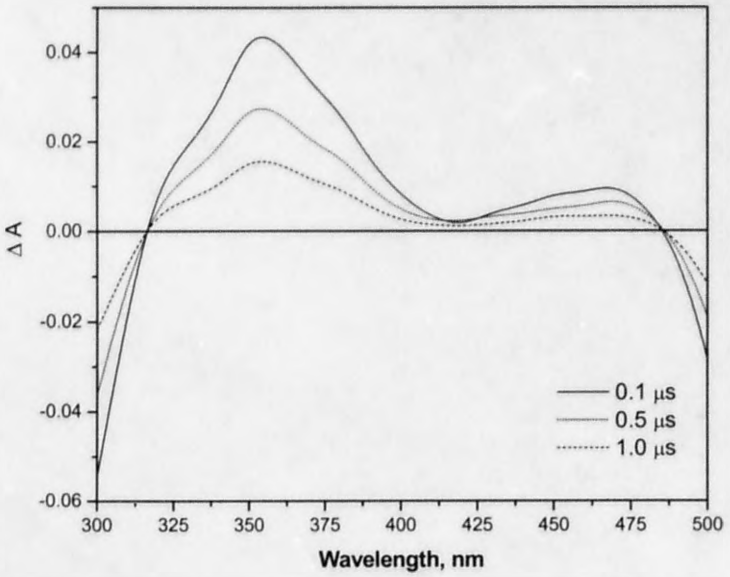

Figure 3.2.10. Transient absorption difference spectra of **2** in deaerated BuCN following 416 nm excitation. The delay times are specified on the spectrum.

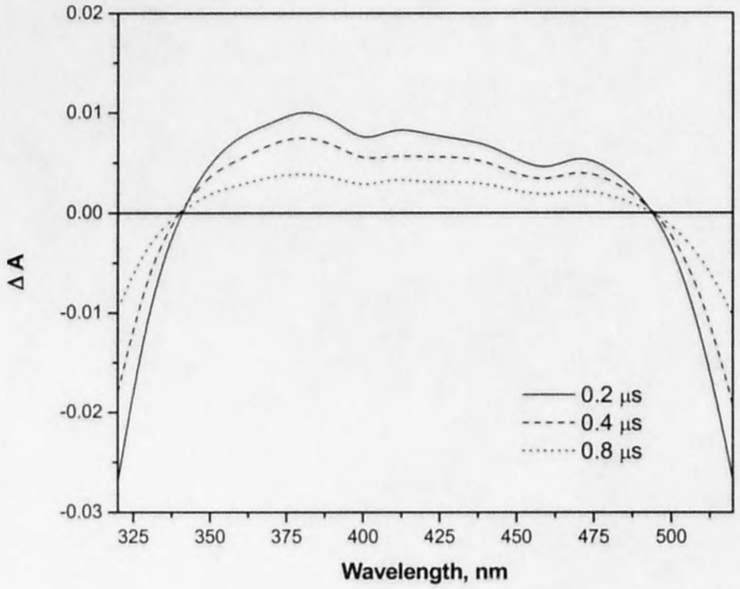

Figure 3.2.11. Transient absorption difference spectra of **5** in deaerated BuCN following 355 nm excitation. The delay times are specified on the spectrum.

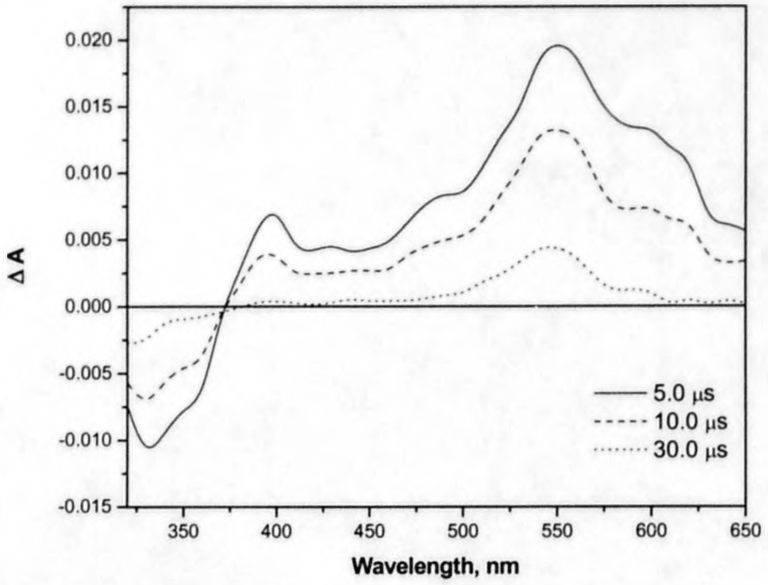

Figure 3.2.12. Transient absorption difference spectra of **6** in deaerated BuCN following 355 nm excitation. The delay times are specified on the spectrum.

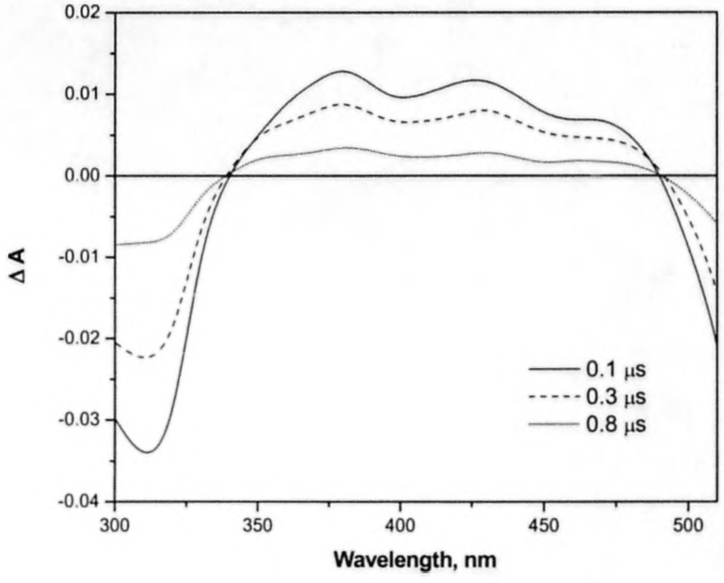

Figure 3.2.13. Transient absorption difference spectra of **5** in CH_3CN (DCE added for solubility) excited at 416 nm. The delay times are specified on the spectrum.

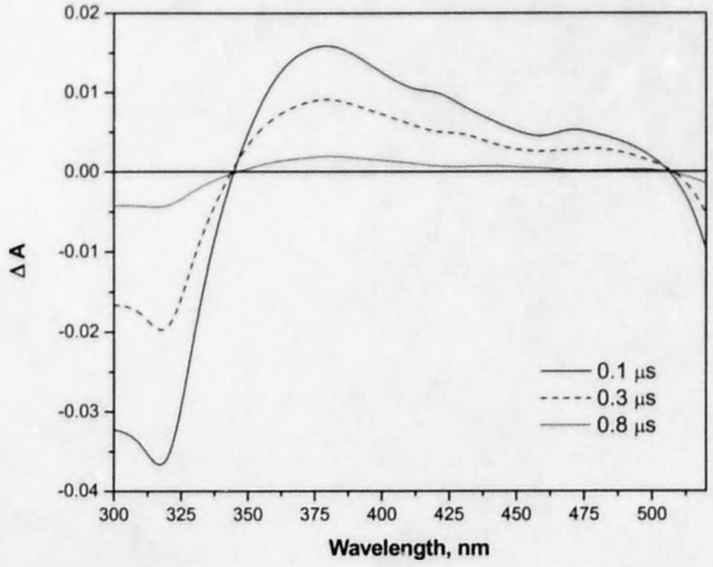

Figure 3.2.14. Transient absorption difference spectra of **5** in MTHF excited at 416 nm. The delay times are specified on the spectrum.

Low-Temperature Photoluminescence

The emission spectra of compound **5** and **2** in BuCN at room temperature and in a 77 K glass are presented in Figures 3.2.15 and 3.2.16 respectively. As it was already established above, room temperature photoluminescence properties of **5** and **2** are well consistent with the ^{3}MLCT manifold. It can be noticed that model compound **2** displays a significant value of thermally induced Stokes shift (ΔE_s = 2677 cm^{-1}), which is consistent with previous observations from the Schanze group.[58] This suggests the charge-transfer nature of the excited state in **2**, as there are clearly large differences in ground and excited state dipole moments.[36]

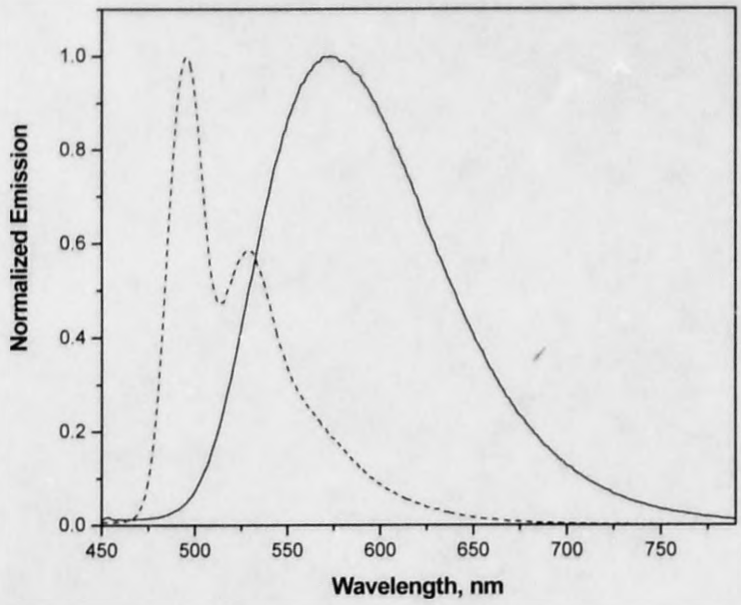

Figure 3.2.15. Room temperature (solid line) and 77 K (dashed line) spectra of **5** in BuCN.

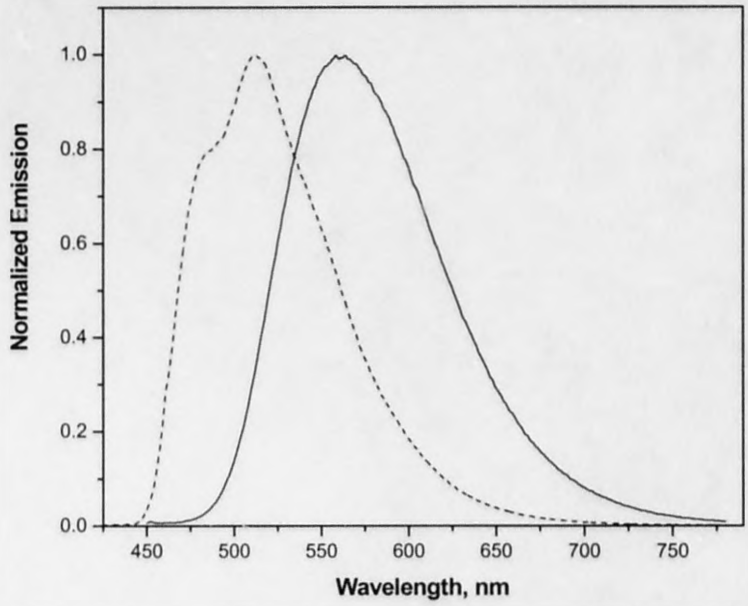

Figure 3.2.16. Room temperature (solid line) and 77 K (dashed line) spectra of **2** in BuCN.

However, the 77 K spectrum of **5** in BuCN is shaped very differently then that of **2**, it is relatively sharp in comparison with pronounced vibronic transition (1298 cm^{-1}) suggesting that the emission of **5** is not attributed to MLCT parentage, Figure 3.2.15.

The 77 K and RT emissions of model compound **6** in BuCN are depicted in Figure 3.2.17. Photophysical properties of **6** are dominated by the π-π^* manifold which is in agreement with the modest ΔE_s value (759 cm^{-1}). Interestingly, the emission spectrum of **5** at 77 K become significantly superimposable with that of **6** and adopts its vibronic spacing (1319 cm^{-1}) within experimental error, Figure 3.2.18. These results strongly suggest that it glassy solution at 77 K the lowest excited state in **5** is biphenylacetylide-centered ^{3}IL.

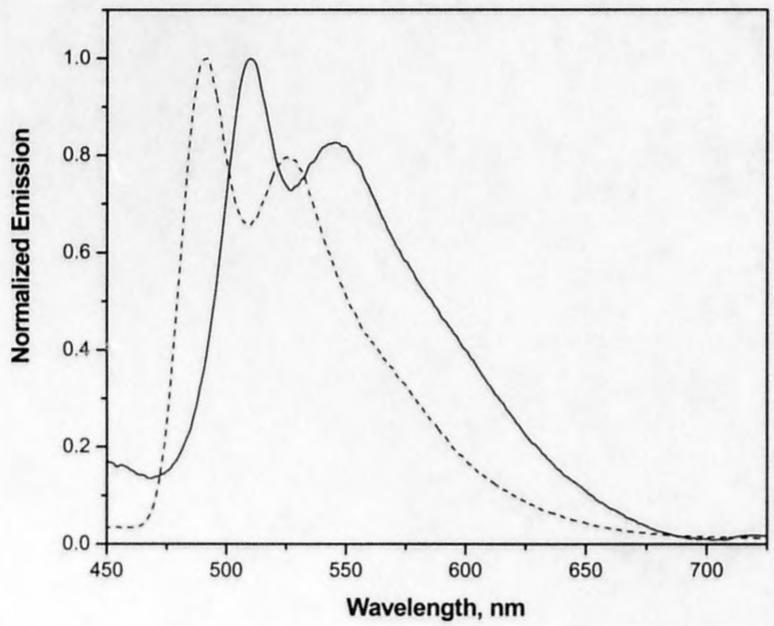

Figure 3.2.17. Room temperature (solid line) and 77K (dashed line) spectra of **6** in BuCN.

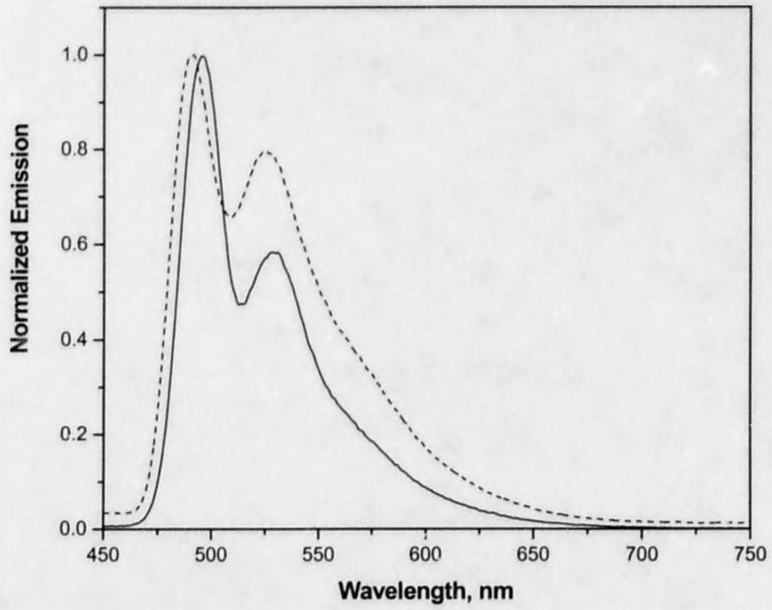

Figure 3.2.18. 77 K spectra of **5** (solid line) and **6** (dashed line) in BuCN glasses.

This can be easily rationalized by the fact that due to the "luminescence rigidochromism" in frozen media,[36] the energy gap between the ground and ^{3}MLCT excited state significantly increases, while the energy of π-π^* transition remain unaffected because of its non-polar nature. This makes energy transfer from ^{3}MLCT to ^{3}IL biphenylacetylide-based state energetically favorable.

CHAPTER III.III. SOLVENT SWITCHING BETWEEN CHARGE TRANSFER AND INTRALIGAND EXCITED STATES IN A MULTICHROMOPHORIC Pt(II) COMPLEX

Introduction

In this chapter, we set out to design a new molecule where the ^{3}IL states on the arylacetylide ligands would be energetically proximate to the luminescent ^{3}MLCT state. This motif features the possibility of observing radiative decay from two distinct triplet states at room temperature and permits the evaluation of potential excited triplet state interactions. Through well-established synthetic protocols, we were able to assemble the multichromophoric system, Pt(dbbpy)(C≡C-Naphthalene)$_2$ (**7**) (dbbpy = 4,4'-(di-*tert*-butyl)-2,2'-bipyridine; C≡C-Napthalene = 1-ethynylnaphthalene), whose triplet energy levels were coarse-adjusted by design and synthetically imparted into the structure. Although several publications have commented on the strong negative solvatochromism displayed by the low energy charge transfer absorptions in Pt(diimine)(C≡C-R)$_2$ chromophores,[54,63] to our knowledge nobody has attempted to use this dependence to systematically modulate the excited state properties in this class of molecules. In this study we chose four different solvents to test this hypothesis: acetonitrile (CH_3CN), dichloromethane (CH_2Cl_2), 2-methyltetrahydrofuran (MTHF), and toluene. We postulated that the solvent polarity dependence could be used to fine-adjust the ^{3}MLCT energy relative to the $^3\pi$-π^* levels in **7**, potentially accessing a variety of excited state behaviors in a single molecular system. Indeed this is the case as the solvent polarity increases the nature of the excited state becomes more ^{3}IL-like, as revealed by static and dynamic absorption and luminescence spectroscopy.

Structures

All of the Pt(II) complexes used in this study were prepared in accordance with standard procedures with final purification achieved by chromatography over silica. All complexes are stable solids at room temperature and are readily soluble in a variety of organic solvents.

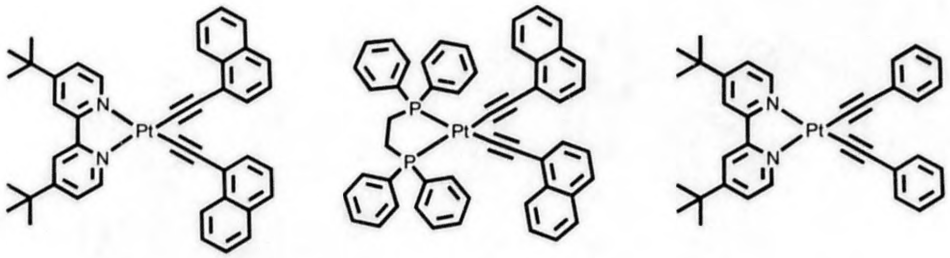

7 **10** **2**

Compounds **7, 10, 2** were structurally characterized by NMR, mass spectrometry, and elemental analysis. Multichromophoric **7** possesses a combination of low-lying ^{3}MLCT and ^{3}IL excited states whereas **10** is a reference compound containing the metal-perturbed naphthaleneacetylide chromophores arranged in a *cis*-geometry around the Pt(II) center, enforced by the bidentate dppe ligand (dppe = 1,2-bis(diphenylphosphino)ethane). Structure **10** lacks a low lying charge transfer state and will be used to model the ^{3}IL manifold resident on the naphthaleneacetylide ligands, whereas compound **2** is intended to represent the ^{3}MLCT state in **7**.

Room Temperature Absorption and Photoluminescence

The room temperature spectroscopic and photophysical properties of all the complexes investigated in this study are collected in Table 3.3.1. Figure 3.3.1 displays the

absorption spectra of Pt(dbbpy)(C≡C-Napthalene)$_2$ measured in different solvents. It is clear that the low energy MLCT absorption (ε_{CH3CN} = 7,900 $M^{-1}cm^{-1}$ at 386 nm) blue shifts with increasing solvent polarity. This is not surprising as negative solvatochromism has been previously observed for Pt(dbbpy)(C≡C-Ph)$_2$ (and structurally related molecules),[54,63] resulting from a large ground state dipole moment. We have performed density functional theory (DFT) calculations on the ground states of **7** and **2** to estimate each dipole moment.[71] Using optimized structures in Gaussian 98 (BP86 functional with a double zeta basis set using an effective core potential for Pt),[71] the calculated values of the ground state dipole moments are 10.8 D and 10.6 D, respectively, consistent with the transient DC photoconductivity study performed by Hupp and coworkers in a structurally related Pt(II) diimine dithiolate complex.[72] In both cases the ground state dipole moment vector directly opposes that produced by MLCT excitation. The higher energy ligand-localized π-π* transitions between 300 and 350 nm resulting from electronic transitions within the naphthaleneacetylide fragments are not significantly perturbed by solvent polarity. These observations are easily confirmed by the absorption spectra in Figure 3.3.1 as well as that displayed by the structural model **10**, Figure 3.3.2. In essence, solvent polarity can be used to tune the MLCT energy in relation to the π-π* energy of the C≡C-nap chromophores in **7**. The absorption spectra of **2** in solvents of different polarity are displayed on Figure 3.3.3.

The luminescence spectra of **7** obtained in various solvents are displayed in Figure 3.3.4. The spectra observed in MTHF and toluene are broad and structureless, closely resembling the breadth and shape measured for **2** in the same solvents, Figure 3.3.5. Therefore, we tentatively assign the photoluminescence of **7** in those solvents as

MLCT-based. The photoluminescence spectrum of **7** measured in CH_3CN is qualitatively similar to the spectrum observed for **10**, Figure 3.3.6. In this case, the emission appears to be most consistent with ^{3}IL phosphorescence emanating from a naphthaleneacetylide moiety. The luminescence spectrum of **7** measured in CH_2Cl_2 is intriguing as it lies somewhat in-between that observed in CH_3CN and MTHF, Figure 3.3.4. The static luminescence data at room temperature strongly suggest that the ^{3}MLCT and ^{3}IL states crossover in energy as the solvent polarity is increased from MTHF to CH_3CN. In low polarity solvents, the emission is dominated by the MLCT state whereas in higher polarity media, the emission appears to be dictated by the ^{3}IL state residing on one of the C≡C-napthalene ligands.

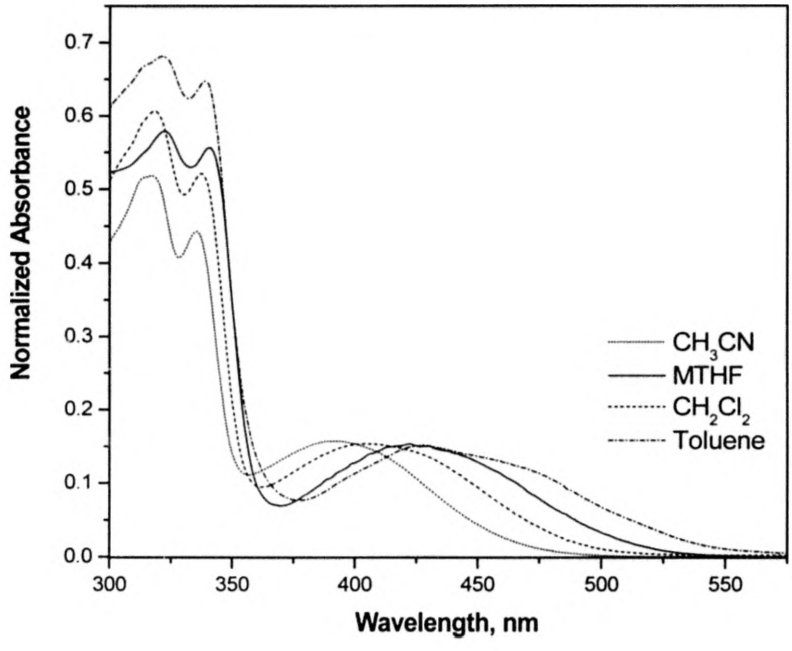

Figure 3.3.1. UV-Vis absorption spectra of **7** in CH_3CN, MTHF, CH_2Cl_2, and toluene.

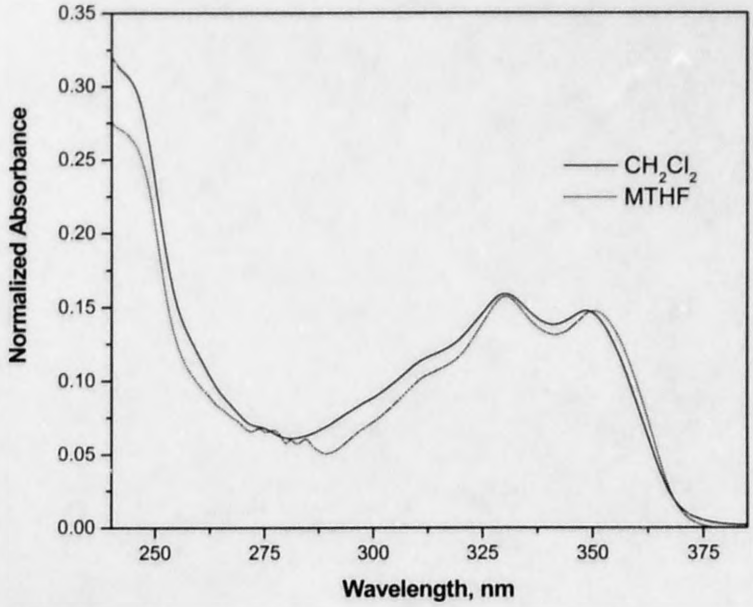

Figure 3.3.2. UV-Vis absorption spectra of **10** in MTHF and CH_2Cl_2.

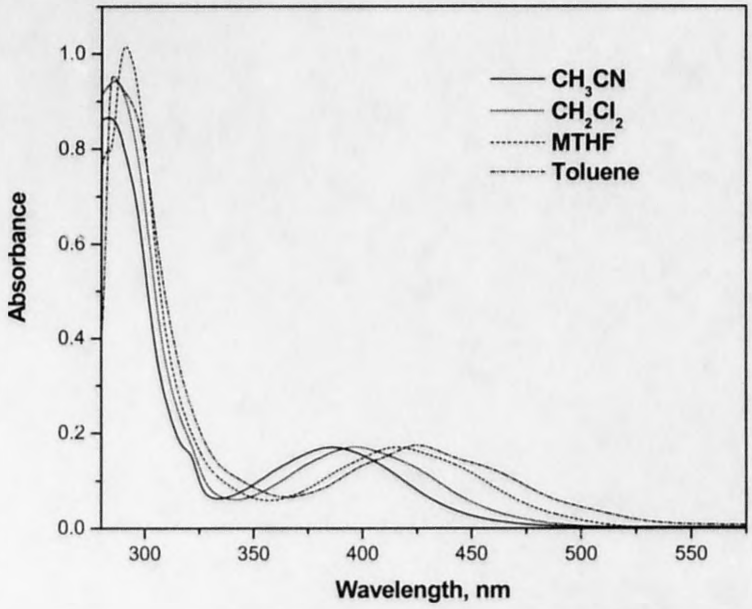

Figure 3.3.3. UV-Vis absorption spectra of **2** in CH_3CN, MTHF, CH_2Cl_2, and toluene.

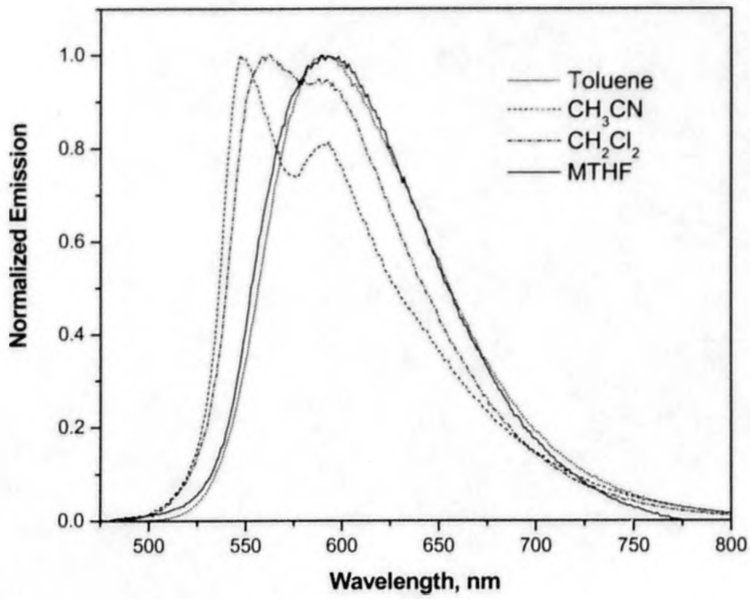

Figure 3.3.4. Static photoluminescence spectra of **7** in CH_3CN, MTHF, CH_2Cl_2, and toluene.

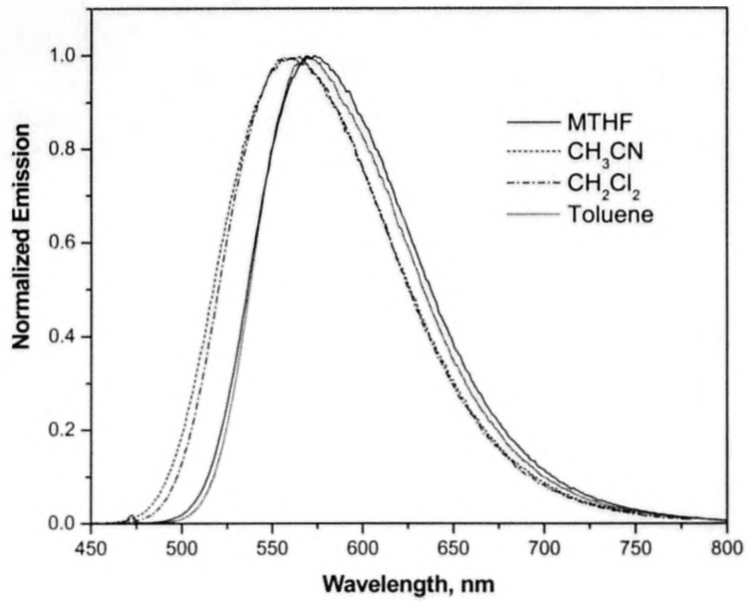

Figure 3.3.5. Static photoluminescence spectra of **2** in CH_3CN, MTHF, CH_2Cl_2, and toluene.

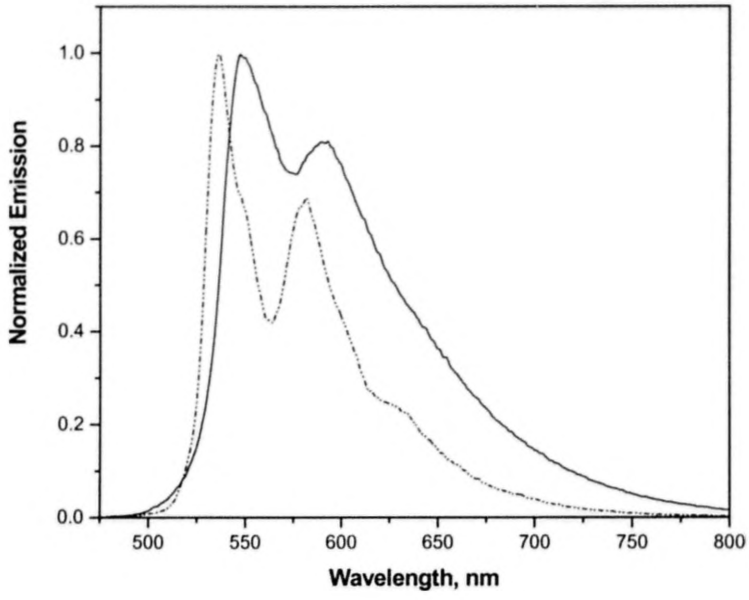

Figure 3.3.6. Photoluminescence spectra of **7** (solid line) and **10** (dashed line) in CH_3CN.

With the notable exception of MTHF, the photoluminescence quantum yields observed for **7** are significantly lower than those measured for **2**, Table 3.3.1. When the quantum yields and excited state lifetimes (see below) are taken into account in both molecules, the calculated values of k_r and k_{nr} (Table 3.3.1) provide evidence of the proposed state inversion in **7**. The radiative decay rates observed for **7** in CH_3CN and CH_2Cl_2 are an order of magnitude smaller than those measured for **2** in the same solvents, while the k_{nr} values are respectively smaller. This drop in k_r and k_{nr} may reflect more of a ^{3}IL character in the excited state decay.[58] In toluene, where the ^{3}MLCT is lower in energy, the k_r and k_{nr} values measured for **7** are of the same magnitude as those seen for **2**, suggesting that the ^{3}MLCT manifold is largely responsible for the radiative decay. The data obtained in MTHF cannot be readily interpreted as the emission spectrum and

lifetime are consistent with a ^{3}MLCT excited state but values of k_r and k_{nr} are both smaller than the values obtained for **2** in the same solvent.

We have noted that the emission spectrum of **7** is symmetrically quenched in all solvents investigated when the solution environment changes from argon-purged to air-saturated. This seemingly simple result is important as it suggests that the emission manifold is comprised of one state or two closely lying states in rapid thermal equilibrium. The corrected excitation spectra of **7** and **10** were largely superimposable with corresponding absorption spectra at all wavelengths above 300 nm and were completely invariant to the monitoring wavelength. Representative examples for **7** and **10** are depicted on Figures 3.3.7. and 3.3.8. respectively.

Table 3.3.1. Photophysical data at room temperature.[a]

Compound	Solvent	λ_{abs}, nm	λ_{em}, nm	τ_{em},[b] μs	τ_{TA},[c] μs	Φ_{em}[d]	k_r, $*10^{-5}$ s^{-1} [e]	k_{nr}, $*10^{-5}$ s^{-1} [f]
7	CH_3CN	392	548m 591	2.8	3.5	0.046	0.16	3.41
	CH_2Cl_2	404	562m 591	3.0	2.7[g]	0.11	0.36	2.97
	Toluene	427	591	0.87	0.75	0.168	1.93	9.56
	MTHF	422	593	0.54	0.52	0.023	0.43	18.09
2	CH_3CN	386	561	0.69	0.60	0.15	2.20	12.29
	CH_2Cl_2	396	562	1.36	-	0.34	2.50	4.85
	Toluene	425	569	1.05	1.02	0.307	2.92	6.60
	MTHF	416	573	0.16	0.15	0.047	2.94	59.56
10	MTHF	330 350	542m 587	100	69	-	-	-

[a]Argon degassed solutions; [b]Emission intensity decay lifetime, ± 5%; [c]Absorption transient lifetime, ± 10%; [d]Quantum yield of photoluminescence relative to $[Ru(bpy)_3]^{2+}$ in CH_3CN ($\Phi_{em} = 0.062$); [e]Radiative decay rate, calculated by $k_r = \Phi_{em}/\tau_{em}$; [f]Nonradiative decay rate, calculated by $k_{nr} = (1-\Phi_{em})/\tau_{em}$; [g]Measured in 1,2-dichloroethane.

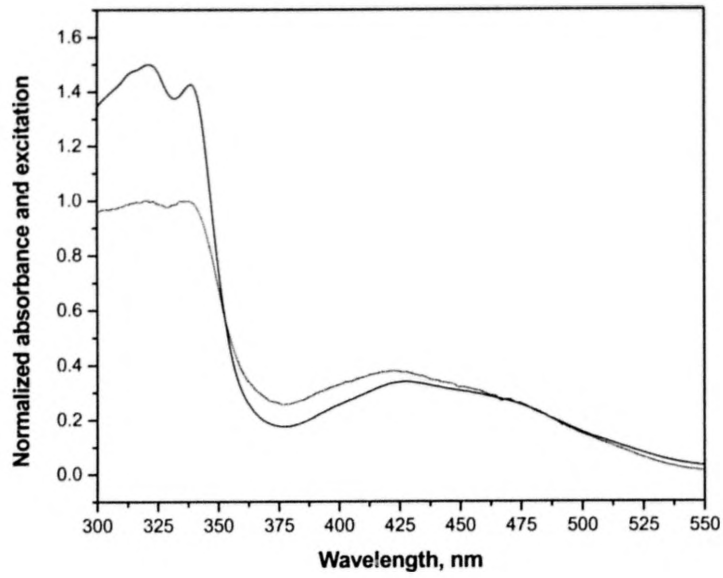

Figure 3.3.7. Normalized absorbance (solid line) and excitation (dotted line) spectra of 7 in Toluene.

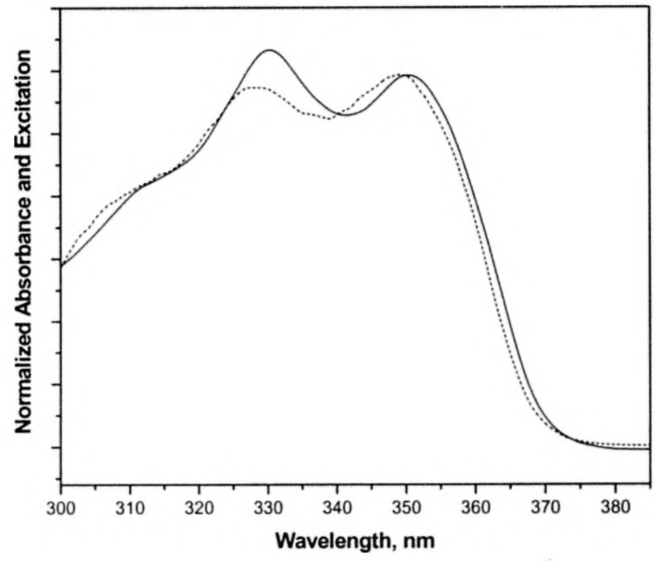

Figure 3.3.8. Normalized absorbance (solid line) and excitation (dotted line) spectra of **10** in MTHF.

Photoluminescence Dynamics

The excited state luminescence lifetimes of **7** measured in optically dilute (10^{-6}-10^{-5} M) deaerated solutions of MTHF, toluene, CH_2Cl_2, and CH_3CN are 0.54, 0.87, 3.0, and 2.8 μs, respectively and represented on Figures 3.3.9-3.3.12. The recovered lifetimes were invariant at the low sample concentrations used in these experiments. In all cases the emission intensity decays were well modeled by single exponential kinetics and lifetimes were constant as a function of the emission monitoring wavelength. This suggests that in every solvent there is only one type of emitting state, consistent with the static data described above. However, all results are also compatible with a solvent-dependent fast equilibrium between ^{3}MLCT and ^{3}IL excited state. In MTHF and toluene, we believe that the lifetimes are most consistent with a lowest excited state composed primarily of ^{3}MLCT character. Indeed these lifetimes are in the range of values typically observed in Pt(diimine)(C≡C-R)$_2$ complexes, whose excited states are derived from MLCT composition.[53,54,57,58,64] In CH_2Cl_2 and CH_3CN the lifetimes of the emissions increase to ~3.0 μs, suggesting that significant ^{3}IL character is present in the excited state manifold. The lifetime of **10** measured in CH_3CN with 337 nm excitation is 100 μs, Figure 3.3.13 This value is ~ 30 times larger than the similar radiative decay process in **7**. Although the static emission spectrum appears to be consistent with a ^{3}IL assignment, the observed dynamics suggest that there is some degree of MLCT character in the excited state decay of **7**, which substantially shortens the lifetime relative to a purely ^{3}IL excited state.

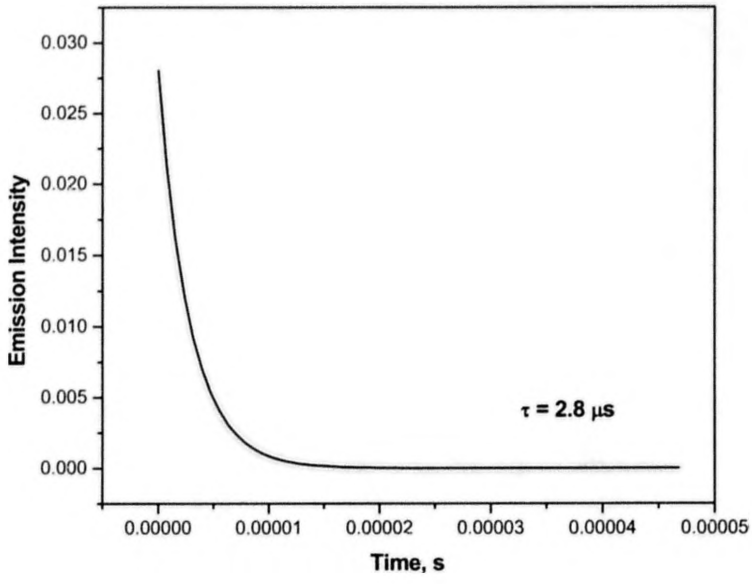

Figure 3.3.9. Room temperature emission decay of **7** in CH_3CN monitored at 548 nm. Solid line is the single exponential fit (2.8 μs).

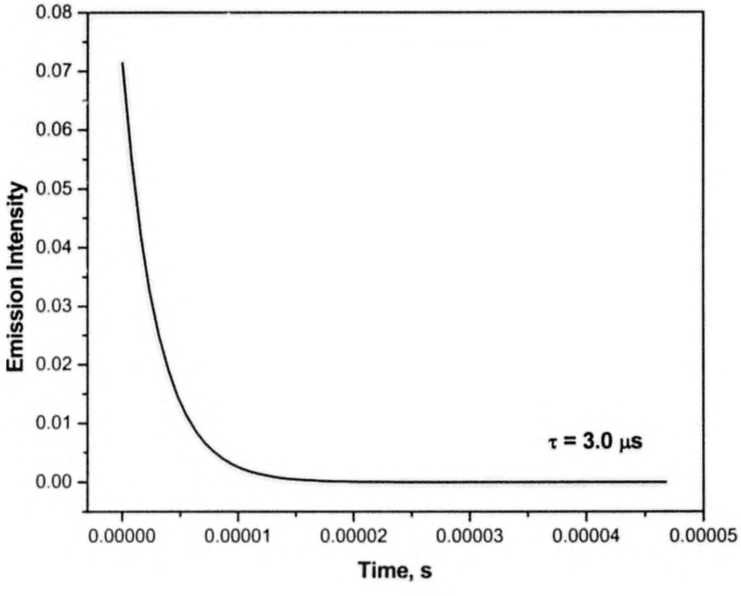

Figure 3.3.10. Room temperature emission decay of **7** in CH_2Cl_2 monitored at 562 nm. Solid line is the single exponential fit (3.0 μs).

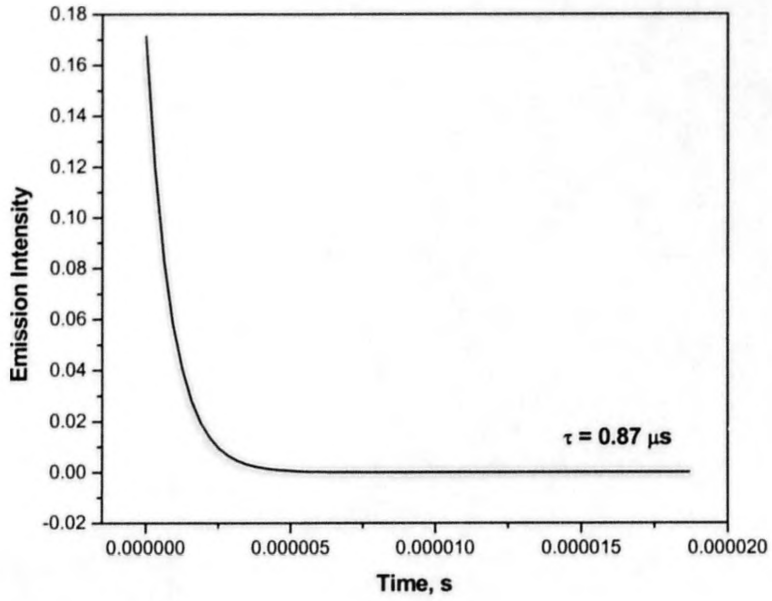

Figure 3.3.11. Room temperature emission decay of **7** in Toluene monitored at 591 nm. Solid line is the single exponential fit (0.87 μs).

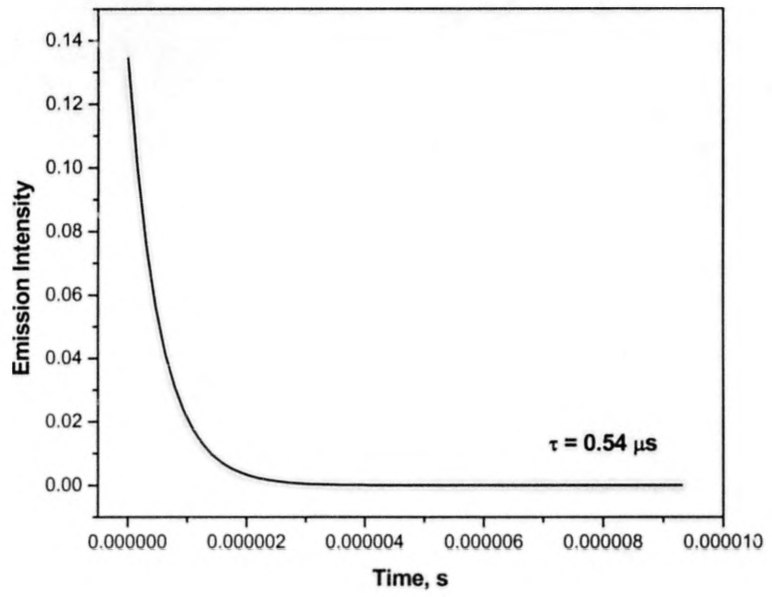

Figure 3.3.12. Room temperature emission decay of **7** in MTHF monitored at 593 nm. Solid line is the single exponential fit (0.54 μs).

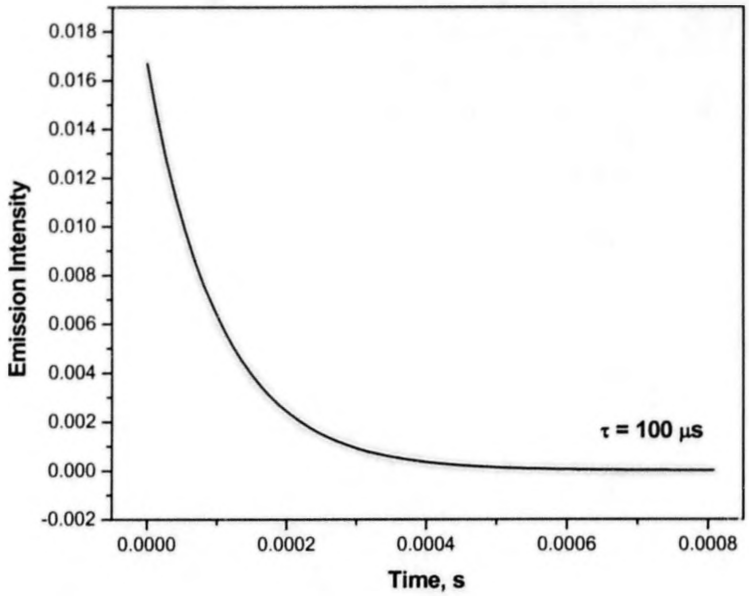

Figure 3.3.13. Room temperature emission decay of **10** in MTHF monitored at 541 nm. Solid line is the single exponential fit (100 μs).

This is quite different than what we have observed previously in Pt(dbbpy)(C≡C-Pyrene)$_2$, where the excited state could be readily interpreted as largely ^{3}IL (pyrenylacetylide) in nature.[17] The major difference is that in the latter multichromophoric system, the pyrenylacetylide triplet states were substantially lower in energy relative to the ^{3}MLCT manifold, preventing any mixing or thermal equilibration between the two triplets. Based upon the luminescence data, it appears that the ^{3}MLCT and ^{3}IL states in **7** are interacting in some manner at room temperature and solvent media dictates the extent of the interaction.

Transient Absorption

The transient absorption spectra of **7** following visible excitation at 416 nm in toluene and CH_3CN are displayed in Figure 3.4.14-17. This excitation wavelength was chosen in order to preferentially pump the low energy MLCT transitions. In these experiments, the concentrations used were slightly larger than in the luminescence experiments, and minor variations in excited state lifetime were observed, Table 3.3.1.[56] It is apparent that the relative intensities in the observed absorption transients markedly change with solvent, while the positions of the same bands do not shift dramatically, Figure 3.3.14-17. In toluene, the excited state absorptions occur at ~380 and ~485 nm, with the 380 nm band possessing slightly more intensity, Figure 3.3.14.

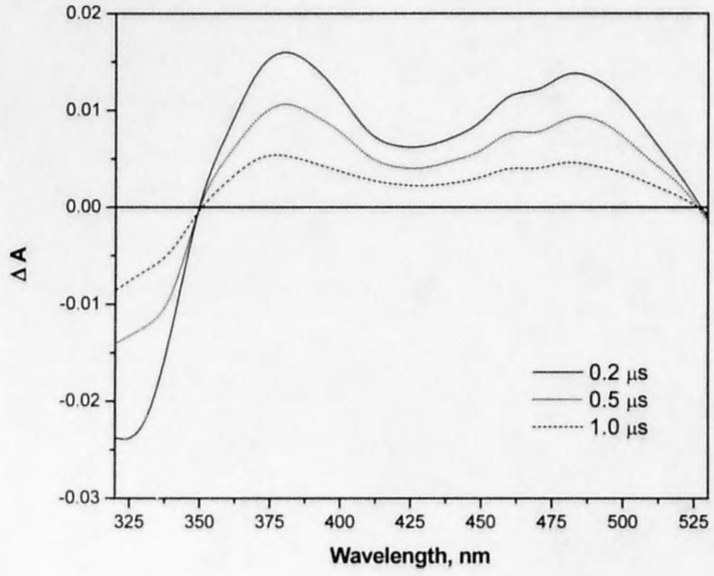

Figure 3.3.14. Excited state absorption difference spectra of **7** in Toluene following 416 nm excitation. The delay times are specified on the spectrum.

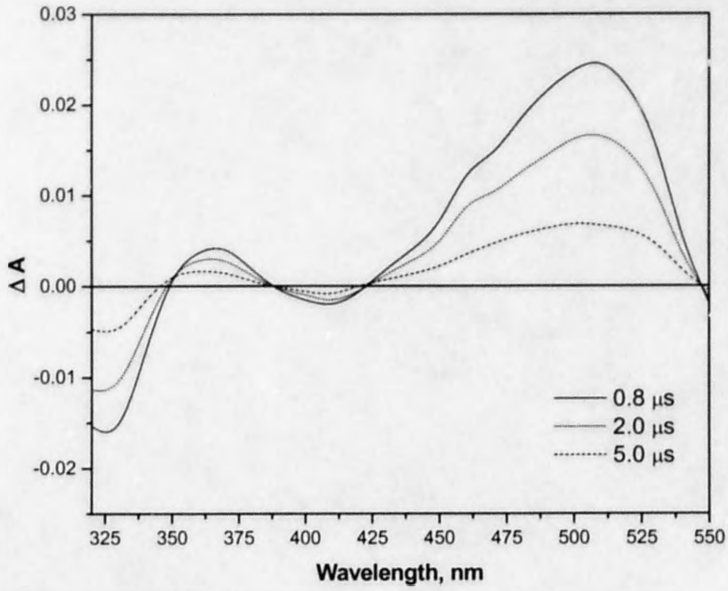

Figure 3.3.15. Excited state absorption difference spectra of **7** in CH_3CN following 416 nm excitation. The delay times are specified on the spectrum.

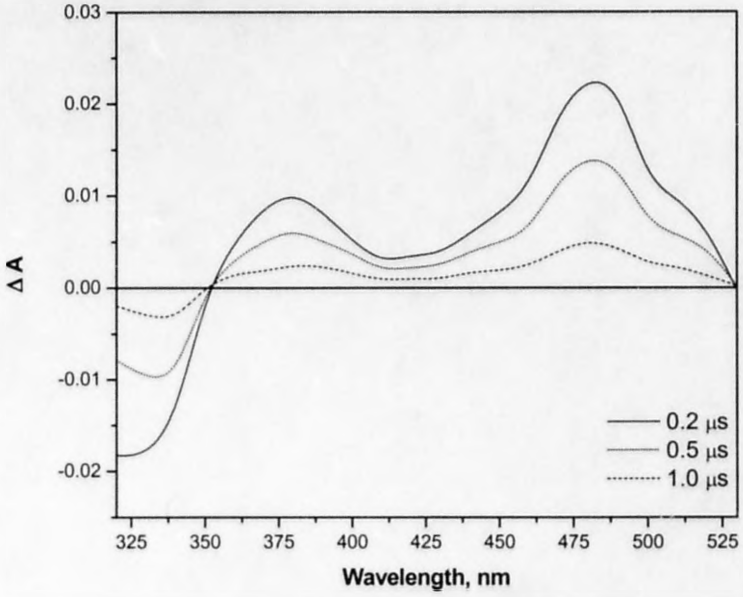

Figure 3.3.16. Excited state absorption difference spectra of **7** in MTHF following 416 nm excitation. The delay times are specified on the spectrum.

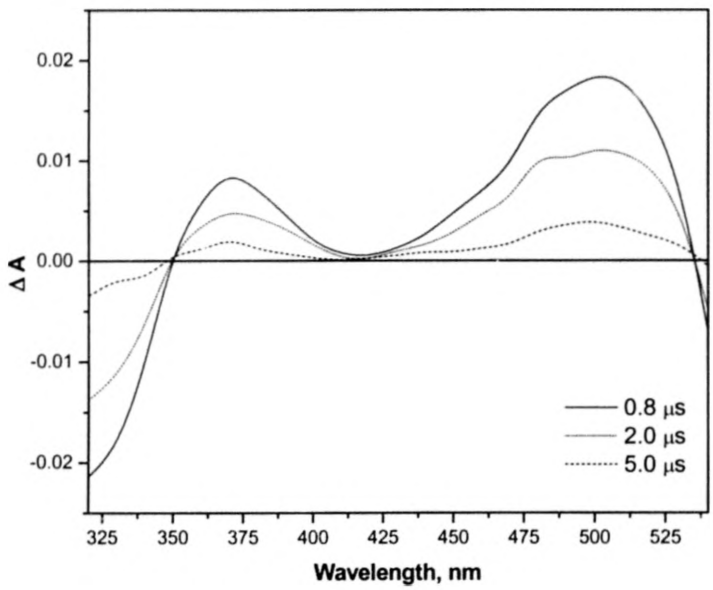

Figure 3.3.17. Excited state absorption difference spectra of **7** in DCE following 416 nm excitation. The delay times are specified on the spectrum.

The absorption signatures obtained for **7** in CH_3CN tell a different story as the band positions are slightly shifted ~365 and ~510 nm, and most of the transient absorption intensity can be found in the low energy band at ~510 nm, Figure 3.3.15. It is now worthwhile to make direct spectroscopic comparisons to the reference chromophores **10** and **2**. Compound **2** in toluene, believed to possess a low energy MLCT excited state, features excited state absorptions at ~360 and ~485 nm, with most of the intensity present in the high energy 360 nm band, Figure 3.3.18.

This data is consistent with the excited state difference spectra measured by Schanze and coworkers in structurally related Pt(II) systems.[58] The first-order kinetics displayed by the absorption transients as well as the bleach recoveries for **10** and **2** in deaerated toluene were in quantitative agreement within experimental error of their

respective luminescence intensity decays, Table 3.3.1. If the solvent is changed to CH_3CN, the absorption transients observed in **2** both experience a ~10-15 nm blue shift relative to toluene, with peak band positions at ~350 and ~470 nm, Figure 3.3.19. However, the relative intensities of the bands are comparable to that observed for **2** in toluene. The same is true for MTHF and BuCN, Figure 3.3.20 and 3.3.21, illustrating that **2** possesses a lowest energy ^{3}MLCT state in all solvents investigated, in agreement with the literature.[54,57,58] The excited state absorption difference spectrum obtained for **10** in MTHF (λ_{ex} = 355 nm) exhibits a strong absorption transient near 530 nm along with a strong ground state bleaching signal below 375 nm, Figure 3.3.22. We note that there is no significant solvent dependence for the transient absorption spectrum of **10**, so only the data obtained in MTHF will be discussed. The absorption at 530 nm is assigned to the triplet-to-triplet absorption of the naphthaleneacetylide chromophore, as no other absorption transients are expected for this model system. The single exponential lifetime of the absorption transients measured for **10** are well beyond that observed in **7**, mirroring the kinetic behavior seen in the time-resolved photoluminescence experiments, Table 3.3.1.

The entire collection of transient absorption data yields significant insight into the proposed solvent-induced reordering of the lowest excited state in **7**. Similar to that observed in the luminescence intensity decays, in all instances the transients self-consistently exhibit similar lifetimes throughout the absorption envelope, illustrating that a single type of excited state is probably responsible for the experimental observations. It should be noted that the nanosecond flash photolysis data does not yield any insight into the dynamics occurring within the 7 ns laser pulse, so it is possible that this data reflects

transients associated with the lowest of two states connected together via thermal equilibrium. This possibility requires further investigation with ultrafast transient absorption spectroscopy. Figures 3.3.14 and 3.3.15 show that in the two extremes of solvent polarity (toluene vs. CH_3CN), the major difference in the observed transients is in the relative magnitude of their absorption intensities, the band in the red being greatly enhanced as the solvent polarity is increased. The enhancement of this low energy band is most consistent with the formation of ^{3}IL states in the naphthaleneacetylide chromophore(s), as can be easily ascertained by the data provided in the model system **10**, Figure 3.3.22. What is interesting is that in all solvents investigated, the relative intensities of the two transient absorption bands vary but they never approach the ratio seen in **2**, which is expected for a "pure" ^{3}MLCT excited state,[58] Figures 3.3.18 - 21. This data implies that in all solvents, the excited state manifold in **7** can best be described as something intermediate of ^{3}MLCT and ^{3}IL. However, we do believe that the transient absorption data reveal the proposed reordering of the lowest excited state in **7** from predominately ^{3}MLCT to ^{3}IL as the solvent polarity is increased. Since the absorption bands characteristic of both triplet states severely overlap, we cannot definitively say that one state or the other (or a combination of the two) solely exist in any given solvent at room temperature. However, the independently measured excited state dynamics support the notion that both triplet states interact at room temperature and the photophysical properties observed as a function of solvent likely represent different composites of the two states.

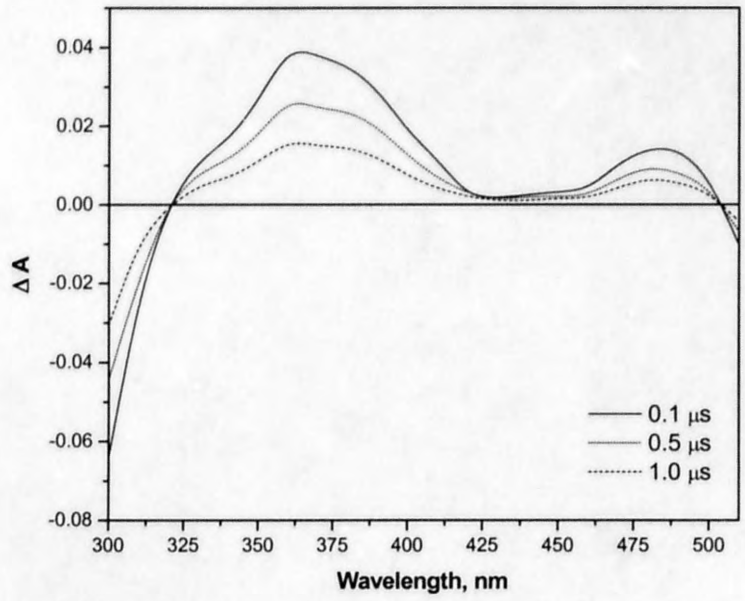

Figure 3.3.18. Excited state absorption difference spectra of **2** in toluene following 416 nm excitation. The delay times are specified on the spectrum.

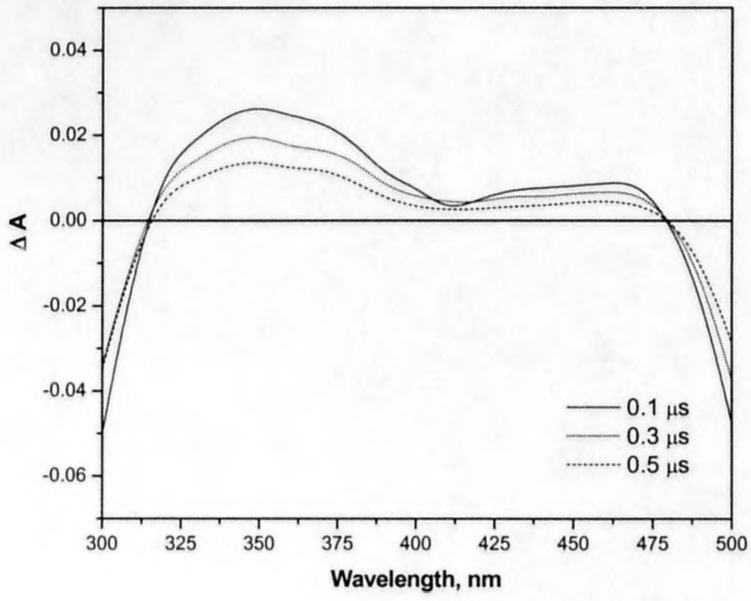

Figure 3.3.19. Excited state absorption difference spectra of **2** in CH_3CN following 416 nm excitation. The delay times are specified on the spectrum.

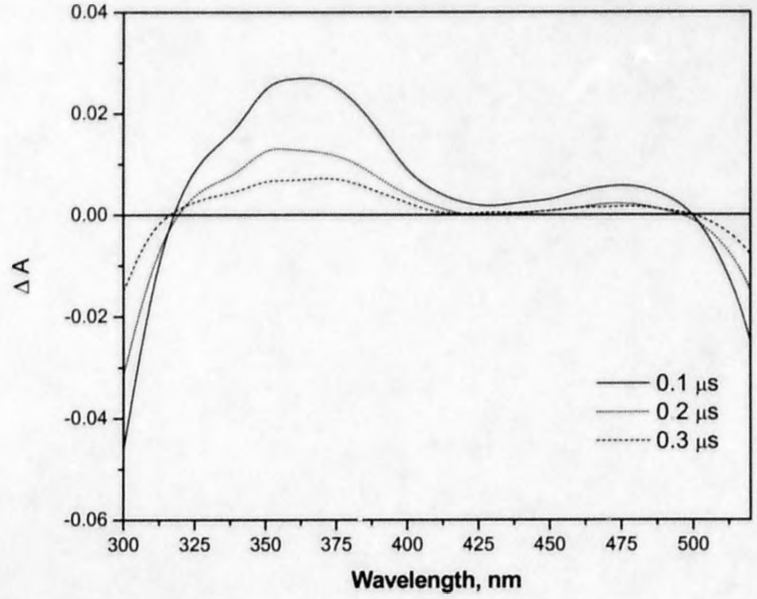

Figure 3.3.20. Excited state absorption difference spectra of **2** in MTHF following 416 nm excitation. The delay times are specified on the spectrum.

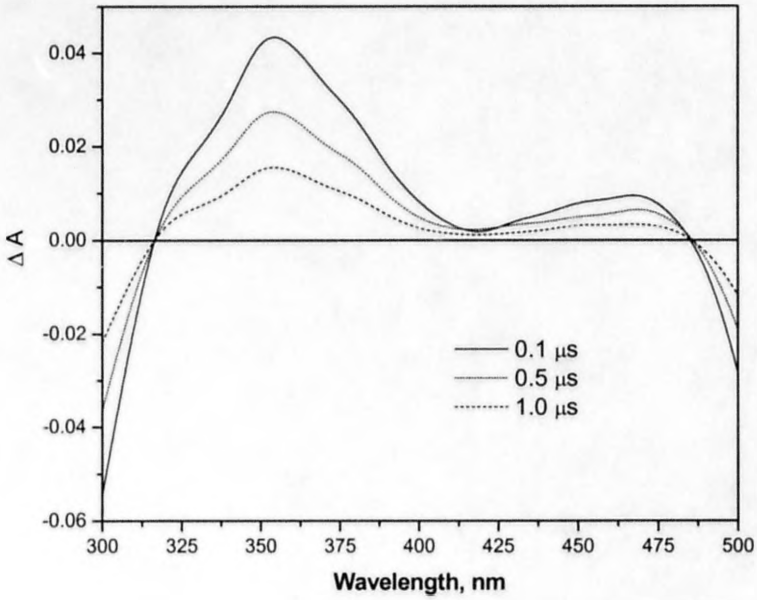

Figure 3.3.21. Excited state absorption difference spectra of **2** in BuCN following 416 nm excitation. The delay times are specified on the spectrum.

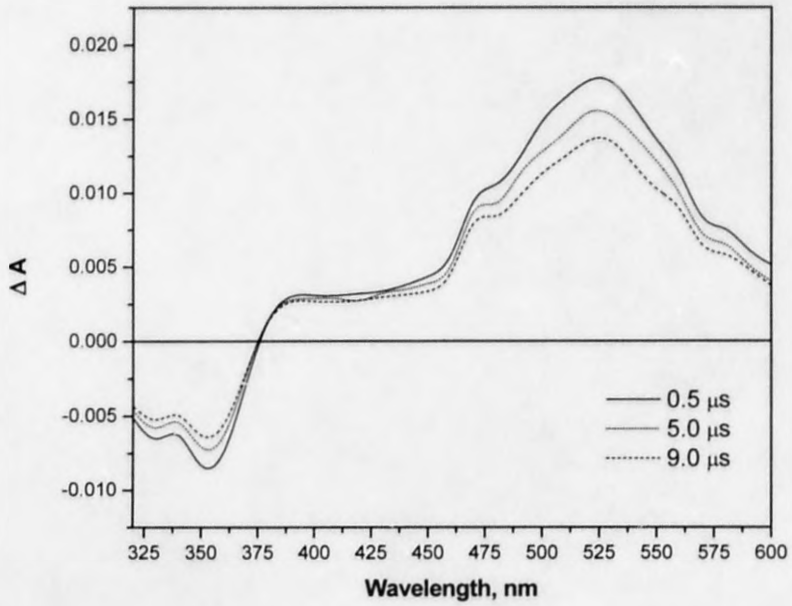

Figure 3.3.22. Excited state absorption difference spectra of **10** in MTHF following 355 nm excitation. The delay times are specified on the spectrum.

Low Temperature Photoluminescence

Luminescence spectra obtained at 77 K also yield some insight into the nature of the lowest excited state in **7**. All low temperature luminescence data are cataloged in Table 3.3.2. Figures 3.3.23, 3.3.25 and 3.3.26 present the room temperature and 77 K spectra of compounds **7, 10, 2** measured in MTHF, selected because of its low polarity and capacity to readily form high quality low temperature glasses. Immediately one notices that the thermally-induced Stokes shifts ($\Delta E_s = E_{00}(77\ K) - E_{00}(298\ K)$) observed for **2** are extraordinarily large in the nonpolar MTHF solvent (ΔE_s = 2470 cm^{-1}), consistent with previous observations from the Schanze laboratory in related complexes[58], Figure 3.3.25.

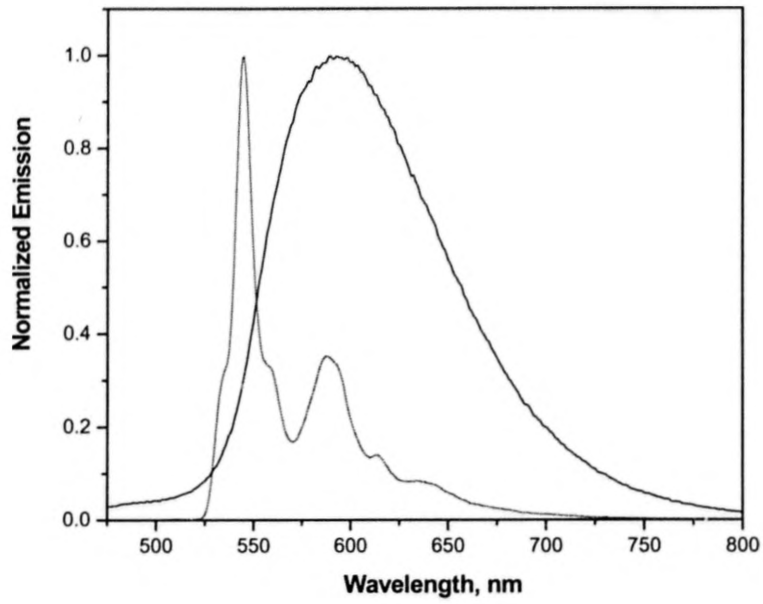

Figure 3.3.23. Room temperature (solid line) and 77K (dotted line) spectra of **7** in MTHF.

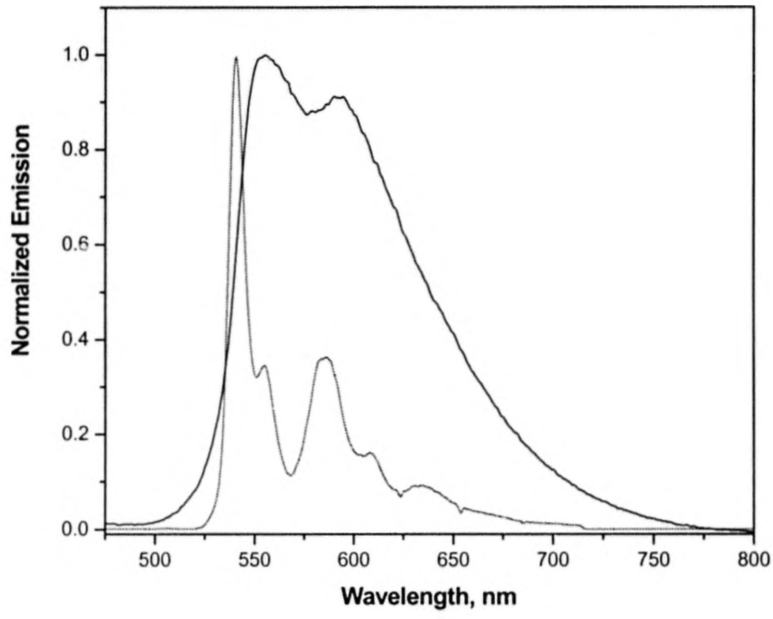

Figure 3.3.24. Room temperature (solid line) and 77K (dotted line) spectra of **7** in BuCN.

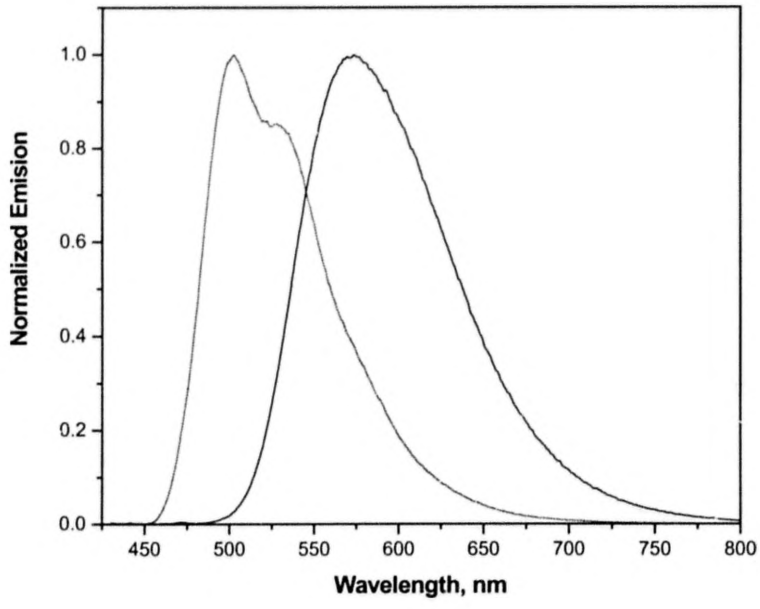

Figure 3.3.25. Room temperature (solid line) and 77K (dotted line) spectra of **2** in MTHF.

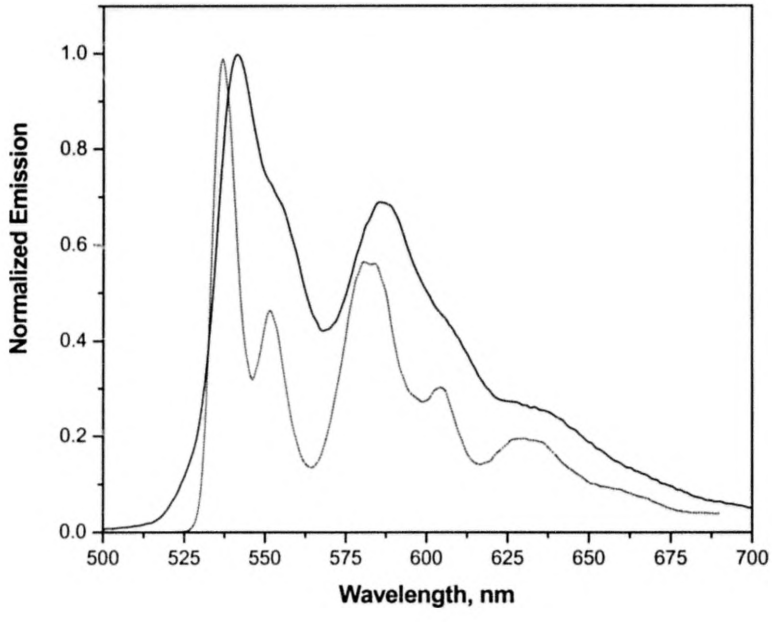

Figure 3.3.26. Room temperature (solid line) and 77K (dotted line) spectra of **10** in MTHF.

This indicates the likelihood of a charge-transfer excited state in **2**, as there are clearly large differences in ground and excited state dipole moments.[36] In the model system **10**, ΔE_s plummets to ~170 cm^{-1} (Figure 3.3.26), signaling the low level of charge redistribution typically associated with π-π^*-based intraligand transitions, such as those expected from the phosphorescence of the naphthaleneacetylide ligands. Therefore, the magnitude of ΔE_s serves as an indicator for the nature of the luminescence from the lowest excited state. Interestingly, the ΔE_s values are very distinct in complex **7**, varying from 1490 cm^{-1} in MTHF (Figure 3.3.23) to 230 cm^{-1} in BuCN (Figure 3.3.24).

We interpret this result in much the same manner as all previous data in the chapter. In more polar solvents, the ΔE_s values in **7** are small and within experimental error of that measured in reference system **10**, more consistent with a ^{3}IL naphthaleneacetylide-based lowest excited state. In low polarity solvents, the ΔE_s values in **7** are large, but not nearly as large as the values obtained in model system **2** (Figure 3.3.25). This latter result suggests that the excited state is composed mainly of ^{3}MLCT character, but there are likely contributions from the ^{3}IL manifold as well. In any case, the ΔE_s values are much smaller in **7** relative to **2** and the emission profiles at low temperature are markedly different, signaling a fundamental difference in the excited state composition of the two Pt(II) chromophores. To further investigate potential triplet state electronic interactions in **7**, we measured the static and dynamic luminescence properties of this complex at 77 K and compared these data to that measured for **2**.[31,73-75] Table 3.3.2 presents the static and dynamic photophysical data obtained for these complexes at 77 K in each solvent glass. In all glass matrices studied, the emission at 77 K in **7** is derived exclusively from the C≡C-Napthalene fragment(s) and its spectrum is

largely invariant to the polarity of each matrix, Figure 3.3.27. In other words, the apparent state reordering seen at room temperature is no longer observed at low temperature. The measured low temperature lifetimes are independent of monitoring wavelength, implying the presence of one type of emitting state. The 77 K spectral data obtained for **2** vary with the nature of the matrix (Figure 3.3.28), blue shifting with increasing polarity. Therefore, we rationalized that the only energy levels that significantly shift with solvent matrix in **7** are those associated with $d\pi$ Pt $\rightarrow \pi^*$ dbbpy MLCT states.

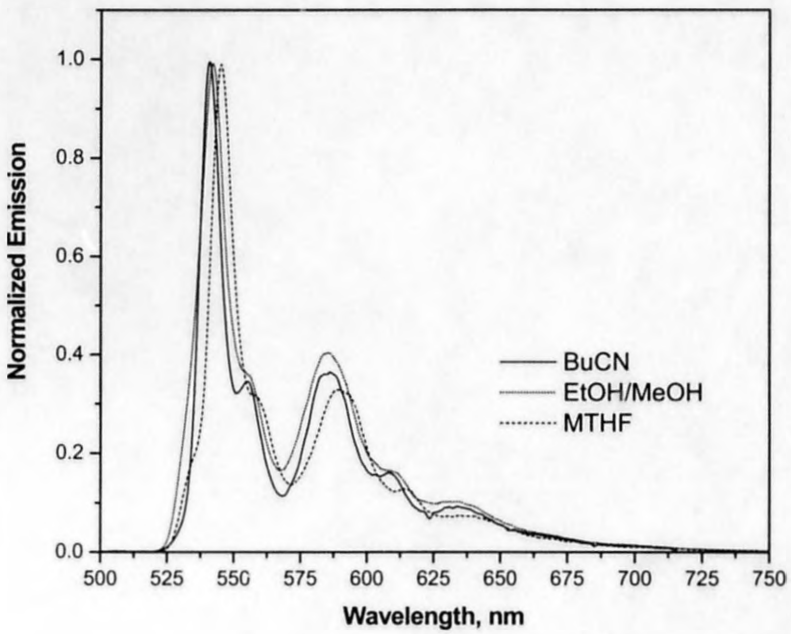

Figure 3.3.27. 77 K spectra of **7** in different matrices (depicted on the figure).

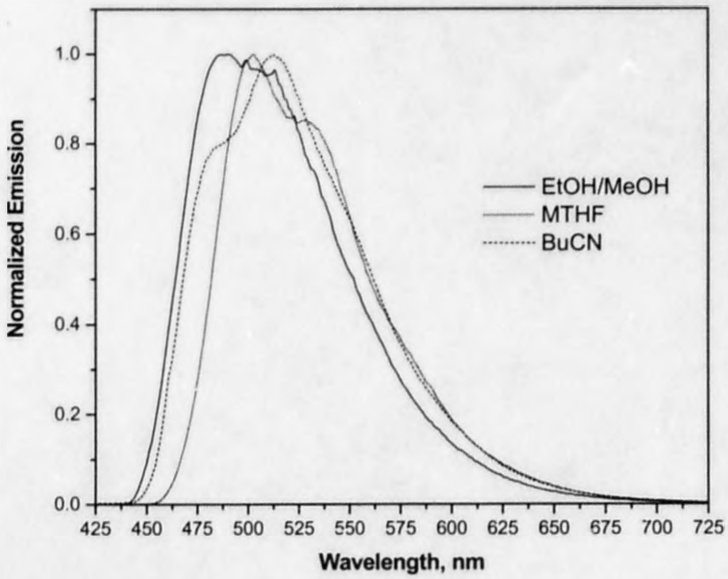

Figure 3.3.28. 77 K spectra of **2** in different matrices (depicted on the figure).

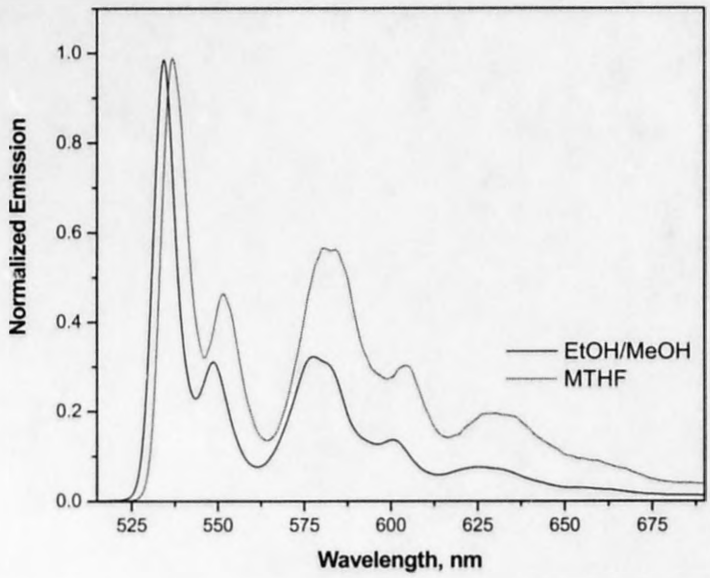

Figure 3.3.29. 77 K spectra of **10** in different matrices (depicted on the figure).

Interestingly, the excited state lifetimes measured at 77 K for **7** are much longer and vary as a function of matrix whereas those measured for **2** are nearly constant and are relatively short lived in comparison, Figure 3.3.32. Qualitatively, as the ^{3}MLCT-^{3}IL energy gap becomes larger (see Table 3.3.2), the lifetimes measured for **7** increase reaching 100 μs in EtOH/MeOH (4:1) matrix, suggesting that there is indeed a perturbation induced on the ^{3}IL level by the ^{3}MLCT state. We believe that the extent of this interaction dictates the lifetime observed from the lowest excited state.[73-75] Emission decay of **7** in BuCN at 77K is presented as an example on Figure 3.3.30.

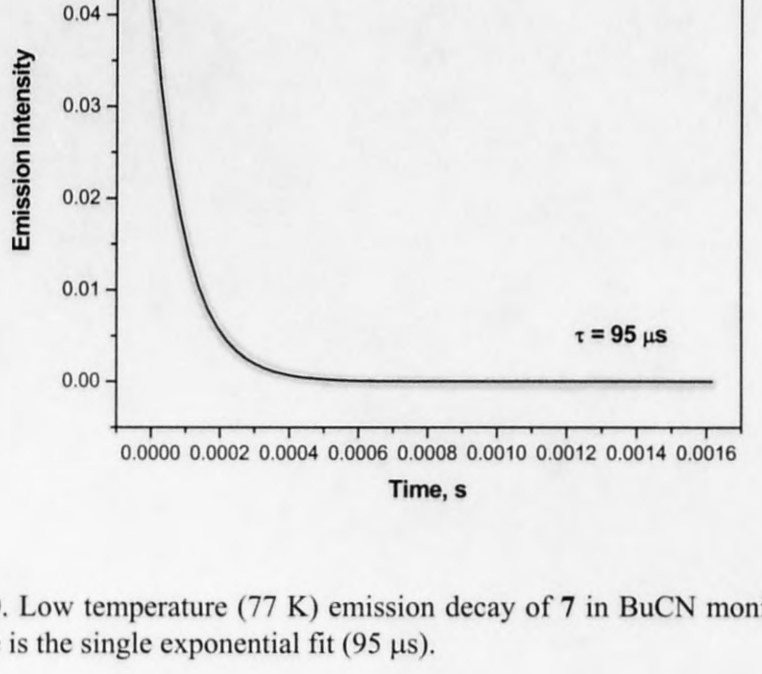

Figure 3.3.30. Low temperature (77 K) emission decay of **7** in BuCN monitored at 541 nm. Solid line is the single exponential fit (95 μs).

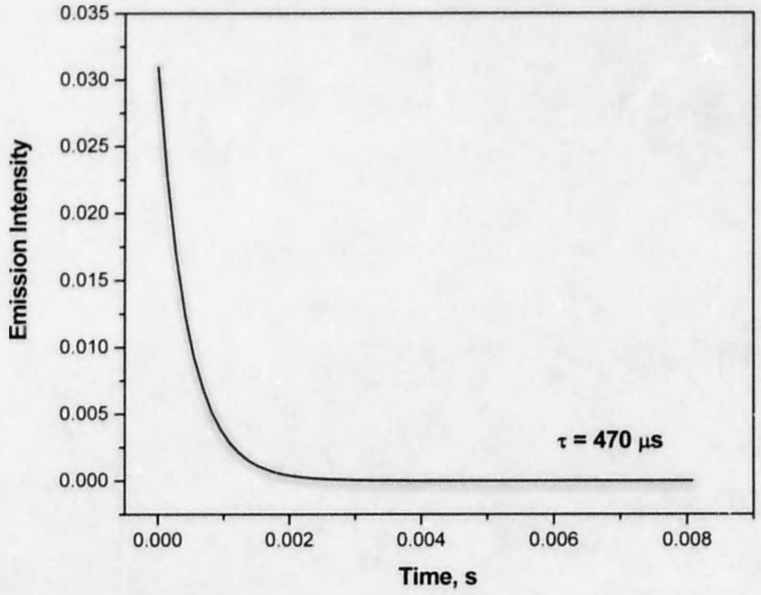

Figure 3.3.31. Low temperature (77 K) emission decay of **10** in MTHF monitored at 537 nm. Solid line is the single exponential fit (470 μs).

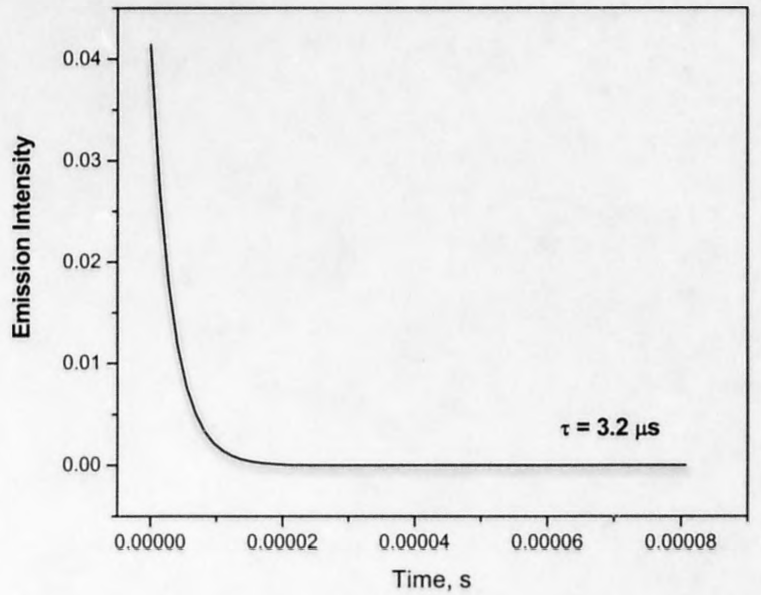

Figure 3.3.32. Low temperature (77 K) emission decay of **2** in BuCN monitored at 487 nm. Solid line is the single exponential fit (3.2 μs).

The longest 77K lifetime observed for **7** is not nearly as large as that of **10**, Figure 3.3.31. Unfortunately, the relative energy levels available in the present case prevent a true test of this model because the two relevant states at 77 K never really approach "resonance."

In 3MP, the solvent with the smallest measured triplet energy gap, the states are separated by ~1480 cm^{-1}, well beyond that required for significant configuration interaction.[31] In any case, our data appear to be qualitatively consistent with the first-order perturbation model proposed by Crosby and coworkers over 30 years ago, used to describe electronic interactions between charge transfer and ligand localized triplet states in Ir(III) diimine complexes at low temperature.[31,73-75]

Table 3.3.2. Luminescence Data at 77 K.

Compound	Solvent Matrix[a]	$\lambda_{em.}$, nm (cm^{-1})[b]	τ, μs[c]	^{3}MLCT-^{3}IL gap, cm^{-1} [d]
7	EtOH/MeOH	542 (18450)	100	1960
	BuCN	541 (18480)	95	2050
	MTHF	545 (18350)	65	1570
	3MP	546 (18310)	61	1640
2	EtOH/MeOH	490 (20410)	3.51	-
	BuCN	487 (20530)[e]	3.20	-
	MTHF	502 (19920)	3.35	-
	3MP	501 (19960)	2.58	-
10	MTHF	537 (18620)	470	-

[a]EtOH/MeOH = 4:1 EtOH/MeOH; BuCN = butyronitrile; 3MP = 3-methylpentane; [b]Emission maximum, ± 2 nm; [c]Emission decay lifetime, ± 10%; [d] ^{3}MLCT/^{3}IL gap, calculated by the difference in the E_{00} energies of **3** and **1** at 77 K in each matrix, ± ~200 cm^{-1}; [e]High energy shoulder.

CHAPTER III.IV. ROOM TEMPERATURE PHOSPHORESCENCE FROM A Pt(II) DIIMINE BIS(ARYLACETYLIDE) COMPLEXES

Structures

In the present work, new Pt(II)diimine complexes, Pt(dbbpy)(C≡C-Pyrene)$_2$ (**12**), Pt(dbbpy)(C≡C-Anthracene)$_2$ (**16**) and Pt(dbbpy)(C≡C-Perylene)$_2$ (**17**), where dbbpy = 4,4'-di(*tert*-butyl)-2,2'-bipyridine (C≡C-Pyrene, C≡C-Anthracene and C≡C-Perylene are 1-ethynylpyrene, 9-ethynylanthracene and 3-ethynylperylene respectively) have been synthesized and their photophysical properties have been thoroughly investigated. Syntheses of compounds **12**, **16** and **17** are described in the synthetic chapter of the thesis. Pt(dbbpy)(C≡C-Perylene)$_2$ (**17**) has been synthesized from the ethynylperylene, generously provided by J. Moore group. The newly synthesized compounds were structurally characterized by multiple analytical methods. As a consequence of the design the ^{3}IL arylacetylide-based states in the molecules are strategically positioned below the Pt $d\pi\rightarrow\pi^*$ (dbbpy) MLCT state therefore intraligand-centered phosphorescence is expected. *trans*-Pt(PBu$_3$)$_2$(C≡C-Pyrene)$_2$ (**13**)[12,13] served as a model for compound **12** and is vital for this study since it does not possess any MLCT excited states but contains the Pt(II) center (to impart the heavy atom effect) and two pyrenylacetylide units in a *trans*-geometry to ensure the absence of intramolecular ground state interactions. Model compound **2** does possess MLCT excited state, but does not exhibit any phosphorescence at RT from solution but rather emits from its ^{3}MLCT state.[57]

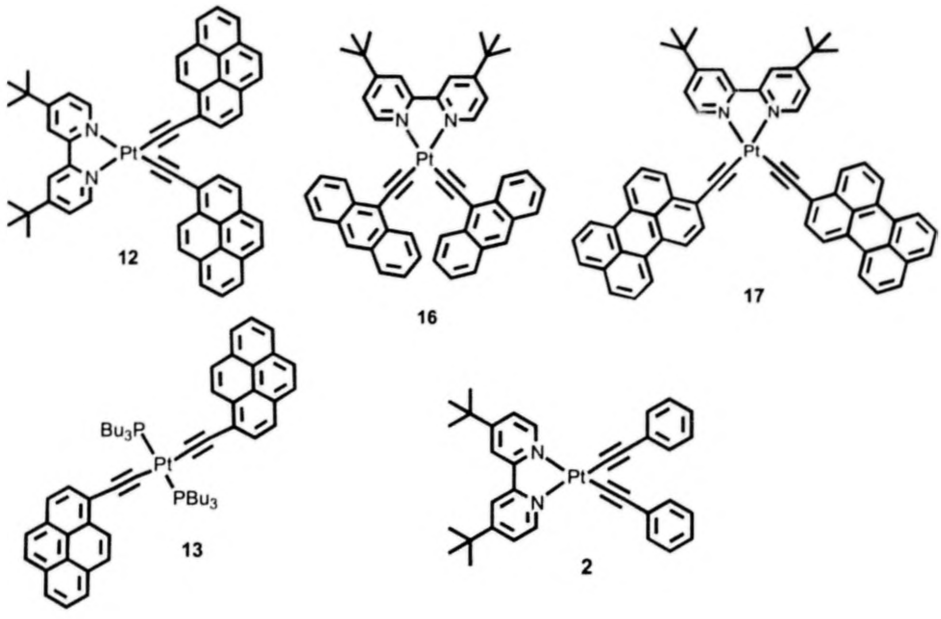

Therefore, Pt(dbbpy)(C≡C-Ph)$_2$ (**2**)[57] serves here as a model representing the ^{3}MLCT manifold in complexes **12, 13** and **16**. Due to the instability of **16** towards light and oxygen, only limited photophysical properties could be investigated.

Absorption properties

The absorption spectra of compounds **12**, **16** and **17** in dichloromethane are depicted on Figure 3.4.1. The arylacetylide chromophores are responsible for the structured π-π* transitions between 325 and 500 nm. The π-π* absorptions in **12** and **17** are substantially red shifted relative to those of free Pyrene-C≡C-H and Perylene-C≡C-H species (Figure 3.4.2 and 3.4.3), suggesting large sigma donation of the arylacetylide electron density to the Pt(II) center, Figure 3.4.2. The shift of the π-π* transitions to the lower energy going from C≡C-pyrene to the C≡C-perylene is due to the more extended conjugation in the series.

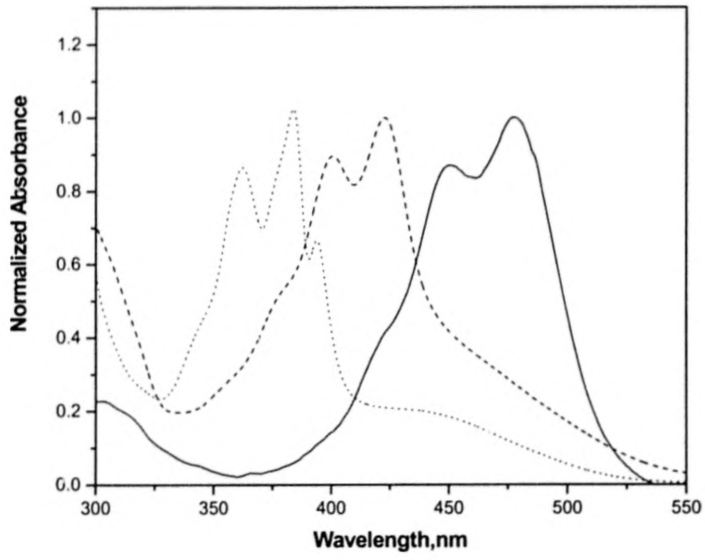

Figure 3.4.1. UV-Vis spectra of **17** in DCE (solid line), **16** in CH_2Cl_2 (dashed line) and **12** in CH_2Cl_2 (dotted line).

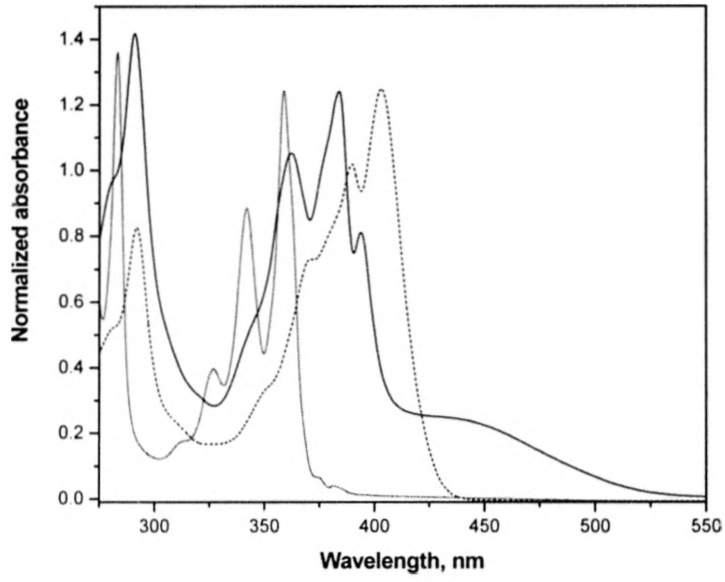

Figure 3.4.2. UV-Vis spectra of compound **12** (solid line), **13** (dashed line) and Pyrene-C≡C-H (dotted line) in CH_2Cl_2.

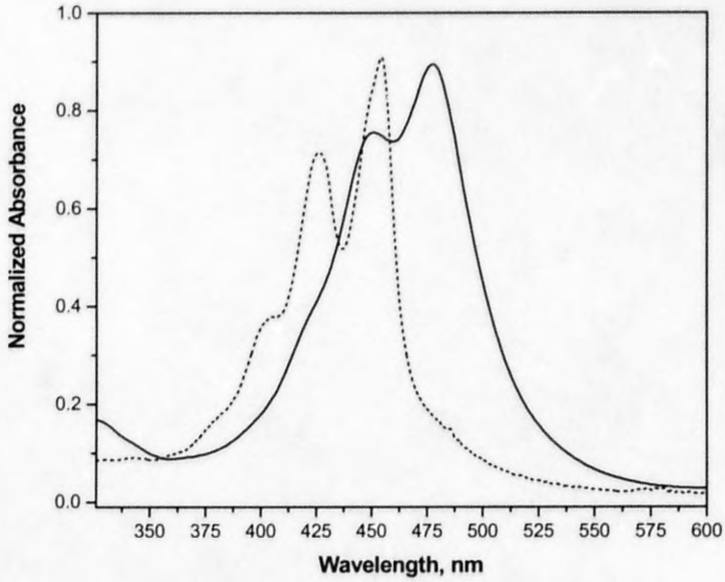

Figure 3.4.3. UV-Vis spectra of **17** (solid line) and Perylene-C≡C-H (dotted line) in MTHF.

The visible absorption bands near 450 nm observed for complexes **12** and **16** are believed to be attributed to the Pt $d\pi \rightarrow \pi^*$ dbbpy MLCT transitions and, although red-shifted, are quantitatively similar to that of **2.** The low energy broad band in **2** centered at 400 nm (Figure 3.4.4) has been already assigned to Pt $d\pi \rightarrow \pi^*$ (dbbpy) MLCT absorption by Eisenberg and co-workers.[57] The ^{1}MLCT band in **17** can't be really distinguished under the broad and structured π-π^* transitions due to the fact that ^{3}IL and therefore ^{1}IL states of C≡C-Perylene ligand in **17** are located much lower in energy then corresponding pyrenylacetylide and anthracenylacetylide-based IL states in **12** and **16** respectively. Therefore, the ^{1}MLCT and ^{1}IL energies become comparable in **17** causing the π-π^* and MLCT transitions to overlap, Figure 3.4.31.

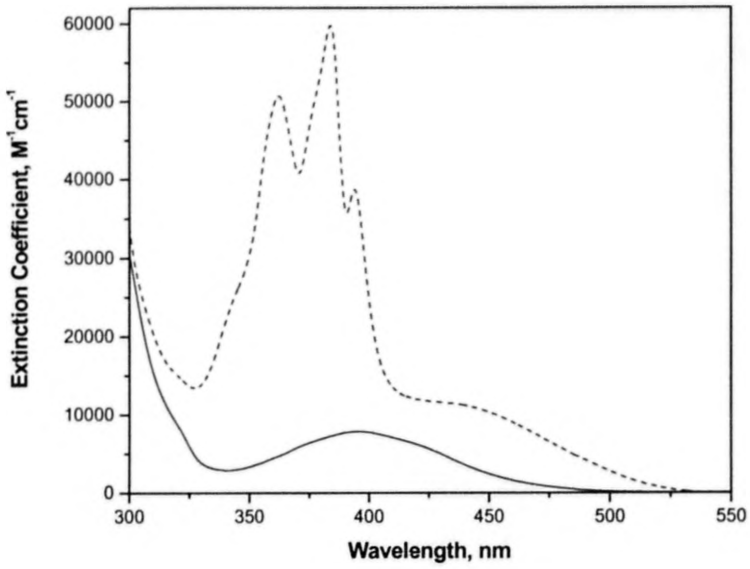

Figure 3.4.4. UV-Vis spectra of compound **12** (solid line) and **2** (dashed line) in deaerated CH_2Cl_2 at room temperature.

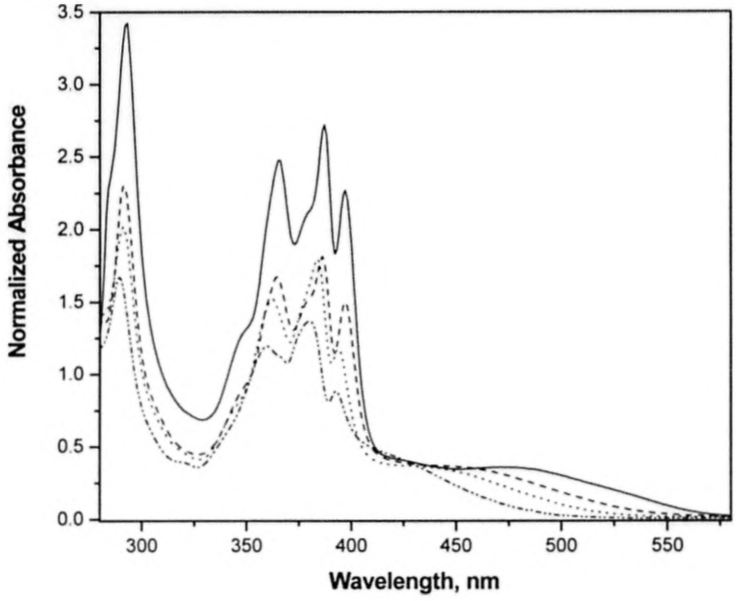

Figure 3.4.5. UV-Vis spectra of compound **12** in CH_2Cl_2 (dotted line), toluene (solid line), MeTHF (dashed line), CH_3CN (dash-dotted line).

MLCT assignment is consistent with the solvatochromic shifts observed for the low energy absorption bands in **12** (and **2**).[36,38,57] The absorption spectra of compound **12** in solvents of different polarities are depicted in Figure 3.4.5 as representative examples.

It should be noted that the sharp absorption features between 350 and 400 nm also exhibit solvatochromism, suggesting that that bands possess some charge transfer character or that they simply overlap with the broad MLCT bands. The red shift in the MLCT absorption band position going from the compound **2** through **12**, **16** to **17** is induced by the increasing of sigma-donation of arylacetylide electron density to the Pt(II) center in this series of compounds, Figures 3.4.4 and 3.4.1. The red shift of the MLCT absorption band upon the enhancing the electron donation ability of appended acetylide ligands has been previously reported by different groups in structurally related Pt(diimine)(C≡C-R)$_2$ complexes.[57,58]

Electrochemistry

The first reduction waves measured for **12** and **2**, obtained with cyclic voltammetry in dichloromethane, occur at the same potential within experimental error (-1.35 V vs. Ag/AgCl), Figure 3.4.6. and 3.4.7. Eisenberg and co-workers have already assigned this process to a dbbpy ligand-based reduction in **2**.[57] Reductive electrochemistry performed on Pyrene-C≡C-H yielded an irreversible process that initiates at -1.73 V. It is therefore reasonable to assume that the lowest acceptor ligand orbital is located on dbbpy in **12**. Consistent with other related Pt(II) diimine bis(acetylide) complexes, **12** and **2** displayed irreversible metal-based oxidations at +0.95 V and +1.11 V, respectively.[57,58,76]

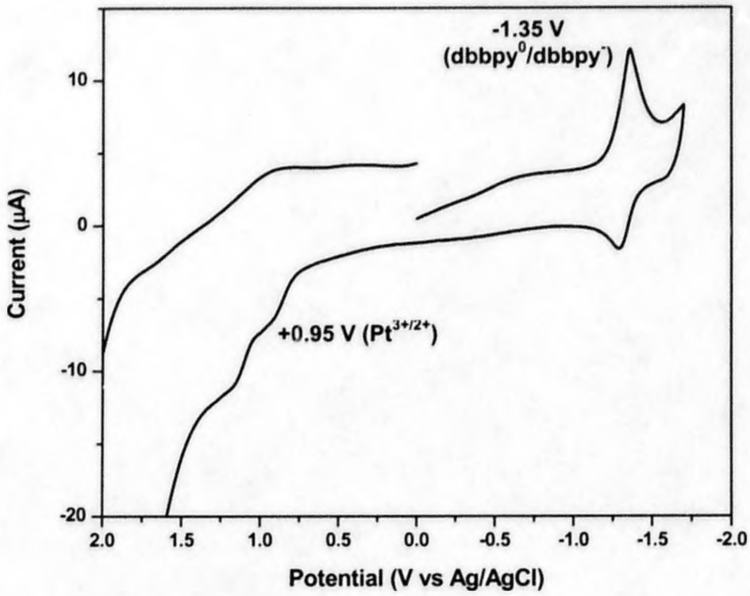

Figure 3.4.6. Cyclic voltammogram of compound **12** in CH_3CN with 0.1 M TBAP.

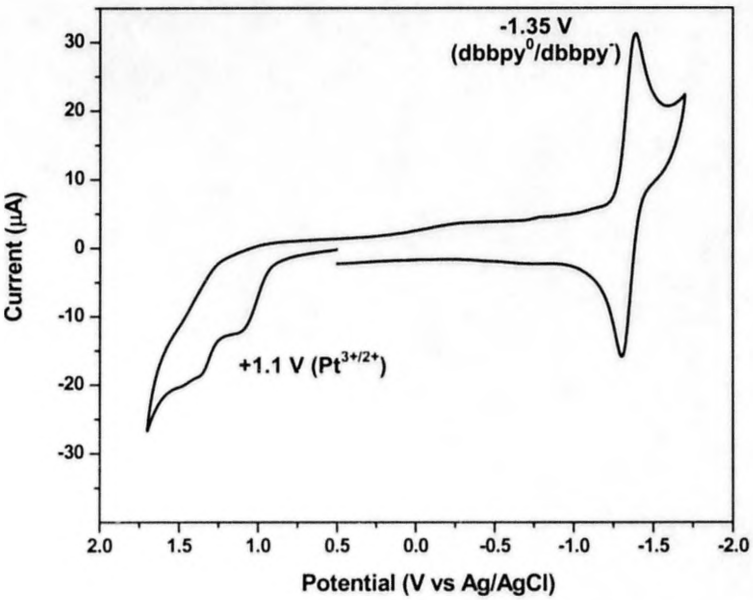

Figure 3.4.7. Cyclic voltammogram of compound **2** in CH_3CN with 0.1 M TBAP.

The fact that the former is shifted to a more negative potential reflects significant sigma donation of electron density from the C≡C-pyrenyl units to the Pt (II) center, consistent with the red shift observed in the absorption spectrum.

Photoluminescence properties

Excitation of **2**, **12** and **16** at 480 nm produces a distinct emission spectrum in each case, Figure 3.4.8. The luminescence in **2** has already been shown to originate from an MLCT manifold,[57,58] whereas the emission from **12** and **16** are red-shifted (up to 200 nm), structured, and relatively sharp in comparison, Figure 3.4.7. Due to the substantial overlap of the $\pi \rightarrow \pi^*$ anthrasenylacetylide and $d\pi$ Pt $\rightarrow \pi^*$ (diimine) absorption bands, the excitation at low energy MLCT transition at 480 nm results in both fluorescence and phosphorescence, emanating from anthracenylacetylide ligands, however, only the phosphorescence is shown in Figure 3.4.8. The observed phosphorescence from the ethynylperylene moieties in **17**, following excitation in the visible region was very weak, nevertheless vibronic transitions are quite distinguishable with a maximum around 1010 nm in the near-IR, Figure 3.4.9. The low emission intensity could be attributed to the expected high rate of non-radiative decay. The result is consistent with the energy gap law, which states that as the energy gap between ground and excited state decreases, k_{nr} increases exponentially.[77] I would like to thank Dr. K. Schanze and co-workers (University of Florida) for measuring the room temperature and 77 K photoluminescence properties of **17** in the near-IR.

The quantum yield for **12**, measured relative to $[Ru(bpy)_3]ClO_4$ was determined to be 0.011 in deaerated dichloromethane. It is important to mention that the quantum yield of **2** in dichloromethane was 0.11 which is ten times larger than quantum yield of **12** measured under the same conditions. The quantum yields for **16** and **17** haven't been specifically measured, but based on experimental observations believed to be below 1%. This observation provides additional evidence that emission of **12**, **16** and **17** does not originate from the MLCT manifold but rather from the ^{3}IL state.

The model compound **13** exhibits both fluorescence and phosphorescence upon the excitation into the pyrenylacetylide π-π^* absorption band. It is clear, that phosphorescence part of the spectra of **13** is superimposable with the emission spectrum of **12**, obtained from direct MLCT excitation, providing the additional evidence for ^{3}IL pyrenylacetylide-based phosphorescence in **12**, Figure 3.4.10

The RT emission spectrum of **2** was easily measured in aerated dichloromethane whereas the corresponding spectra for **12**, **16** and **17** are almost quantitatively quenched by dioxygen, necessitating its removal. The emission spectra of **12** in aerated and deaerated dichlomethane are compared on Figure 3.4.11, as an example.

The corrected excitation spectra of compounds **12**, **16** and **17** were largely identical with the corresponding absorption spectrum at all wavelengths above 400 nm and were completely invariant to the monitoring wavelength, indicating that the ^{3}IL phosphorescence from the arylacetylide manifold can be sensitized by MLCT excitation. The normalized absorption and excitation spectra of **12** in CH_2Cl_2 are presented in Figure 3.4.12.

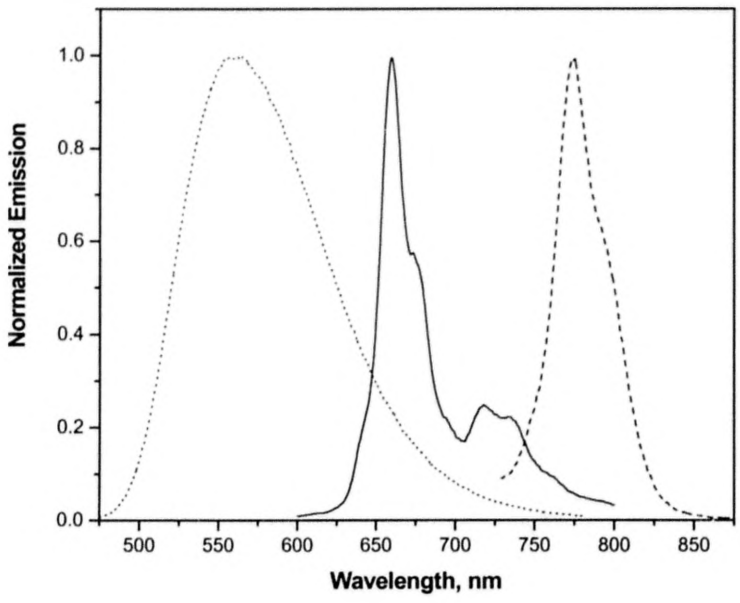

Figure 3.4.8. Normalized emission spectra of **12** (solid line), **16** (dashed line) and **2** (dotted line) in deaerated CH_2Cl_2 recorded using 480 ± 2 nm excitation.

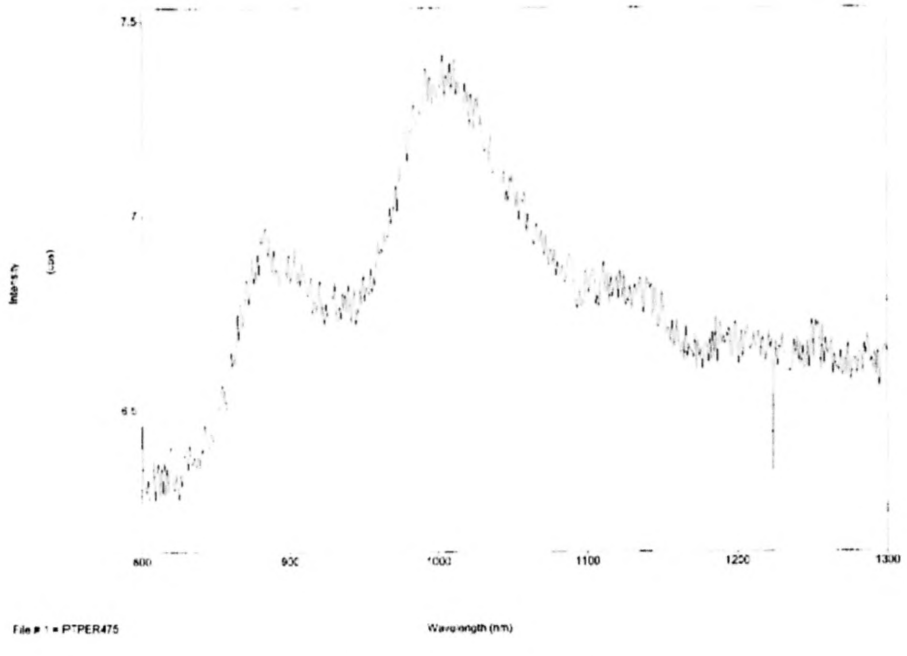

Figure 3.4.9. Emission spectrum of **17** in deaerated MTHF.

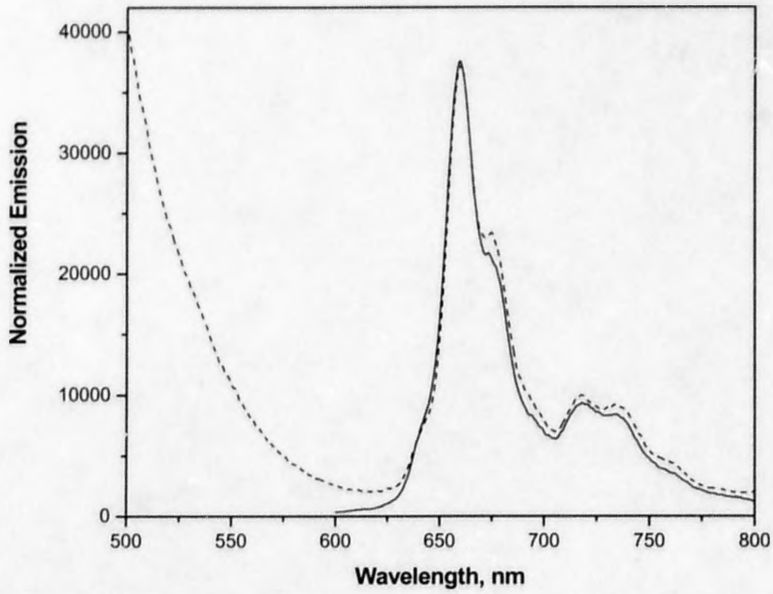

Figure 3.4.10. Normalized emission spectra of **12** (solid line) and **13** (dashed line) in deaerated CH_2Cl_2 recorded using 480 ± 2 nm and 400 ± 2 nm excitations respectively.

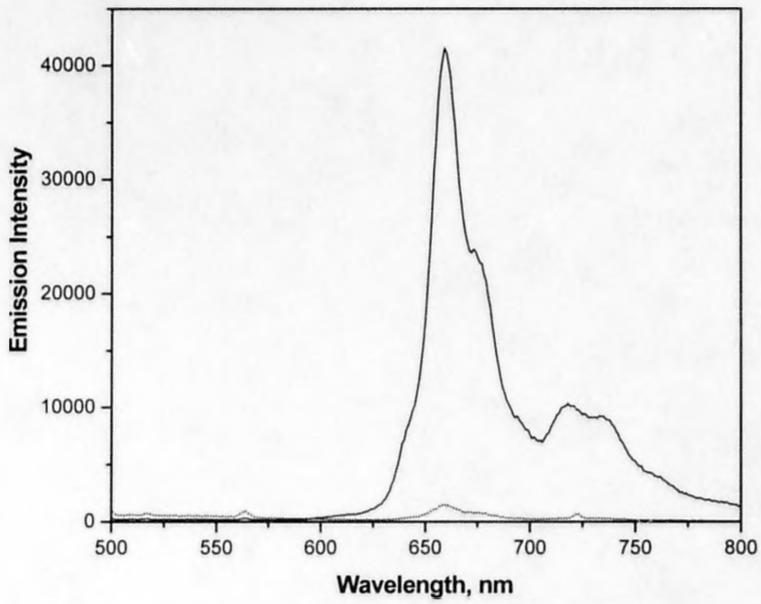

Figure 3.4.11. Emission spectrum of **12** in aerated (dashed line) and deaerated (solid line) CH_2Cl_2.

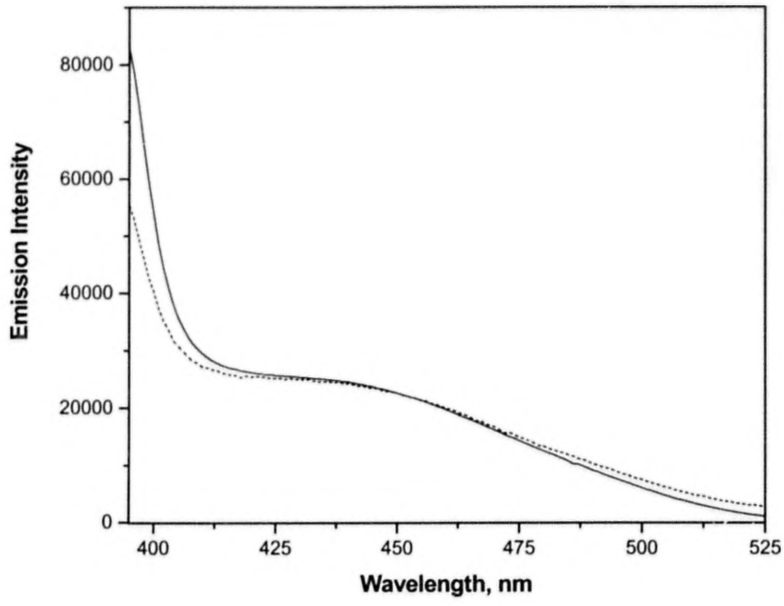

Figure 3.4.12. Normalized absorption (solid line) and excitation (dashed line) spectra of **12** in deaerated CH_2Cl_2 monitored at 660 nm.

The insignificant deviation from the ideal overlap in the absorption and excitation spectra could be accounted for the wavelength dependence of the fluorimeter wavelength response and presence of multiple chromophores in the molecule.[78]

The excitation spectrum of **17** was quite noisy and didn't show pronounced structured π-π^* transitions observed in corresponding absorption spectrum due to the very weak intensity of the emission at room temperature, Figure 3.4.13. For the model compound **2**, the excitation spectrum also displayed a significant overlap with absorption spectrum in the region of MLCT transition (340-400 nm) and was invariant to the monitoring wavelength, Figure 3.4.14.

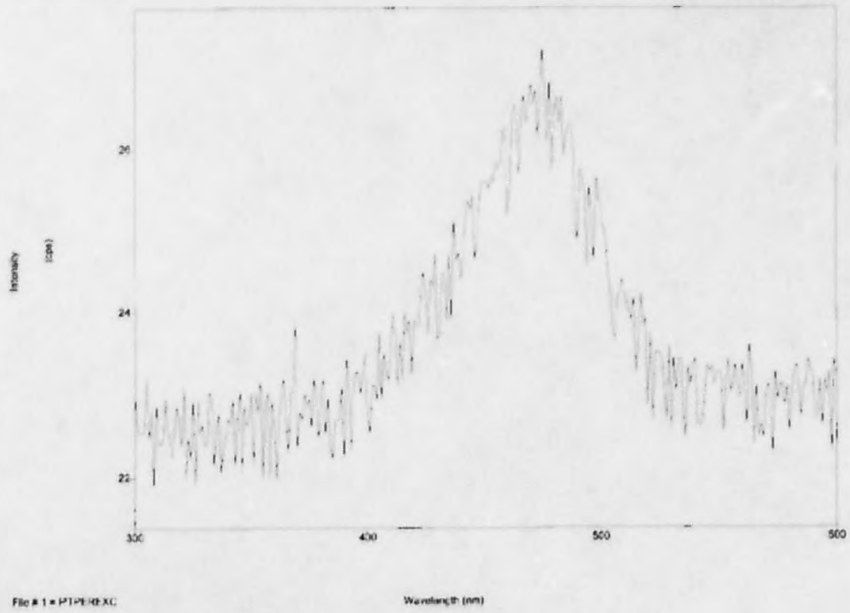

Figure 3.4.13. Excitation spectrum of **17** in MTHF.

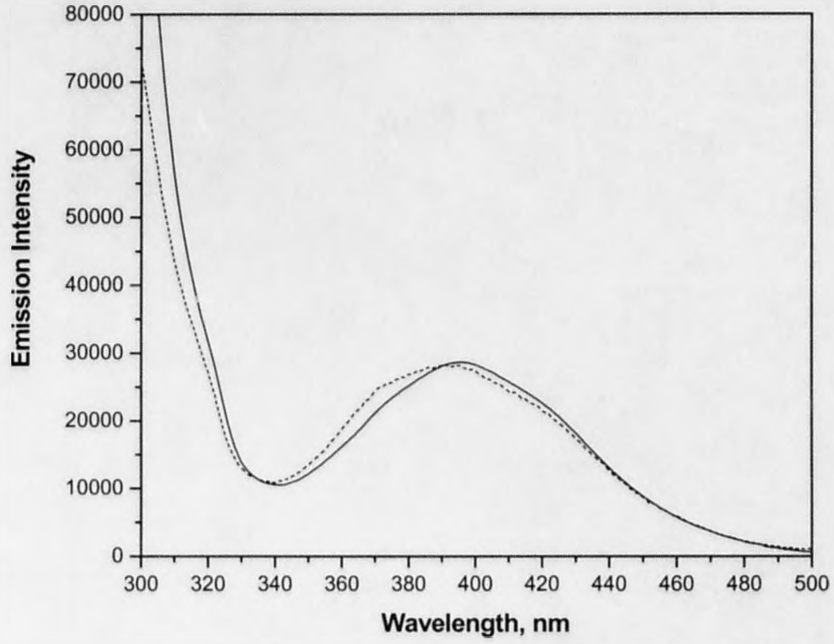

Figure 3.4.14. Normalized absorption (solid line) and excitation (dashed line) spectra of **2** in deaerated CH_2Cl_2 monitored at 560 nm.

Room Temperature Photoluminescence Dynamics

Since Pt(II) chromophores of this type are known to undergo excited state self-quenching reactions,[52,56-58,62] all luminescence experiments were performed at or below 10 μM, where the measured lifetimes were invariant to concentration. The excitation wavelength of 460 nm was used for compounds **2**, **12** and **16** in order to predominantly excite the low-energy MLCT state. The RT luminescence lifetimes of **12, 16** and **2**, measured with a broadband N_2-pumped dye laser (460 ± 2 nm, 500 ps fwhm) in deaerated CH_2Cl_2, were also strikingly different, 48.5 μs, 8.4 μs and 1.25 μs respectively. All emission decays followed single-exponential kinetics and are presented in Figures 3.4.15 - 3.4.17. Using 357 nm excitation, the lifetime of the phosphorescence of **13** in deaerated CH_2Cl_2 was determined to be 68 μs (Figure 3.4.18), which is similar to that measured for **12** following visible MLCT excitation. Therefore, the photophysical properties of **12** are clearly not attributed to an excited state composed of MLCT parentage.

The lifetime of **17** estimated from the TA experiment was 8 μs, Figure 3.4.19. The relatively long lifetime of **16** and **17** provide additional evidence to ^{3}IL origin of lowest excited state in the molecules.

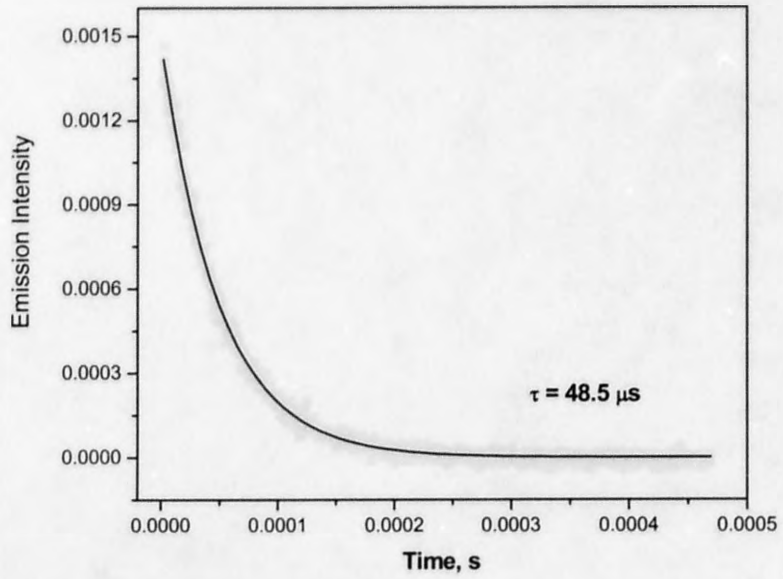

Figure 3.4.15. Phosphorescence lifetime of **12** in deaerated CH_2Cl_2 followed by 460 ± 2 nm excitation. Solid line is the single exponential fit (48.4 μs).

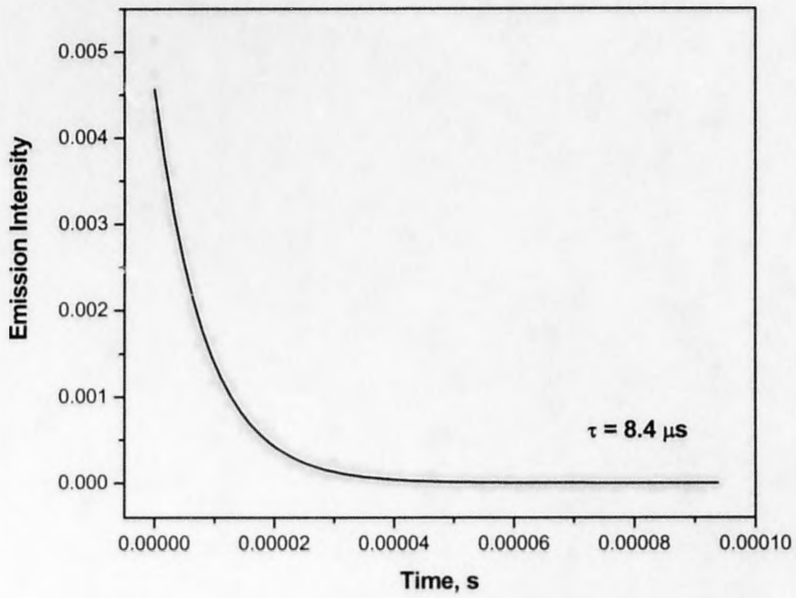

Figure 3.4.16. Room temperature emission decay of **16** in deaerated CH_2Cl_2 followed by 460 ± 2 nm excitation. Solid line is the single exponential fit (8.4 μs).

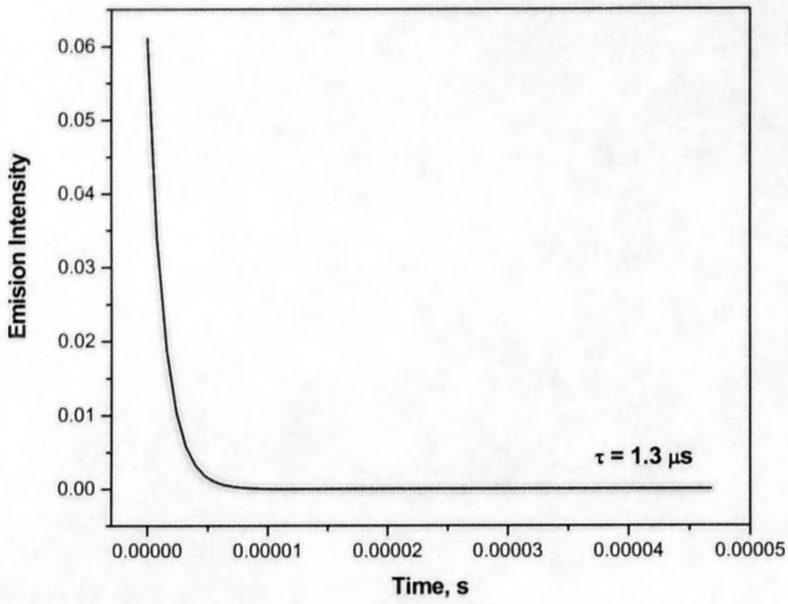

Figure 3.4.17. Luminescence lifetime decay of **2** in deaerated CH_2Cl_2 followed by 460 ± 2 nm excitation. Solid line is the single exponential fit (1.3 μs).

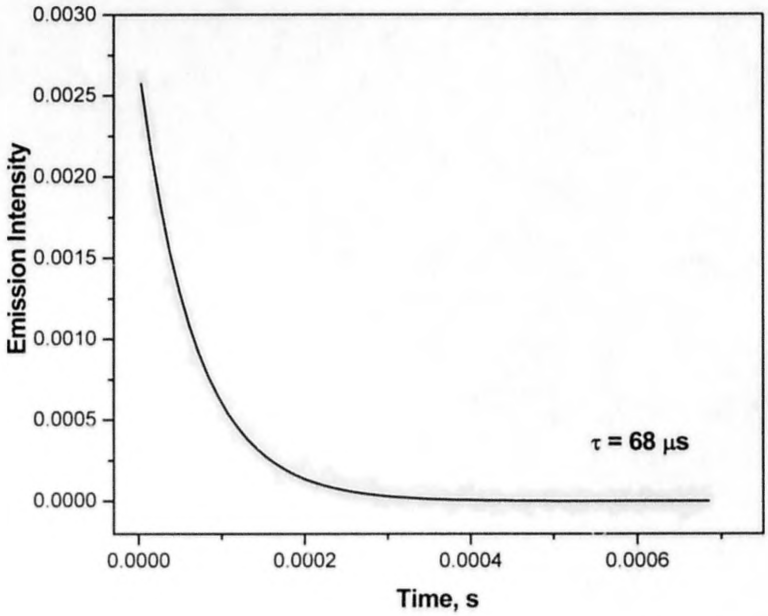

Figure 3.4.18. Phosphorescence lifetime decay of **13** in deaerated CH_2Cl_2 followed 357 nm excitation. Solid line is the single exponential fit (68 μs).

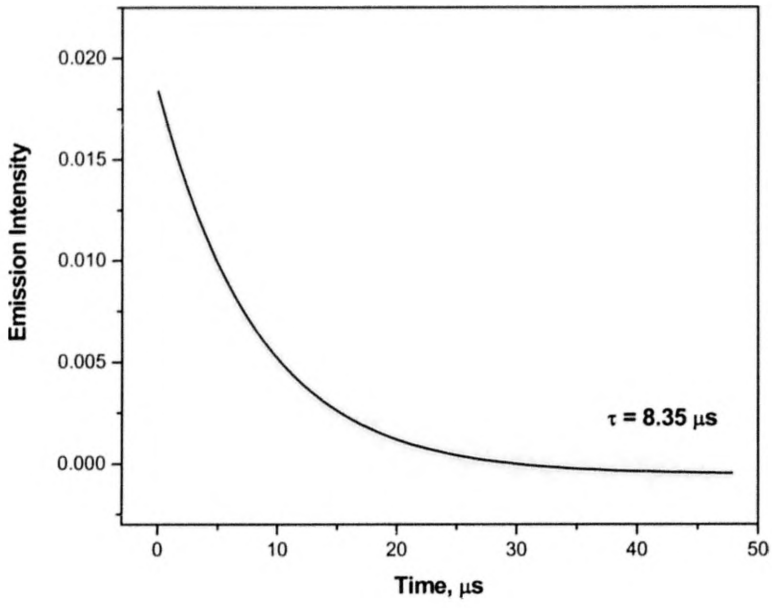

Figure 3.4.19. TA lifetime of **17** in deaerated MTHF monitored at 560 nm, followed by 416 nm laser flash. Solid line is the single exponential fit (8.35 μs).

Low-Temperature Photoluminescence

The emission spectra of **12** and **13** obtained at RT and 77 K in 4:1 EtOH/MeOH glass are compared in Figures 3.4.20 and 3.4.21. The difference in the RT and 77 K emission energies, or thermally induced Stokes shift (ΔE_s), is extremely small for both compounds, ~ 70 cm^{-1}. Under the same conditions, the luminescence from **2** displayed a substantial ΔE_s value of 2800 cm^{-1} (0.35 eV). Large values of ΔE_s are correlated with significant changes in dipole moment between ground and excited states, such as those attributed to MLCT excited states.[36,58] The small value of ΔE_s in the case of **12** indicates that the emission does not originate from MLCT excited state. The emission spectra obtained for **12** and **13** at both temperatures are nearly identical in shape and vibronic

spacing, illustrating that the emitting state in **12** is ^{3}IL phosphorescence from appended C≡C-Pyrenyl units. Surprisingly, the spectra are identical even though the pyrenyl fragments are in different molecular geometries around the Pt(II) center (*cis* in **12** and *trans* in **13**). The emission results strongly suggest that the two pyrenyl units do not interact (intramolecularly) at all in **12**. The 77 K emission spectrum of **12** is also identical in shape and vibronic spacing to the low temperature emission spectrum of Pyrene-C≡C-H model, Figure 3.4.22. The result provides additional evidence towards ^{3}IL Pyrenyl-C≡C- centered phosphorescence in **12**.

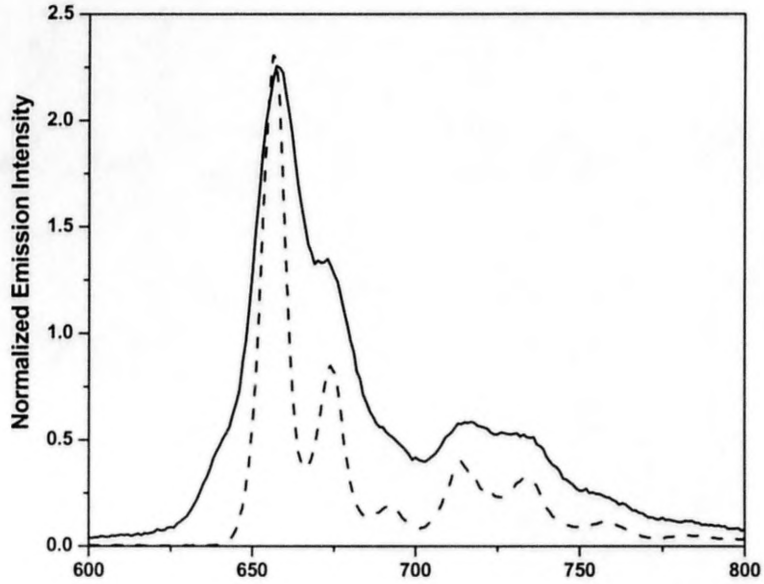

Figure 3.4.20. Emission spectrum (λ_{exc} = 480 ± 2 nm) measured for **12** in deaerated 4:1 EtOH/MeOH at room temperature (solid line) and at 77 K (dashed line).

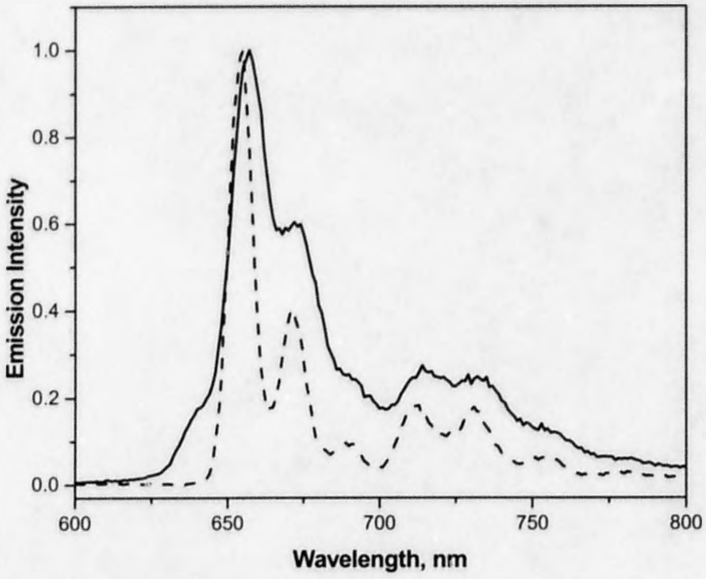

Figure 3.4.21. Emission spectrum (λ_{exc} = 400 ± 2 nm) measured for **13** in deaerated 4:1 EtOH/MeOH at room temperature (solid line) and at 77 K (dashed line).

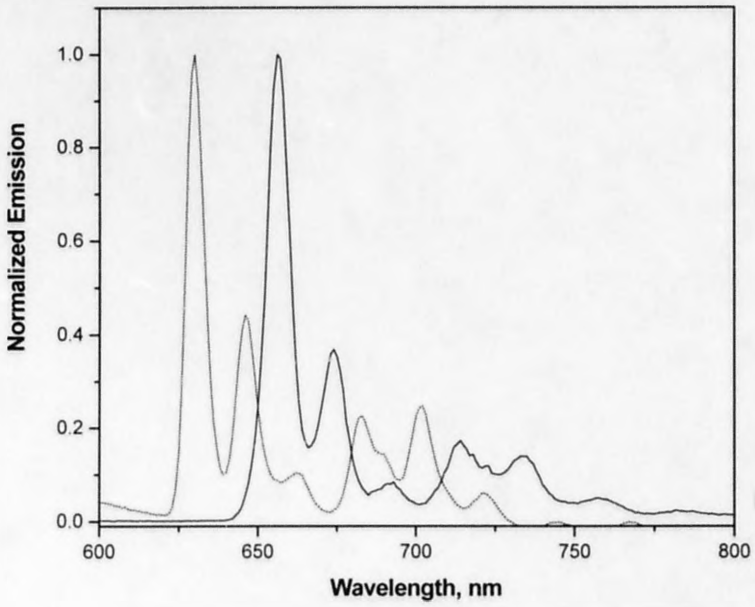

Figure 3.4.22. Phosphorescence spectrum of **12** (λ_{exc} = 480 ± 2 nm) (solid line) and Pyrene-C≡C-H in the presence of 10% ethyl iodide (λ_{exc} = 357 ± 2 nm) (doted line) at 77 K in a 4:1 EtOH/MeOH.

The room temperature and 77 K emission spectra of **16** at are compared in Figure 3.4.23. Importantly, that fluorescence in **16** becomes more structured at 77 K, exhibiting small values of thermally induced Stokes shifts confirming its anthracenylacetylide origin. The magnitude of ΔE_s for phosphorescence (~ 84 cm^{-1}) clearly points towards the ^{3}IL manifold. The low-temperature photoluminescence spectra of **17** were measured at the University of Florida by Dr. K. Schanze and co-workers. The experiment was performed in a cryostat and emission spectrum was taken every 20 K. The 77 K emission spectra of **17** in MTHF glass at different temperatures are shown on Figure 3.4.24 and display four distinctive vibronic transitions. It was observed, that the phosphorescence intensity grows dramatically (~ 8 times) as the temperature decreases from 220 to 80 K.

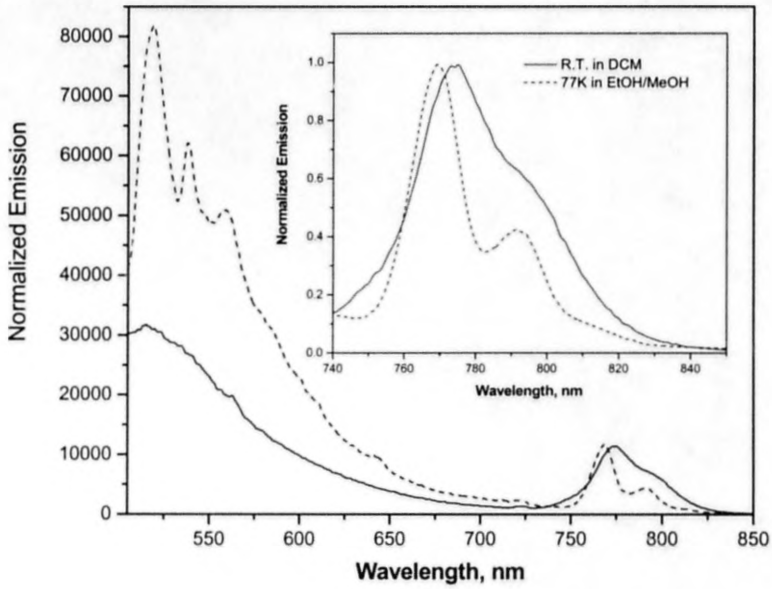

Figure 3.4.23. Emission spectra of **16** in deaerated CH_2Cl_2 at room temperature (solid line) and 77 K (dashed line) in EtOH/ MeOH (4:1) glass followed 480 nm excitation, normalized at ~ 775 nm.

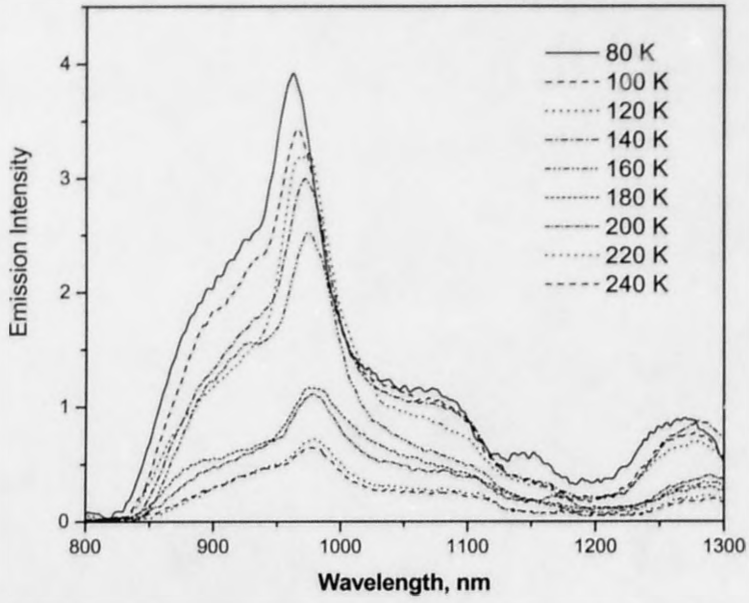

Figure 3.4.24. Emission spectra of **17** in MTHF glass in the 240 - 80K temperature interval.

Figure 3.4.25 is intended to summarize the relative shifts in phosphorescence maxima for all three ^{3}IL emitting complexes **12** and **16** in EtOH/MeOH glass at 77 K and **17** in MTHF at 80 K. The comparison of the all phosphorescence spectra in the same glass couldn't be accomplished due to the fact that the 80 K spectrum of **17** wasn't measured in-house. Nevertheless, the comparison can be justified by the fact that the energy of π-π^* states doesn't change significantly with the nature of the solvent. The tremendous changes in the emission maxima were observed, upon variation of the arylacetylide ligand. The photoluminescence properties of **17** can be potentially useful for near-IR emitting molecular devices.

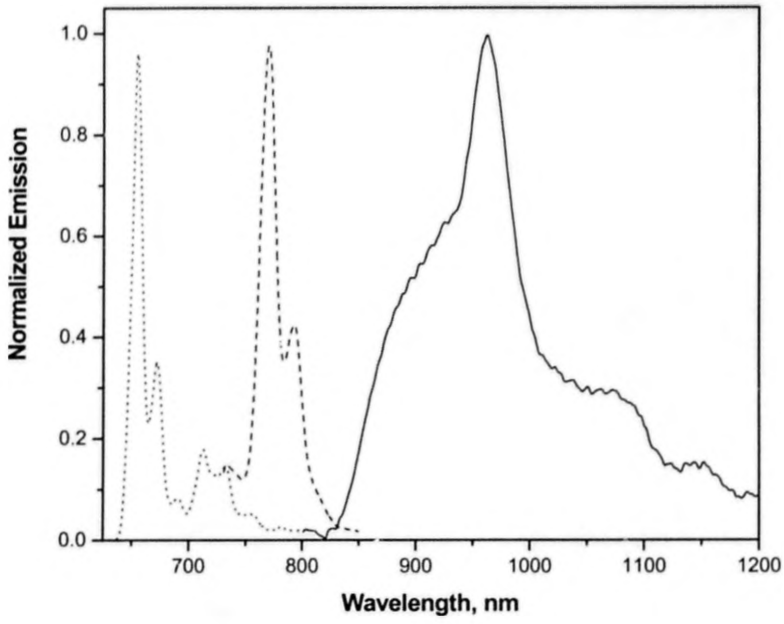

Figure 3.4.25. Normalized 77 K emission spectrum of **17** in MTHF galss (solid line), **16** (dashed line) and **12** (dotted line) in a EtOH / MeOH (4:1) glass.

Transient absorption

Additional support for the sensitization of the C≡C-Aryl-based ^{3}IL excited states in **12** and **17** comes from TA measurements. The TA experiments haven't been performed on **16** due to the sample decomposition. The absorption features observed for **2** are consistent with an MLCT excited state[58] (Figure 3.4.26), whereas the transients in **12** and **17** are completely different. Figures 3.4.27 and 3.4.29 display the absorption transient spectra obtained for **12** and **17** following a 355 nm and 416 nm laser flash respectively. The spectrum observed for **12** and **17** appeared promptly within the 15 ns instrument response so no information could be obtained on the evolution of the transients.

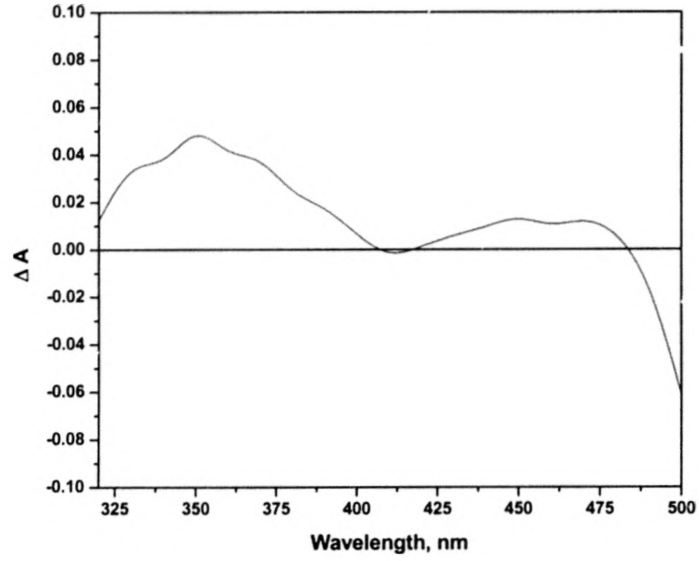

Figure 3.4.26. Transient absorption difference spectrum of **2** in deaerated CH_2Cl_2 measured 100 ns after 355 nm laser pulse.

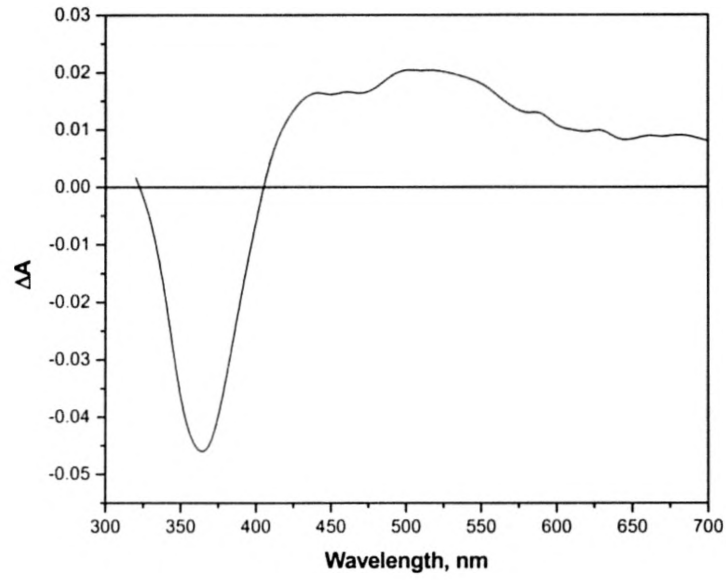

Figure 3.4.27. Transient absorption difference spectrum of **12** in deaerated CH_2Cl_2 measured 500 ns after 355 nm laser pulse.

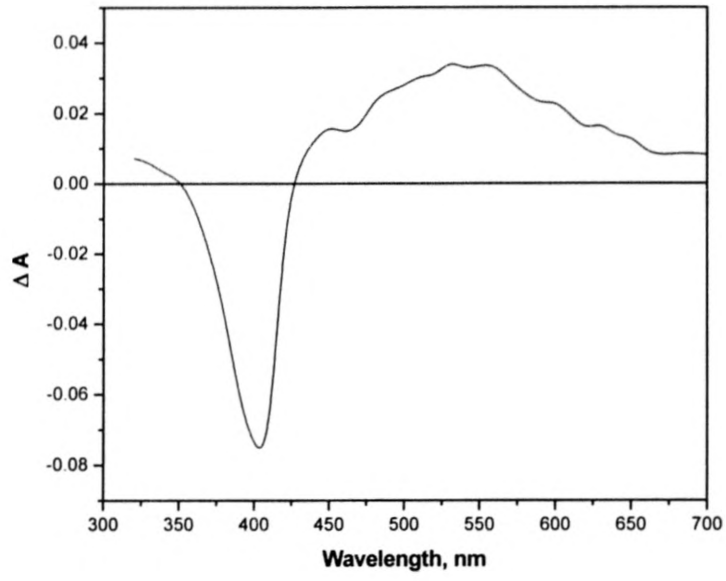

Figure 3.4.28. Transient absorption difference spectrum of **13** in deaerated CH_2Cl_2 measured 20 μs after 355 nm laser pulse.

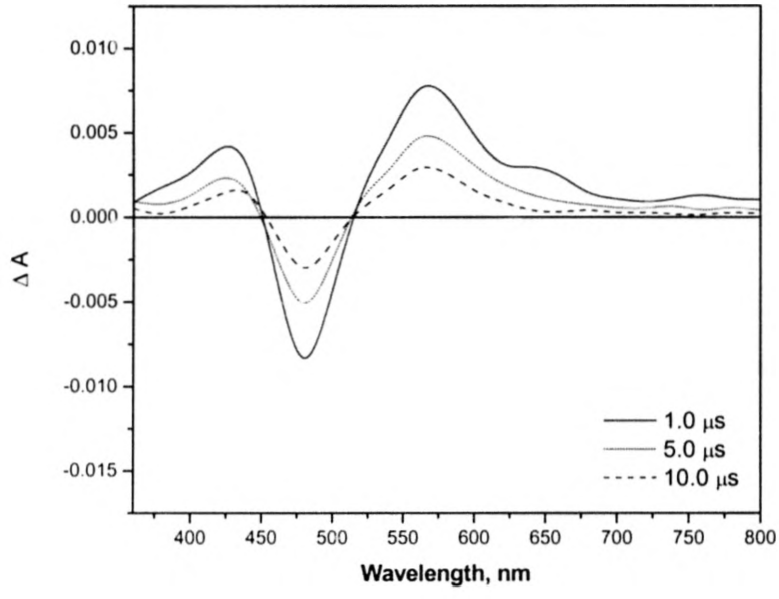

Figure 3.4.29. Transient absorption difference spectrum of **17** in deaerated MTHF, followed by 416 nm laser pulse.

Flash photolysis performed on **13** generated a similar transient to that of **12** through the visible region, Figure 3.4.28. However, the ground state bleaching of the pyrenyl units occurs at lower energy in **13** then in **12**, which is consistent with differences in their relative C≡C-Pyrenyl absorption band positions (see Figure 3.4.2). On the basis of the transient data the absorptions in **12** are assigned to the ground state bleaching (λ = 325-410 nm) and to the triplet-to-triplet absorption (λ = 410-800 nm) of C≡C-Pyrene units. The bleach recovery and the absorption decays followed similar single-exponential kinetics that exhibit concentration-dependent lifetimes on the order of tens of microseconds. The absorption transient in **17** centered at ~550 nm is proposed to be attributed to the triplet-to-triplet absorption of the –C≡C-Perylene moieties based on its shape and lifetime (8 μs). The absorption kinetics paralleled the time-resolved emission decays in all cases, illustrating that the absorption transients are likely of the same origin as the phosphorescence.

CONCLUSIONS

A variety of new complexes, Pt(II) diimine bis(arylacetylides) (**5**, **7**, **12**, **16**, **17**) and a corresponding structural model Pt(dppe)(C≡C-Naphthalene)$_2$ (**10**), were synthesized, structurally characterized, and their photophysical properties were thoroughly investigated.

According to our design, the ^{3}IL arylacetylide-centered excited states in complexes **12**, **16** and **17** are strategically positioned below the ^{3}MLCT manifold, therefore ^{3}IL phosphorescence is expected for this group of molecules. It was established that excitation into the low-energy MLCT absorption band in **12**, **16** and **17** sensitizes long lived phosphorescence from the appended C≡C-Aryl ligands at room temperature in a fluid solution. The relatively strong ^{3}IL phosphorescence is a consequence to the presence of internal Pt heavy atom. Compounds **12**, **16** and **17** represent an alternative molecular design that imparts long lifetime red (and even near-IR in **17**) photoluminescence into synthetically facile metal-organic systems. Such molecules have important potential applications in emerging luminescence-based technologies.

The ^{3}IL state in **7** is almost isoinergetic to the Pt d$\pi\rightarrow\pi^*$ (dbbpy) ^{3}MLCT excited state, therefore we proposed that by variation of solvent media and temperature it should be possible to fine-tune the ^{3}MLCT energy relative to ^{3}IL state accessing the wide variety of the interesting and potentially useful photophysical properties. The photophysics of **7** have been explored and compared to the model chromophores **10** and **2** as a function of solvent and two extremes of temperature. The excited state properties of **7** at room temperature can be described as possessing a combination of charge transfer and intraligand character, where the lower-lying state dominates the behavior and solvent

media allows transitioning between these two limits. The data obtained in solvents of low polarity are consistent with an excited state composed of primarily ^{3}MLCT character, whereas the situation becomes inverted in solvents of higher polarity. In the latter cases, the static and dynamic optical data are most consistent with an excited state whose photophysics is largely determined by the ^{3}IL states resident on the naphthaleneacetylide unit(s). Interestingly, in solvents of higher polarity, excited state decay is not exclusively determined by the ^{3}IL state(s), as the lifetimes are significantly shorter than one would expect for a pure $^3\pi$-π^* intraligand state. These results suggest that the ^{3}MLCT state actively influences the decay of the excited state at room temperature, most likely due to mixing of the triplet states, although we cannot rule out contributions from thermal equilibrium.[1,3,4,8,12,13,15,19,79] The magnitude of the thermally induced Stokes shifts indicate a lack of "purity" in the emission properties of **7**, i.e. "pure ^{3}MLCT" verses "pure ^{3}IL." The luminescence data obtained at low temperature as a function of glass matrix are qualitatively consistent with a ^{3}IL excited state decay whose rate is influenced by the presence of an energetically proximate ^{3}MLCT state, suggestive of an electronic perturbation occurring between the two triplets. In order to quantitatively examine the perturbation model, the new structures need to be prepared that will maintain the ^{3}IL level and simultaneously lower the ^{3}MLCT level. These minor structural and energetic changes should yield additional insight into the photophysics of Pt(diimine)(C≡C-R)$_2$ chromophores containing multiple, nearly isoenergetic triplet states.

In general, the photophysical properties observed for **5** at room temperature are consistent with a lowest ^{3}MLCT excited state and similar to that of model compound **2** the properties of which has been already ascribed to the MLCT manifold.[57] This behavior

was quite expected due to the fact that, according to the structural design, ^{3}IL biphenylacetylide-centered excited state in **5** lies far above the ^{3}MLCT level. Interestingly, the situation becomes inverted at 77 K when emission in **5** emanates predominantly from the ^{3}IL state due to the increasing energy of the MLCT manifold and subsequent energy transfer from the later to the ^{3}IL excited state. Pt(dbbpy)(C≡C-Biphenyl)$_2$ compound **5** serve to further enhance our knowledge regarding manipulation of molecular excited states.

References

(1) Tyson, D. S.; Castellano, F. N. *J. Phys. Chem. A* **1999**, *103*, 10955-10960.

(2) Tyson, D. S.; Gryczynski, I.; Castellano, F. N. *J. Phys. Chem. A* **2000**, *104*, 2919-2924.

(3) Tyson, D. S.; Luman, C. R.; Zhou, X.; Castellano, F. N. *Inorg. Chem.* **2001**, *40*, 4063-4071.

(4) Tyson, D. S.; Henbest, K. B.; Bialecki, J.; Castellano, F. N. *J. Phys. Chem. A* **2001**, *105*, 8154-8161.

(5) Tyson, D. S.; Bignozzi, C. A.; Castellano, F. N. *J. Am. Chem. Soc.* **2002**, *124*, 4562-4563.

(6) Tyson, D. S.; Luman, C. R.; Castellano, F. N. *Inorg. Chem.* **2002**, *41*, 3578-3586.

(7) Trouts, T. D.; Tyson, D. S.; Pohl, R.; Kozlov, D. V.; Waldron, A. G.; Castellano, F. N. *Adv. Funct. Mater.* **2003**, *13*, 398-402.

(8) Ford, W. E.; Rodgers, M. A. J. *J. Phys. Chem.* **1992**, *96*, 389-394.

(9) Wilson, G. J.; Launikonis, A.; Sasse, W. H. F.; Mau, A. W.-H. *J. Phys. Chem. A* **1997**, *101*, 4860-4866.

(10) Simon, J. A.; Curry, S. L.; Schmehl, R. H.; Schatz, T. R.; Piotrowiak, P.; Jin, X. Q.; Thummel, R. P. *J. Am. Chem. Soc.* **1997**, *119*, 11012-11022.

(11) Zhou, X.; Tyson, D. S.; Castellano, F. N. *Angew. Chem. Int. Ed.* **2000**, *39*, 4301-4305.

(12) Harriman, A.; Hissler, M.; Khatyr, A.; Ziessel, R. *Chem. Commun.* **1999**, 735-736.

(13) Hissler, M.; Harriman, A.; Khatyr, A.; Ziessel, R. *Chem. Eur. J.* **1999**, *11*, 3366-3381.

(14) Guerzo, A. D.; Leroy, S.; Fages, F.; Schmehl, R. H. *Inorg. Chem.* **2002**, *41*, 359-366.

(15) McClenaghan, N. D.; Barigelletti, F.; Maubert, B.; Campagna, S. *Chem. Commun.* **2002**, 602-603.

(16) Goze, C.; Kozlov, D. V.; Tyson, D. S.; Ziessel, R.; Castellano, F. N. *New. J. Chem.* **2003**, *27*, 1679-1683.

(17) Pomestchenko, I. E.; Luman, C. R.; Hissler, M.; Ziessel, R.; Castellano, F. N. *Inorg. Chem.* **2003**, *42*, 1394-1396.

(18) Liu, Y.; DeNicola, A.; Reiff, O.; Ziessel, R.; Schanze, K. S. *J. Phys. Chem. A* **2003**, *107*, 3476-3485.

(19) Indelli, M. T.; Ghirotti, M.; Prodi, A.; Chiorboli, C.; Scandola, F.; McClenaghan, N. D.; Puntoriero, F.; Campagna, S. *Inorg. Chem.* **2003**, *42*, 5489-5497.

(20) Balzani, V.; Scandola, F. *Supramolecular Photochemistry*; Horwood: Chichester, 1991.

(21) Liu, Y.; Jiang, S.; Glusac, K.; Powell, D. H.; Anderson, D. F.; Schanze, K. S. *J. Am. Chem. Soc.* **2002**, *124*, 12421-12413.

(22) Lee, J. L.; Luman, C. R.; Castellano, F. N.; Lin, W. *Chem. Commun.* **2003**, 2124-2125.

(23) Paris, J. P.; Brandt, W. W. *J. Am. Chem. Soc.* **1959**, *81*, 5001-5002.

(24) Meyer, T. J. *Prog. Inorg. Chem.* **1983**, *30*, 389-440.

(25) Meyer, T. J. *Acc. Chem. Res.* **1989**, *22*, 364-371.

(26) Juris, A.; Balzani, V.; Barigelletti, F.; Campagna, S.; Belser, P.; von Zelewsky, A. *Coord. Chem. Rev.* **1988**, *84*, 85-277.

(27) Demas, J. N.; Crosby, G. A. *J. Mol. Spectrosc.* **1968**, *26*, 72-77.

(28) Hager, G. D.; Crosby, G. A. *J. Am. Chem. Soc.* **1975**, *97*, 7031-7037.

(29) Hager, G. D.; Watts, R. J.; Crosby, G. A. *J. Am. Chem. Soc.* **1975**, *97*, 7037-7042.

(30) Hipps, K. W.; Crosby, G. A. *J. Am. Chem. Soc.* **1975**, *97*, 7042-7048.

(31) Crosby, G. A. *Acc. Chem. Res.* **1975**, *8*, 231-238.

(32) Caspar, J. V.; Meyer, T. J. *J. Am. Chem. Soc.* **1983**, *105*, 5583-5590.

(33) Caspar, J. V.; Meyer, T. J. *J. Phys. Chem.* **1983**, *87*, 952-957.

(34) Wrighton, M.; Morse, D. L. *J. Am. Chem. Soc.* **1974**, *96*, 998-1003.

(35) Van Houten, J.; Watts, R. J. *J. Am. Chem. Soc.* **1976**, *98*, 4853-4858.

(36) Chen, P.; Meyer, T. J. *Chem. Rev.* **1998**, *98*, 1439-1477.

(37) Kober, E. M.; Meyer, T. J. *Inorg. Chem.* **1984**, *23*, 3877-3886.

(38) Kober, E. M.; Sullivan, B. P.; Meyer, T. J. *Inorg. Chem.* **1984**, *23*, 2098-2104.

(39) Damrauer, N. H.; Cerullo, G.; Yeh, A.; Boussie, T. R.; Shank, C. V.; McCusker, J. K. *Science* **1997**, *275*, 54-57.

(40) Yeh, A. T.; Shank, C. V.; McCusker, J. K. *Science* **2000**, *289*, 935-938.

(41) McCusker, J. K. *Acc. Chem. Res.* **2003**, *36*, 876-887.

(42) Bhasikuttan, A. C.; Suzuki, M.; Nakashima, S.; Okada, T. *J. Am. Chem. Soc.* **2002**, *124*, 8398-8405.

(43) Hagfeldt, A.; Gratzel, M. *Chem. Rev.* **1995**, *95*, 49-68.

(44) Anzenbacher Jr., P.; Tyson, D. S.; Jursikova, K.; Castellano, F. N. *J. Am. Chem. Soc.* **2002**, *124*, 6232-6233.

(45) Xu, W. Y.; Kneas, K. A.; Demas, J. N.; DeGraff, B. A. *Anal. Chem.* **1996**, *68*, 2605-2609.

(46) Lyons, C. H.; Abbas, E. D.; Lee, J.-K.; Rubner, M. F. *J. Am. Chem. Soc.* **1998**, *120*, 12100-12107.

(47) Rudmann, H.; Shimada, S.; Rubner, M. F. *J. Am. Chem. Soc.* **2002**, *124*, 4918-4921.

(48) Gao, F. G.; Bard, A. J. *J. Am. Chem. Soc.* **2000**, *122*, 7426-7427.

(49) Buda, M.; Kalyuzhny, G.; Bard, A. J. *J. Am. Chem. Soc.* **2002**, *124*, 6090-6098.

(50) Miskowski, V. M.; Houlding, V. H. *Inorg. Chem.* **1989**, *28*, 1529-1533.

(51) Miskowski, V. M.; Houlding, V. H.; Che, C.-M.; Wang, Y. *Inorg. Chem.* **1993**, *32*, 2518-2524.

(52) Kunkely, H.; Vogler, A. *J. Am. Chem. Soc.* **1990**, *112*, 5625-5627.

(53) Chan, C.-W.; Cheng, L.-K.; Che, C.-M. *Coord. Chem. Rev.* **1994**, *132*, 87-97.

(54) Chan, S.-C.; Chan, M. C. W.; Wang, Y.; Che, C.-M.; Cheung, K.-K.; Zhu, N. *Chem. Eur. J.* **2001**, *7*, 4180-4190.

(55) Cummings, S. D.; Eisenberg, R. *J. Am. Chem. Soc.* **1996**, *118*, 1949-1960.

(56) Connick, W. B.; Geiger, D.; Eisenberg, R. *Inorg. Chem.* **1999**, *38*, 3264-3265.

(57) Hissler, M.; Connick, W. B.; Geiger, D. K.; McGarrah, J. E.; Lipa, D.; Lachicotte, R. J.; Eisenberg, R. *Inorg. Chem.* **2000**, *39*, 447-457.

(58) Whittle, C. E.; Weinstein, J. A.; George, M. W.; Schanze, K. S. *Inorg. Chem.* **2001**, *40*, 4053-4062.

(59) James, S. L.; Younus, M.; Raithby, P. R.; Lewis, J. *J. Organomet. Chem.* **1997**, *543*, 233-235.

(60) Adams, C. J.; James, S. L.; Liu, X.; Raithby, P. R.; Yellowless, L. J. *J. Chem. Soc. Dalton Trans.* **2000**, 63-67.

(61) Blanton, C. B.; Murtaza, Z.; Shaver, R. J.; Rillema, D. P. *Inorg. Chem.* **1992**, *31*, 3230-3235.

(62) Wan, K.-T.; Che, C.-M.; Cho, K.-C. *J. Chem. Soc. Dalton Trans.* **1991**, 1077-1080.

(63) McGarrah, J. E.; Eisenberg, R. *Inorg. Chem.* **2003**, *42*, 4355-4365.

(64) Wadas, T. J.; Lachicotte, R. J.; Eisenberg, R. *Inorg. Chem.* **2003**, *42*, 3772-3778.

(65) Vogel, A. I. *Vogel's Textbook of Practical Organic Chemistry*; 5th ed. ed. New York, 1989.

(66) Hodges, K. D.; Rund, J. V. *Inorg. Chem.* **1975**, *14*, 525-528.

(67) Bruce, M. I.; Davy, J. R.; Hall, B. C.; Jansen van Galen, Y.; Skelton, B. W.; White, A. H. *Appl. Organometal. Chem.* **2002**, *16*, 559-568.

(68) Appleton, T. G.; Bennett, M. A.; Tompkins, B. *J. Chem. Soc. Dalton Trans.* **1976**, 439-446.

(69) Wright, M. E.; Schorzman, D. A. *Macromol.* **2001**, *34*, 4768-4773.

(70) Kauffman, G. B.; Teter, L. A. *Inorg. Syn.* **1963**, *7*, 24-29.

(71) Klein, A.; van Slagreren, J.; Zalis, S. *Eur. J. Inorg. Chem.* **2003**, 1917-1928.

(72) Vanhelmont, F. W. M.; Johnson, R. C.; Hupp, J. T. *Inorg. Chem.* **2000**, *39*, 1814-1816.

(73) Watts, R. J.; Crosby, G. A. *J. Am. Chem. Soc.* **1971**, *93*, 3184-3188.

(74) Watts, R. J.; Crosby, G. A. *Chem. Phys. Lett.* **1972**, *13*, 619-621.

(75) Watts, R. J.; Crosby, G. A.; Sansregret, J. L. *Inorg. Chem.* **1972**, *11*, 1474-1483.

(76) Yang, Q.-Z.; Wu, L.-Z.; Wu, Z.-X.; Zhang, L.-P.; Tung, C.-H. *Inorg. Chem.* **2002**, *41*, 5653-5655.

(77) Gilbert, A.; Baggott, J. *Essentials of Molecular Photochemistry*; Blackwell Science Ltd.: Cambridge, 1991.

(78) Lakowicz, J. R. *Principles of Fluorescence Spectroscopy*; Kluver Academic/Plenum Publishers: New York, 1999.

(79) Tyson, D. S.; Bialecki, J.; Castellano, F. N. *Chem. Commun.* **2000**, 2355-2356.

CHAPTER IV. SYNTHESIS OF Re(I) AND Au(I) ACETYLIDE COMPLEXES AND INFLUENCE OF A Au(I)-ACETYLIDE SUBUNIT ON THE PHOTOPHYSICS OF Re(Phen)$(CO)_3$Cl

Introduction

Since the first report by Wrighton and Morse in 1974,[1] the photophysics and photochemistry of complexes of the general formula Re(L-L)$(CO)_3$Cl, L-L is a diimine ligand, have been widely developed. Particularly noteworthy are the contributions from Meyer's group, which outlined the systematic structure-photophysical property relationships as a function of either non-chromophoric (replacement of Cl) or chromophoric (diimine) ligand substitutions.[2,3] Of course, many investigators have used Re(I) complexes in a variety of fundamental and applied research projects as their photophysical properties are largely predictable prior to synthesis.[2-24] Recently, Schanze's group has developed a new class of π-conjugated Re(I) chromophores where various arylethynylenes are appended to the 5,5'-ends of 2,2-bipyridine.[25-28] These metal-organic oligomers possess photophysical properties that are not as predictable as their structurally simpler predecessors, yielding room temperature excited state decay that can best be described as a composite of metal-to-ligand charge transfer (^{3}MLCT) and oligomer-based $^3\pi$-π^* intraligand (^{3}IL) character. Clearly, the addition of the conjugated organic ethynylene units dramatically affect the radiative decay processes in Re(I) complexes. Over the past several years Yam's group in Hong Kong has looked at the photophysical properties of a variety of Re(I)-acetylides of the general formula Re(L-L)$(CO)_3$(C≡CR), where R are various organic-based substituents.[29-32] The σ-donating ability of the acetylides render the Re(I) center more electron rich and therefore systematic variation of the MLCT energies are observed as a function of R.

These structures have been further elaborated into various carbon-rich polynuclear luminescent materials.[32]

Upon consideration of the above experimental results, we rationalized that placing metal-containing conjugated substituents within the diimine ligand framework should promote interesting electronic effects in Re(I) complexes. As typically observed in Re(I) compounds which contain a single chromophoric diimine unit, we expect any electronic effects to be communicated through the resultant photophysical and electrochemical properties. In addition, we were interested in the question of whether the placement of a metal-ethynyl substituent possessing low energy triplet states within the diimine ligand structure of a simple Re(I) complex would markedly influence excited state decay. Here, we selected a gold(I)-acetylide system to serve as a substituent in the 5-position of 1,10-phenanthroline which is appended to a $Re(CO)_3Cl$ skeleton. The newly synthesized Ph_3P-Au-C≡C-phen-containing Re(I) complex (**21**) possesses several distinguishing features that facilitated its selection for the current study. The Ph_3P-Au-C≡C-fragment serves an electron-donating substituent while at the same time the gold(I)-acetylide linkage yields a near-visible absorbing chromophore with low-lying triplet states. Therefore, the opportunity presents itself to see if the Au-acetylide states are able to sensitize the formation of as well as interact with the lowest MLCT excited state. As the photophysical properties of the MLCT excited states of Re(I) complexes are well-documented, evaluating the properties of **21** and appropriate reference chromophores (**20** and **18**) with a battery of spectroscopic techniques will yield a detailed understanding of excited state decay in Re(I) complexes appended with Au-acetylide conjugated substituents.

Materials and Methods

All reagents not specifically listed below were obtained from commercial sources and used as received. Anhydrous dichloromethane was purchased from Aldrich was distilled over CaH_2. Diisopropylamine and acetone were dried and distilled according to standard procedures prior to use. Potassium carbonate (Aldrich) was dried in an oven (140°C) for at least 12 h before use. Copper(I) iodide, 1,10-phenanthroline (phen), and $Re(CO)_5Cl$ were purchased from Aldrich and used as received. $Au(PPh_3)Cl$ was purchased from Alfa Aesar and used as received. 5-Bromo-1,10-phenanthroline was available from a previous study.[33] Water was deionized by means of Barnstead E-Pure system. Silica gel used in chromatographic separations was obtained from EM Science (Silica Gel 60, 230-400 mesh). All synthetic manipulations were performed under an inert and dry argon atmosphere using standard techniques. Elemental analyses were performed by Atlantic Microlab (Norcross, GA) or QTI (Whitehouse, NJ). ^1H NMR spectra were recorded on a Varian Gemini 300 (300 MHz) spectrometer. All chemical shifts are referenced to residual solvent signals previously referenced to TMS and splitting patterns are designated as s (singlet), d (doublet), t (triplet), q (quartet), m (multiplet), and br (broad). Static IR spectra of solid samples were measured with an IR 200 spectrometer (ThermoNicolet). Electrospray ionization (ESI) mass spectra were measured at the University of Toledo using an Esquire-LC spectrometer. EI mass spectra were measured in-house using a Shimadzu QP5050A spectrometer.

Reaction Schemes

The synthetic procedures used in the chapter are summarized in Schemes 4.1 - 4.4. Details on synthesis of each compound (**18 - 29**) are located in the synthetic section of this chapter.

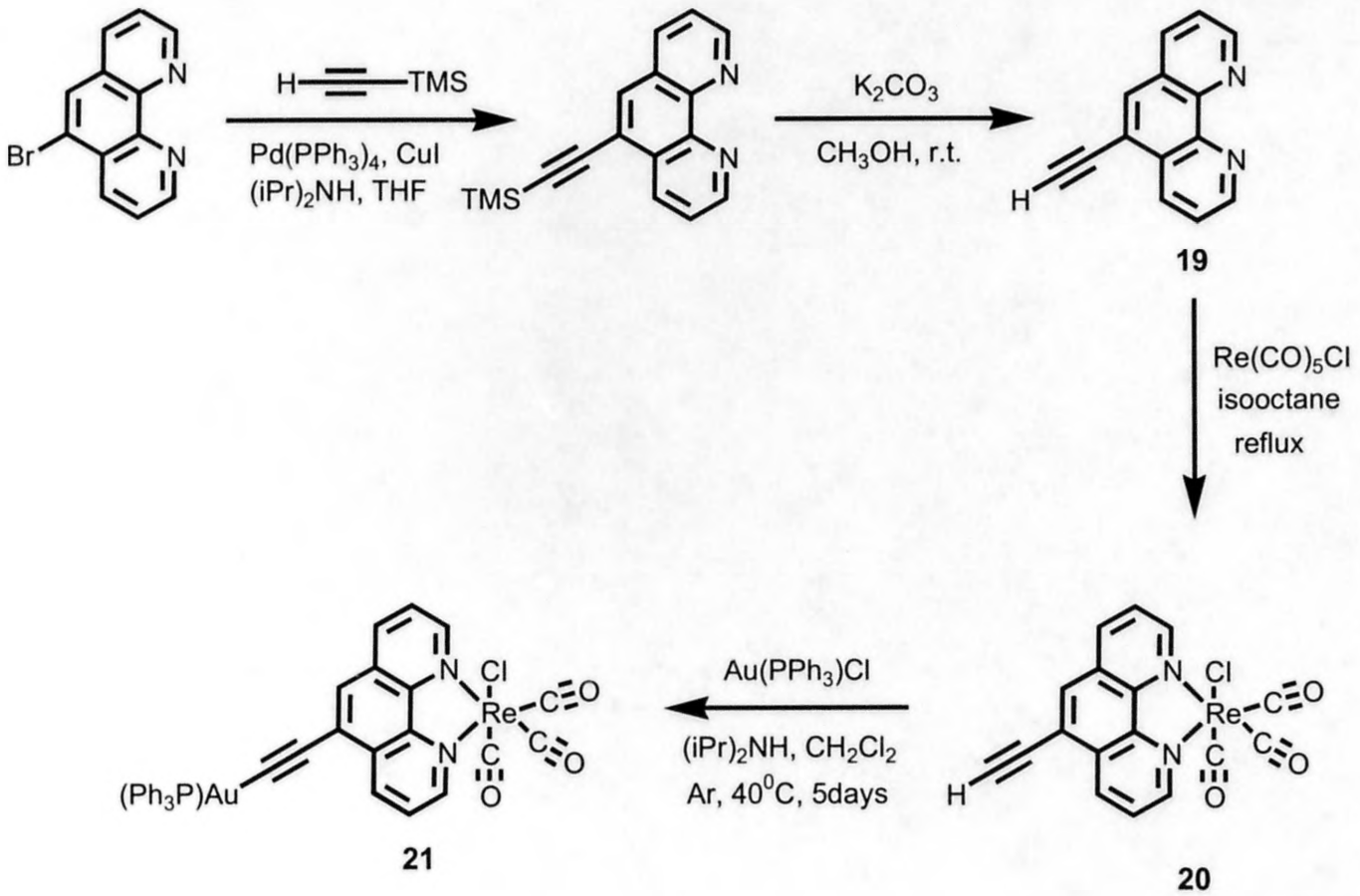

Scheme 4.1. Syntheses of 5-Ethynyl-1,10-phenanthroline (**19**), Re(phen-C≡C-H)$(CO)_3$Cl (**20**) and Re(phen-C≡C-$AuPPh_3$)$(CO)_3$Cl (**21**).

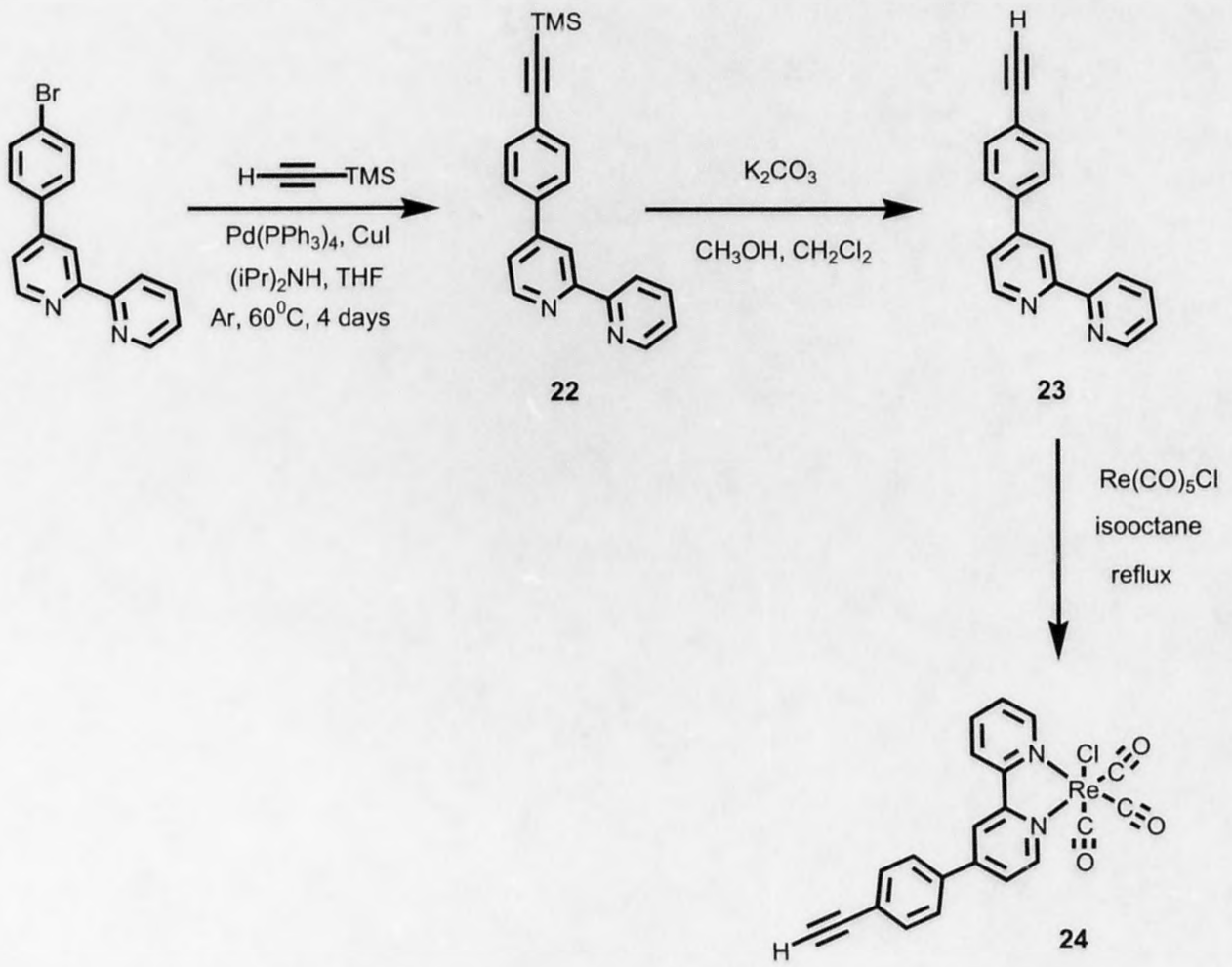

Scheme 4.2. Syntheses of 2.2'-Bipyridine-4'-[4-[(trimethylsilyl)ethynyl]phenyl] (**22**), 2.2'-Bipyridine-4'-(4-ethynylphenyl) (**23**) and Re(bpy-C_6H_4-C≡C-H)$(CO)_3Cl$ (**24**).

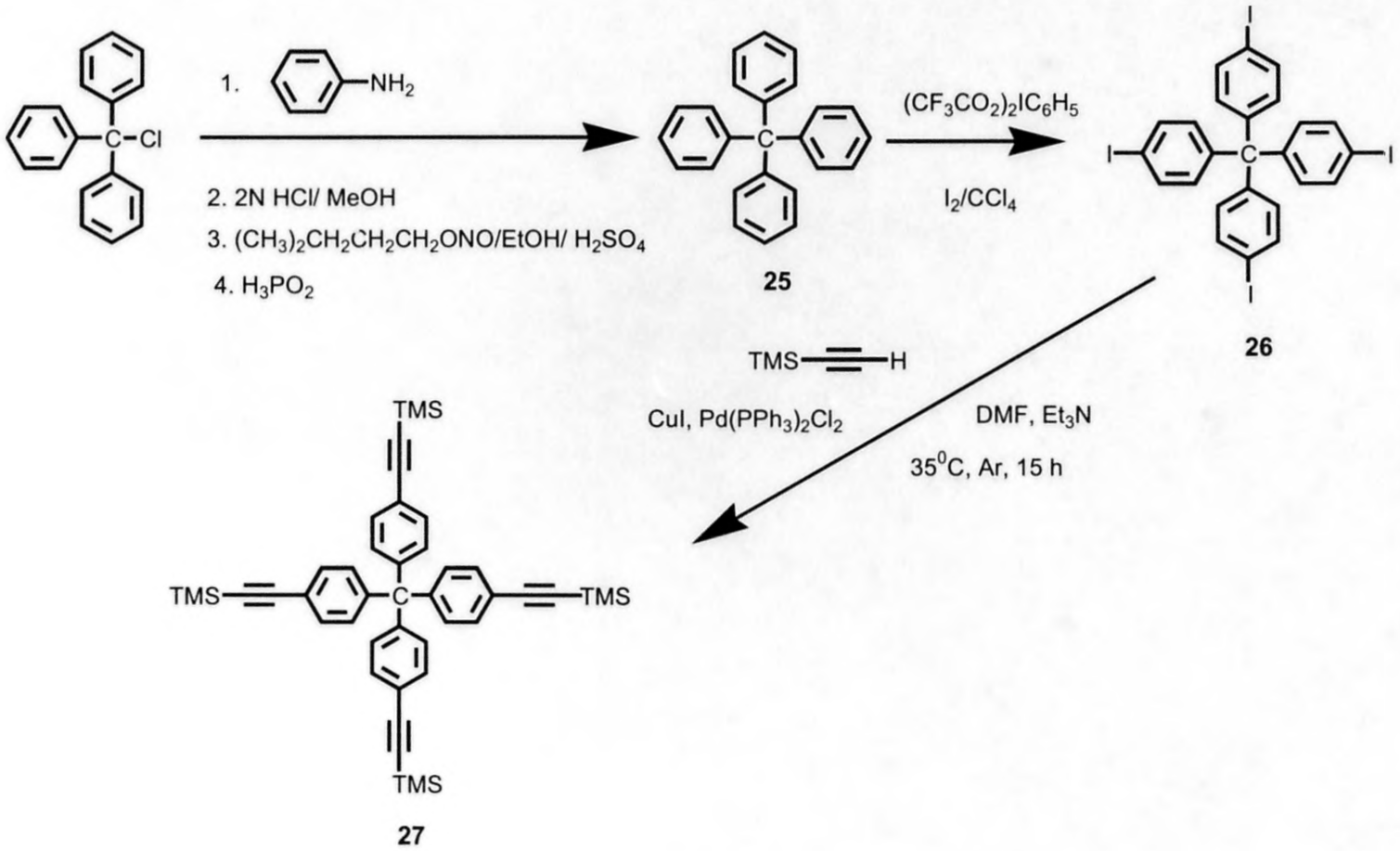

Scheme 4.3. Syntheses of Tetraphenylmethane (**25**), Tetrakis(4-iodophenyl)methane (**26**) and Terakis[4-(trimethylsilylethynyl)phenyl]methane (**27**).

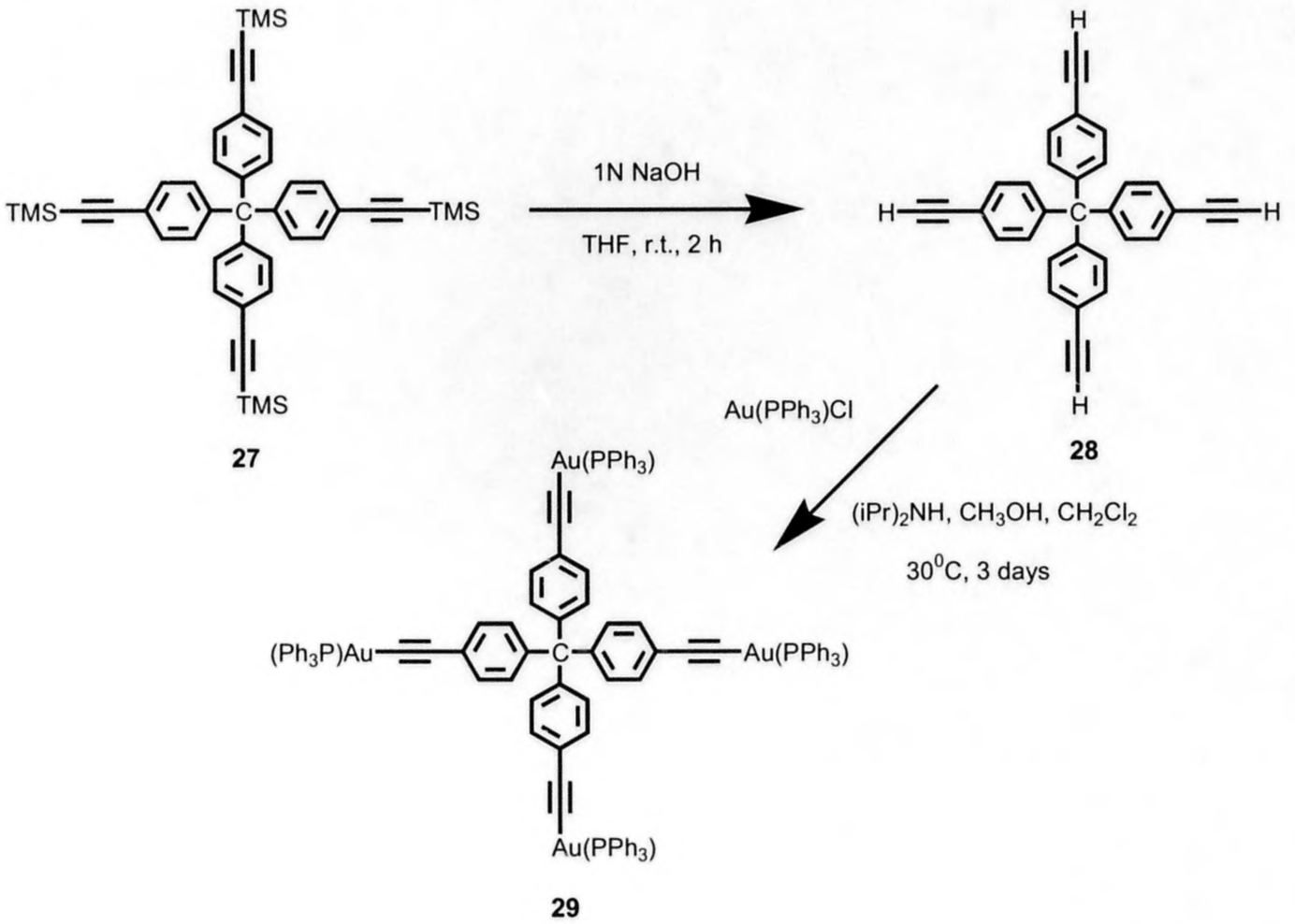

Scheme 4.4. Syntheses of Tetrakis(4-ethynylphenyl)methane (**28**) and $[C\text{-}(C_6H_4\text{-}C{\equiv}C\text{-}AuPPh_3)_4](PF_6)_4$ (**29**).

Synthesis

The synthesis and analysis of each compound presented in this chapter are described below. Previously published procedures have been referenced where appropriate and all compounds (unless specifically noted) were satisfactory characterized by combination of proton nuclear magnetic resonance spectrometry (^{1}H NMR), elemental analysis (El. Anal.), or mass spectrometry.

5-[2-(Trimethysilyl)-1-ethynyl]-1,10-phenanthroline[34] was synthesized by Dr. Radek Pohl and 2,2'-bipyridine-4-(4-bromophenyl)[35] by Daniel Tyson according to literature procedures and yielded satisfactory mass and ^{1}H NMR spectra. Re(phen)$(CO)_3$Cl (**18**)[1-3,36] and 5-Ethynyl-1,10-phenanthroline (**19**)[34] were prepared as described in the literature and yielded satisfactory mass and ^{1}H NMR analyses. Trimethylsilylacetylene, copper (I) iodide, $Re(CO)_5Cl$, were purchased from Aldrich and used as received. Potassium tetrachloroplatinate (II), $Pd(PPh_3)_4$, $Au(PPh_3)Cl$ were purchased from Alfa Aesar and used as received.

20) Re(phen-C≡C-H)$(CO)_3$Cl

5-Ethynyl-1,10-phenanthroline (0.232 g, 1.13 mmol) and $Re(CO)_5Cl$ (0.399 g, 1.10 mmol) were dissolved in isooctane and reaction mixture was brought to reflux for 3 hours. Upon heating yellow precipitate started to appear. The solution was cooled to the room temperature and the precipitate was collected by filtration and washed with cold isooctane. The solid product was purified by column chromatography (SiO_2, 5 vol % of acetone in dichloromethane as an eluent). Experimental yield = 87% yield (0.489 g). Rf = 0.44 (5vol% acetone in CH_2Cl_2); DIP-MS m/z 510. ^{1}H NMR (300 MHz, $CDCl_3$): δ 9.44

(dd, J_1=5.1, J_2=1.2, 1H); 9.40 (dd, J_1=5.1, J_2=1.5, 1H); 9.0 (dd, J_1=8.4, J_2=1.2, 1H); 8.51 (dd, J_1=8.3, J_2 = 1.5, 1H); 8.25 (s, 1H); 7.96 (dd, J_1=8.4, J_2=5.1, 1H); 7.89 (dd, J_1= 8.4, J_2= 5.1, 1H); 3.70 (s, 1H); Anal. Calcd. for $C_{17}H_8ClN_2O_3Re$: C, 40.04; N, 5.49; H, 1.58. Found: C, 40.23; N, 5.32; H, 1.66. Solid state IR $\nu_{C\equiv O}$ (cm^{-1}) 2020; 1927; 1888.

21) Re(phen-C≡C-AuPPh$_3$)(CO)$_3$Cl

Re(phen-C≡C-H)(CO)$_3$Cl (**20**) (0.1 g, 0.196 mmol) was dissolved in dry CH_2Cl_2 (75 ml) in the sealable reaction vessel and solution was degassed with Ar for 15 min. Au(PPh_3)Cl (0.097 g, 0.196 mmol) and freshly distilled $(iPr)_2NH$ (1 ml) were added to the reaction mixture under argon atmosphere. The reaction vessel was sealed with a Teflon screw-cap fitted with an o-ring, and stirred at 40^0C for 1 week. The reaction mixture was filtered and the solvent removed. The remaining orange-yellow residue was dissolved in CH_2Cl_2 and precipitated by addition of isooctane. The solid was collected on a frit, washed with isooctane and purified by column chromatography (SiO_2, 5 vol % of acetone in dichloromethane as an eluent). R_f = 0.53 (5 vol % acetone in CH_2Cl_2); Experimental yield = 85 % (0.160 g). ESI-MS ($CHCl_3$): m/z 966 $[M-H]^+$. ^{1}H NMR (300 MHz; $CDCl_3$): δ 9.37 (dd, J_1= 5.1, J_2= 1.5, 1H); 9.25-9.30 (m, 2H); 8.41 (dd, J_1= 8.4, J_2= 1.2, 1H); 8.11 (s, 1H); 7.88 (dd, J_1=8.4; J_2=5.1, 1H); 7.79 (dd, J_1= 8.1, J_2= 5.1, 1H); 7.48-7.63 (m, 15H). Anal. Calcd. for $C_{35}H_{22}AuClN_2O_3PRe \cdot 1C_3H_6O$: C, 44.47; N, 2.73; H, 2.75. Found: C, 44.77; N, 3.02; H, 2.93. Solid state IR $\nu_{C\equiv O}$ (cm^{-1}) 2015; 1902; 1880.

22) 2,2'-Bipyridine-4'-[4-[(trimethylsilyl)ethynyl]phenyl]

2,2'-bipyridine-4-(4-bromophenyl) (0.1 g, 0.322 mmol) was dissolved in dry THF (25 ml) and solution was degassed with Ar for 15 min. $Pd(PPh_3)_4$ (18.6 mg, 0.016 mmol) and CuI (2.1 mg, 0.016 mmol) were added under Ar atmosphere, flask was closed with septum and the reaction mixture was heated to 60^0C. Solution of trimethylsilylacetylene (0.047 g, 0.482 mmol) in freshly distilled $(iPr)_2NH$ (5 ml) was degassed separately and added to the reaction mixture via syringe under Ar atmosphere. The reaction mixture was stirred at 60 ^{0}C under Ar atmosphere for 4 days. Solvents were removed under vacuum and residue was redissolved in CH_2Cl_2 (20 ml) and washed with 20 ml of aqueous solution of KCN (0.06 M). Organic phase then was washed with H_2O (20 ml) and dried over Na_2SO_4. Dichloromethane was evaporated under reduced pressure and crude product was chromatographed (SiO_2, 5 vol% MeOH in CH_2Cl_2 as an eluent). Evaporation of the solvent yielded **22** in 76% yield (0.080 g) as beige crystalline solid. DIP-MS m/z 328. ^{1}H NMR (DMSO-d_6): δ 8.63-8.77 (m, 3H); 8.42 (d, 1H); 7.76-8.02 (m, 5H); 7.61 (d, 1H); 7.48 (t, 1H); 0.24 (s, 9H).

23) 2,2'-Bipyridine-4'-(4-ethynylphenyl)

2,2'-Bipyridine-4'-[4-[(trimethylsilyl)ethynyl]phenyl] (0.076 g, 0.232 mmol) was dissolved in MeOH (50 ml). Some CH_2Cl_2 was added in order to completely dissolve starting material **22**. Dry K_2CO_3 (2 eq, 0.064 g, 0.464 mmol) and the reaction mixture was stirred at the room temperature for 12 hours. The reaction mixture then was subjected to an aqueous workup and aqueous phase was extracted with CH_2Cl_2. The

combined organic layers were dried over $MgSO_4$. Volatiles were removed under reduced pressure yielding **23** in 87% (0.051 g). DIP-MS m/z 256.

24) Re(bpy-C_6H_4-C≡C-H)$(CO)_3Cl$

2,2'-Bipyridine-4'-(4-ethynylphenyl) (0.51 g, 0.2 mmol) and $Re(CO)_5Cl$ (0.071 g, 0.195 mmol) were dissolved in isooctane and reaction mixture was brought to reflux for 1 hour. Upon heating dark yellow precipitate started to appear. The solution was cooled to the room temperature and the precipitate was collected by filtration and washed with cold isooctane yielding the pure product **24** in 60% yield (0.065 g). DIP-MS m/z 562; ^1H NMR ($CDCl_3$): δ 9.07-9.11 (m, 2H); 8.29-8.32 (m, 2H); 8.10 (dd, J_1= 7.95, J_2=1.5, 1H); 7.65-7.72 (m, 5H); 7.55-7.61 (m, 1H); 3.28 (s, 1H). Anal. Calcd. for $C_{21}H_{12}ClN_2O_3Re$: C, 44.88; N, 4.98; H, 2.15. Found: C, 43.31; N, 4.57; H, 2.26.

25) Tetraphenylmethane

Tetraphenylmethane was prepared according to the literature procedure.[37] Triphenylmethylchloride (28.5 g, 0.102 mol) was heated with aniline (25.6 g, 0.274 mol) at 220^{0}C in a sand bath for 5 min. The resulting mixture was cooled down to 90^{0}C and a mixture of HCl (120 ml, 2N) and MeOH (100 ml) was added gradually. The reaction mixture was heated briefly at reflux, cooled to the room temperature and the gray solid was collected on a frit. The resulting solid was redissolved in the mixture of EtOH (250 ml) and H_2SO_4 (30 ml, conc.). The resulting mixture was cooled to -10^{0}C and treated dropwise with isopentylnitrite (20 ml) upon stirring. The reaction mixture was stirred for 30 min., treated with hypophosphorous acid (50 vol%, 50 ml), heated to reflux and then

cooled to the room temperature. The crude product (olive solid) was collected by filtration and washed with EtOH. Recrystallization from dioxane/ EtOH gave out **25** as a pale-collored solid in quantitative yield. Product was pure by GC-MS analyses. Tetraphenylmethane was used for the next step without further purification. GC-MS m/z 320.

26) Tetrakis(4-iodophenyl)methane

Compound **26** was prepared according to the literature procedure.[37] A suspension of tetraphenylmethane (1 g, 3.1 mmol), bis(trifluoroacetoxy)iodobebenzene (3.1 g, 7.2 mmol), and iodine (1.67 g, 6.57 mmol) in CCl_4 (20 ml) was stirred at 50-60^{0}C until the color of iodine disappeared. Carbon tetrachloride was removed by rotary evaporation. The residue was washed with ethanol and acetone. Recrystallization from THF yielded 438 mg (17%) tetrakis(4-iodophenyl)methane as white crystalline solid. DIP-MS m/z 824.

27) Tetrakis[4-(trimethylsilylethynyl)phenyl]methane

Compound **27** was prepared according to the literature procedure.[38] Tetrakis(4-iodophenyl)methane (0.893 g, 1.08 mmol) was dissolved in the mixture of freshly distilled DMF and triethylamine (9:1, 159 ml) under argon atmosphere. Copper iodide (0.0413 g, 0.217 mmol), $Pd(PPh_3)_2Cl_2$ (0.152 g, 0.217 mmol) and ethynyltrimethylsilane (1.061 g, 10.8 mmol) were added and the reaction vessel was sealed under Ar. Reaction mixture was stirred at 35^{0}C for 15h. Volatiles were removed under reduced pressure and

crude product was purified by column chromatography on silica gel using CH_2Cl_2 / Hexane (9:1) as an eluent. Experimental yield = 79.7% (0.306 g). DIP-MS m/z 704.

28) Tetrakis(4-ethynylphenyl)methane

Compound **28** was prepared according to the literature procedure.[38] Tetrakis[4-(trimethylsilylethynyl)phenyl]methane (0.306 g, 0.435 mmol) was dissolved in THF (40 ml) and NaOH (17 ml, 1N) was added. The reaction mixture was stirred at room temperature for 2h. THF was removed by rotary evaporation. Organics were extracted by CH_2Cl_2 (35 ml) and dried over Na_2SO_4. Product **28** was purified by column chromatography on silica gel using CH_2Cl_2/ Hexane (9:1) as an eluent. Experimental yield = 81.6% (0.147 g). DIP-MS m/z 416. ^{1}H NMR ($CDCl_3$): δ 7.39 (d, 8H); 7.12 (d, 8H); 3.06 (s, 4H).

29) [C-(C_6H_4-C≡C-AuPPh$_3$)$_4$](PF_6)$_4$

Au(PPh_3)Cl (0.081 g, 0.164 mmol) was dissolved in the sealable reaction vessel in 50 ml of CH_3OH/ CH_2Cl_2 (7:3) solvent mixture and the solution was degassed for 15 min with Ar. In a separate flask Tetrakis(4-ethynylphenyl)methane (**28**) (0.017 g, 0.041 mmol) was dissolved under Ar atmosphere in a mixture of solvents (22 ml) CH_3OH and CH_2Cl_2 (7:3), freshly distilled $(iPr)_2NH$ (1.5 ml) was added, the solution was degassed for 15 min and transferred to the reaction vessel. The reaction vessel was sealed under the argon with a Teflon screw-cap fitted with an o-ring, and stirred at 30^{0}C for 2 days. White product was collected on a frit and washed with EtOH. The residue was redissolved in CH_2Cl_2 and insoluble impurities were filtered off. Evaporation of the solvent yielded

white crystalline solid **29**. Product was dried under high vacuum for 12 hours. Experimental yield is 47% (0.043 g). ^{1}H NMR (DMSO-d_6): δ 7.48-7.66 (m, 60H); 7.26 (d, 8H); 7.0 (d, 8H). Anal. Calcd. for $C_{105}H_{96}Au_4P_4$: C, 56.06; H, 3.41. Found: C, 55.83; H, 3.40.

Structures

In this chapter we report a comprehensive photophysical study on two newly synthesized compounds, Re(phen-C≡CH)$(CO)_3$Cl (**20**), (phen-C≡CH is 5-ethynyl-1,10-phenanthroline) and Re(phen-C≡C$AuPPh_3$)$(CO)_3$Cl (**21**), in addition to the benchmark Re(phen)$(CO)_3$Cl (**18**) chromophore.

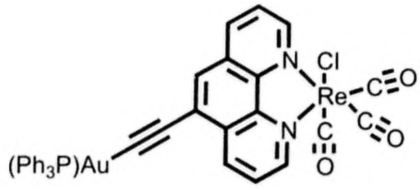

21

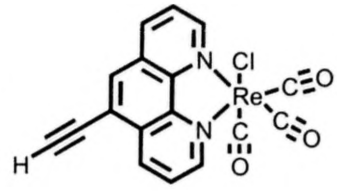

20

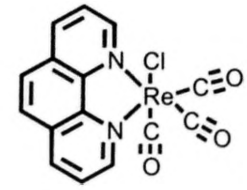

18

Compounds **20** and **18** were prepared by displacement of CO from $Re(CO)_5Cl$ using the appropriate phenanthroline ligand in refluxing isooctane.[36] The synthesis of **21** features a "chemistry on the complex" approach where the acetylene-terminated diimine ligand chelated to the Re(I) center couples to Ph_3PAuCl under mild reaction conditions.[39-42] All complexes were purified by column chromatography on silica gel and final isolated yields were quite significant (≥ 85%). These materials are air-stable solids in addition to being thermally and photochemically stable in solution. All compounds have been structurally characterized with ^{1}H NMR, solid-state IR, elemental analysis, and mass spectrometry. The three-band IR pattern observed in the CO stretching region is consistent with the *facial* arrangement of the three COs in the coordination sphere, as typically observed in related Re(I) organometallic structures.[1-3] In the ^{1}H NMR spectra, all the proton signals residing within the phenanthroline ligand are shifted upfield in **21**

relative to the acetylene precursor **20**. This upfield shift is consistent with back-donation from the gold(I) center to the σ-ethynyl bond in the substituted phenanthroline ligand. A similar upfield shifting effect has been observed in the phenanthroline protons in Ru(II)-systems containing Au-acetylide molecular wires.[43] Elemental analysis and mass spectrometry data are also consistent with the proposed structures.

Absorption Properties

The ground state absorption spectra of complexes **21**, **20** and **18** in MTHF are presented in Figure 4.1. The broad lowest energy absorption feature in all cases is assigned to a dπ (Re) → π* (phen-R) MLCT transition with more intense features at higher energy being of diimine-ligand π-π* origin.

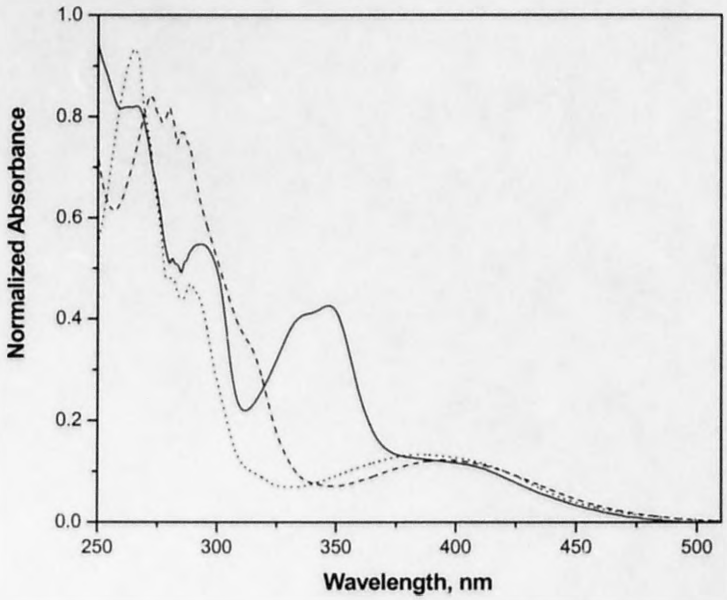

Figure 4.1. Absorption spectra of **21** (solid line) and **20** (dashed line) and **18** (dotted line) in MTHF.

The gold(I)-acetylide chromophore is responsible for the relatively strong near-visible π-π* absorption band centered at 347 nm in **21**.[43-45] This assignment is consistent with observations made in Ru(II) complexes containing Au(I)-acetylides linked in the 3- and 3,8-positions of 1,10-phenanthroline.[43] It is also clear that the low energy MLCT absorption in **21** is slightly blue-shifted with respect to **20**, consistent with a larger energy gap for the charge transfer transition as implied by the electrochemistry below.

Electrochemistry

I would like to thank Dr. Charles R. Luman for his assistance with the electrochemical measurements. The redox behavior of the new complexes measured in CH_3CN by cyclic voltammetry are consistent with data typically obtained in Re(L-L)$(CO)_3$Cl complexes.[3,8,11,21] The first oxidation in **21** and **20** is metal-based, occurring at 1.45 and 1.46 V vs. Ag/AgCl, respectively, Figures 4.2. and 4.3. These oxidations are not completely reversible on the electrochemical time scale and likely result from re-reduction of Re(II) by the solvent or an impurity. The first reduction wave observed in **21** possibly originates from the gold(I)-ethynyl unit bonded to the phenanthroline.[43] Clear reversible phen-based reductions are observed in compounds **21** and **20**, with reduction wave centered at -1.28 and -1.18 V, respectively. Electron back-donation from the Au(I) unit is responsible for the negative shift of the reduction potential of the phenanthroline ligand in **21** compared to **20**, revealing a larger energy gap for the expected charge transfer transitions in the former.[43]

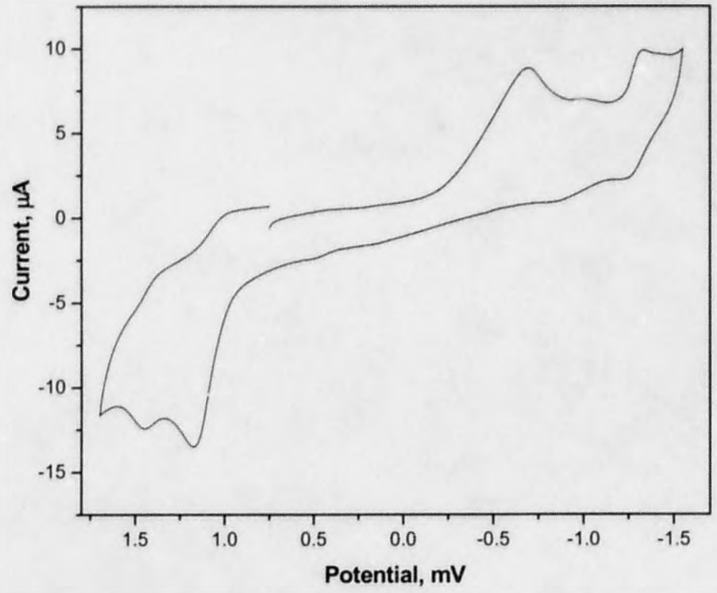

Figure 4.2. Cyclic voltammogram of compound **21** in CH_3CN with 0.1 M TBAP.

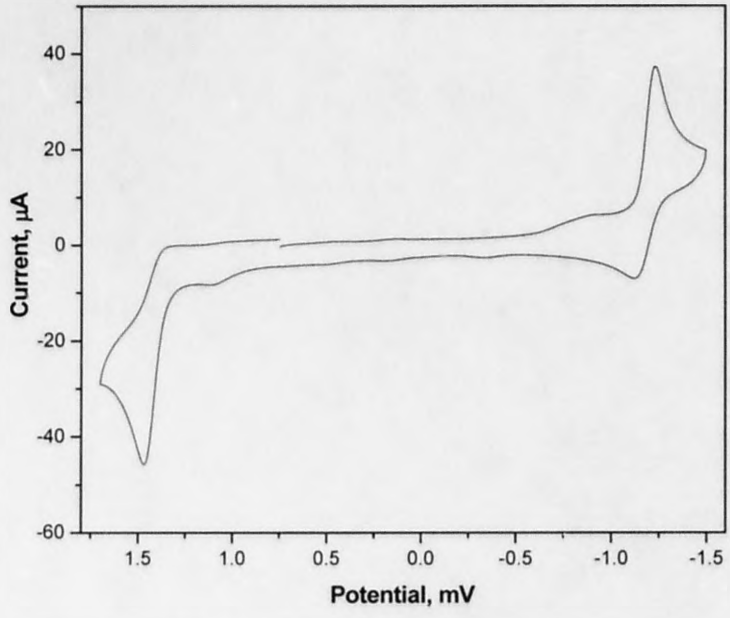

Figure 4.3. Cyclic voltammogram of compound **20** in CH_3CN with 0.1 M TBAP.

Photoluminescence Properties

Complex **21** displays an emission band centered at 598 nm in deaerated MTHF at room temperature, which is completely invariant to the excitation wavelength over the range of 300-480 nm, Figure 4.4. This emission is characteristic of ^{3}MLCT based luminescence typically observed in Re(I) diimine complexes. In fact it is well-established that **18** possesses a lowest energy dπ* MLCT excited state configuration, even at cryogenic temperatures as low as 4 K.[20]

Similarly, photoluminescence centered at 615 nm was observed for the model complex **20** upon excitation into the low energy charge transfer band, Figure 4.4. The blue shift in the emission observed in **21** relative to **20** is consistent with a larger energy gap between ground and excited states.

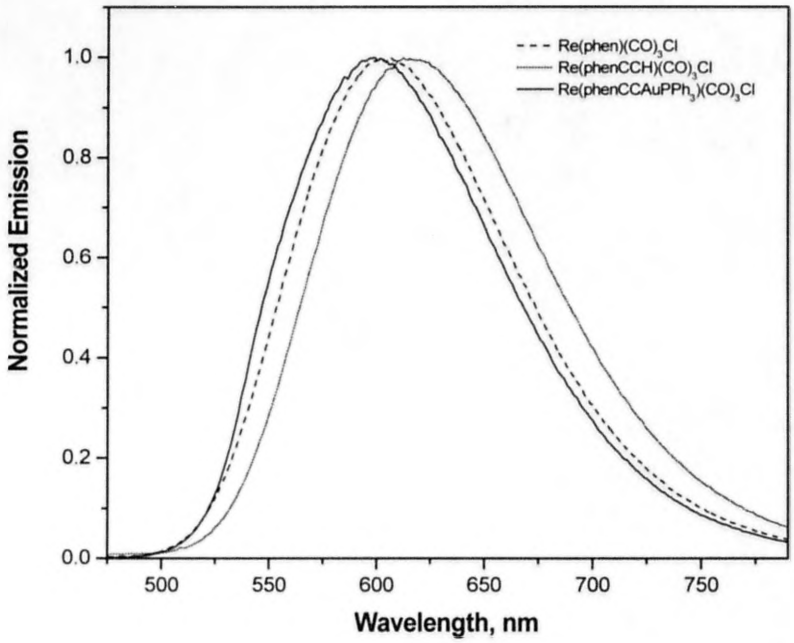

Figure 4.4. Room temperature emission spectra of **21, 20** and **18** in MTHF using 400 nm excitation

The electron rich Ph_3PAu-substituent is clearly responsible for this effect by rendering the phen-ligand harder to reduce in **21**. It should be noted that no emission originating from the Au(I)-acetylide unit could be observed in **21** and the corrected excitation spectrum of **21** between 300 and 500 nm can be largely superimposed with its absorption spectrum. These observations suggest that in **21** the Au(I)-acetylide chromophore harvests near-visible light and efficiently converts it into MLCT-based luminescence.

Photoluminescence Dynamics

The room temperature single exponential photoluminescence lifetimes for **21, 20** and **18** measured in deaerated MTHF are 960, 163, and 227 ns, respectively (Table 4.2.1), Figures 4.5-4.7.

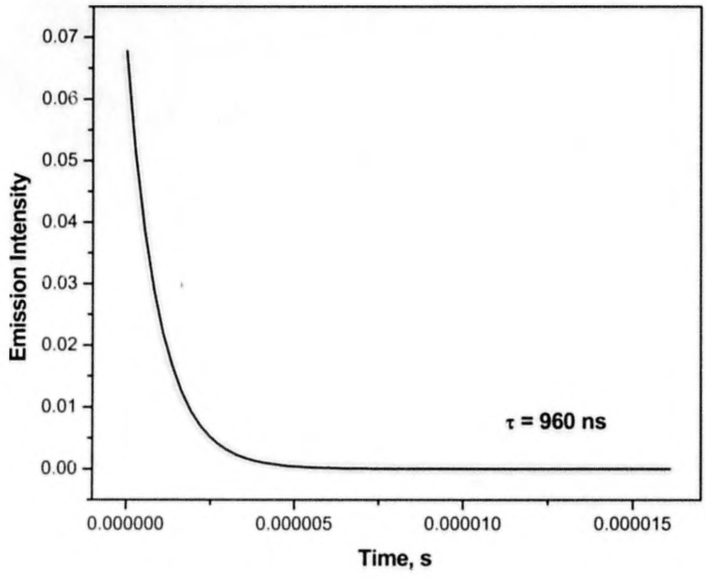

Figure 4.5. Photoluminescence lifetime of **21** in deaerated MTHF followed 385 nm excitation. Solid line – single exponential fit (960 ns).

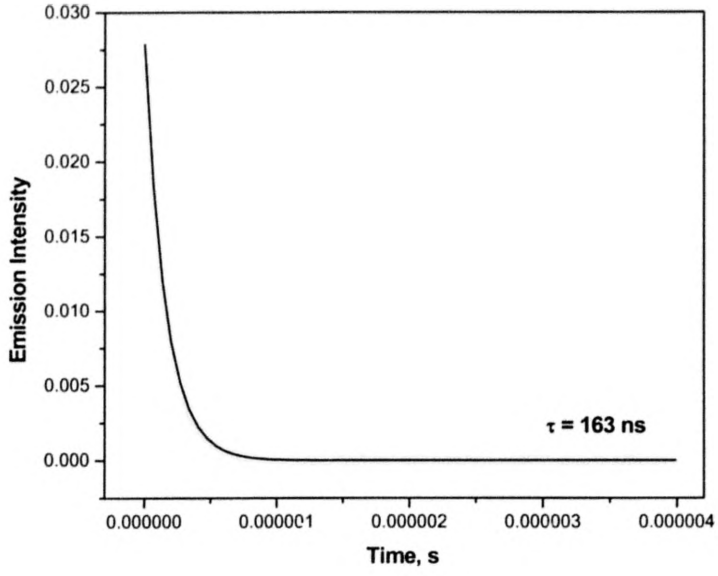

Figure 4.6. Photoluminescence lifetime of **20** in deaerated MTHF followed 365 nm excitation. Solid line – single exponential fit (163 ns).

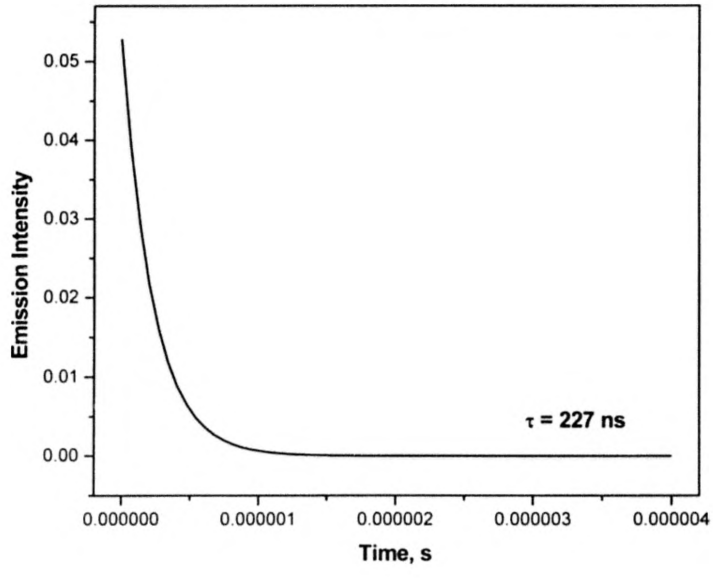

Figure 4.7. Photoluminescence lifetime of **18** in deaerated MTHF followed 450 nm excitation. Solid line – single exponential fit (227 ns).

The longer lifetime observed in **21** reflects a larger energy gap between ground and excited states, decreasing the nonradiative rate constant by a factor of ~ 6 in complex **21** relative to **20**. However, there is likely a contribution associated with electron delocalization into the Au-acetylide fragment in **21** that enhances the excited state lifetime.[46,47] All measured and derived photophysical parameters are collected in Table 4.2.1 and in each case the room temperature photoluminescence properties are consistent with a lowest energy MLCT excited state.

Low Temperature Photoluminescence

Since **21** was designed in the hopes of producing interesting excited state behavior by introducing a low-lying Au(I)-acetylide-based triplet state energetically proximate to the ^{3}MLCT state, we attempted to see if the charge transfer and ligand-based triplet states would interact as a result of a variation in temperature. This was accomplished by studying the emission properties of **21, 20** and **18** in MTHF at room temperature and as low temperature glasses at 77 K. The emission manifold in **18** is broad and structureless at 77 K (Figure 4.8), consistent with radiative decay from a MLCT manifold whose vibronic components are broadened as a result of large solvent reorganizational energies and greater distortions in the low-frequency modes coupling the ground and excited states.[3] The large reorganization energy in **18** is apparent from the large energetic difference between the RT and 77 K spectra (2190 cm^{-1}), also called the thermally induced Stokes shift, ΔE_s, which can be roughly approximated 2 λ_s, where λ_s is the outer-sphere reorganization energy for the MLCT excited state.[48,49] The emission lifetime of **18** at 77 K is 7.6 μs, thus benchmarking the lifetime expected for a ^{3}MLCT excited state in a

Re(I)-phen complex at low temperature. The static 77 K spectra of compounds **21** and **20** contain well-defined structured vibronic components (Figure 4.8), immediately suggesting that the emission is not of MLCT origin. Although the low temperature spectra of **21** and **20** are shifted in energy, the vibronic spacing of the two highest energy bands are identical (1450 cm^{-1}), implying that these emissions are both diimine ligand based. We are uncertain of why **20** displays a larger rigidochromic effect relative to **21** at this juncture but propose that the excited state is more delocalized in the latter, owing to the Au-acetylide linkage. The recovered lifetime of **21** at 77 K is 456 μs whereas the decay in **20** is biexponential with two long-lifetime components (30 and 410 μs). The important finding here is that these lifetimes are well beyond that expected for Re(I)-diimine based MLCT excited states.

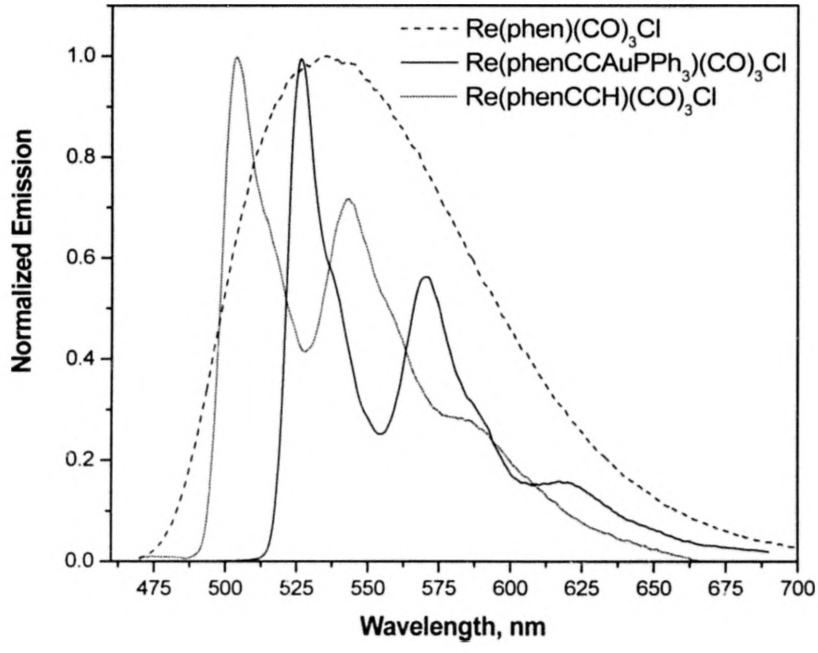

Figure 4.8. Emission spectra of **21, 20** and **18** measured at 77 K in MTHF glasses using 400 nm excitation.

Taken together, the 77 K results are consistent with an intraligand-based π-π* phosphorescence emanating from each respective phenanthroline ligand. This phenomenon is not unprecedented and since it is well established that the ^{3}MLCT level in Re(I) complexes increases with decreasing temperature while the ^{3}IL states are largely unaffected by environment,[1,12,15,18] it is not surprising that the ^{3}IL and ^{3}MLCT states invert at low temperature in **21** and **20**. This state inversion leads to emission from the lowest excited state which can be largely attributed to the ^{3}IL state localized on the diimine ligand structure in **21** and **20**.

Transient Absorption

Nanosecond flash photolysis experiments were performed on compounds **18**, **20** and **21** in MTHF solutions at room temperature using 355 nm excitation, Figures 4.9-4.11. In all three cases the absorption transients decay with the same single exponential kinetics observed in the respective luminescence intensity decays within a few percent, Table 4.2.1. The data obtained for **18** represent the absorption spectral features associated with the MLCT excited state in MTHF, which display transient absorptions throughout the entire spectrum, except at wavelengths above 520 nm where the photoluminescence dominates the signal, Figure 4.9. The ground state bleaching of the MLCT band appears as a depression between 375 and 450 nm whereas broad features are observed in the range of 450-520 nm while a large transient is obtained near 300 nm. This difference spectrum is in complete agreement with that reported for the same complex in CH_3CN where the absorptions near 305 and ~ 480 nm were assigned to reduced phen in the MLCT excited state.[10]

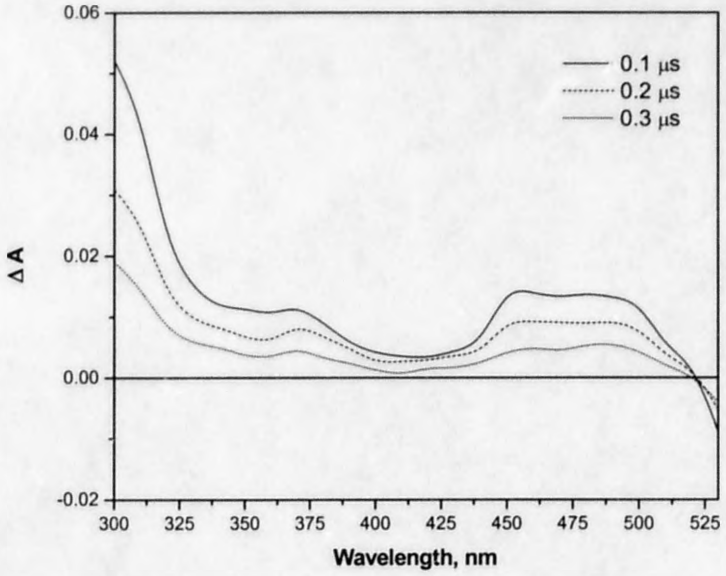

Figure 4.9. Excited state absorption difference spectra of **18** in MTHF followed by 355 nm excitation at 4 mJ/pulse. The delay times are specified on the graph.

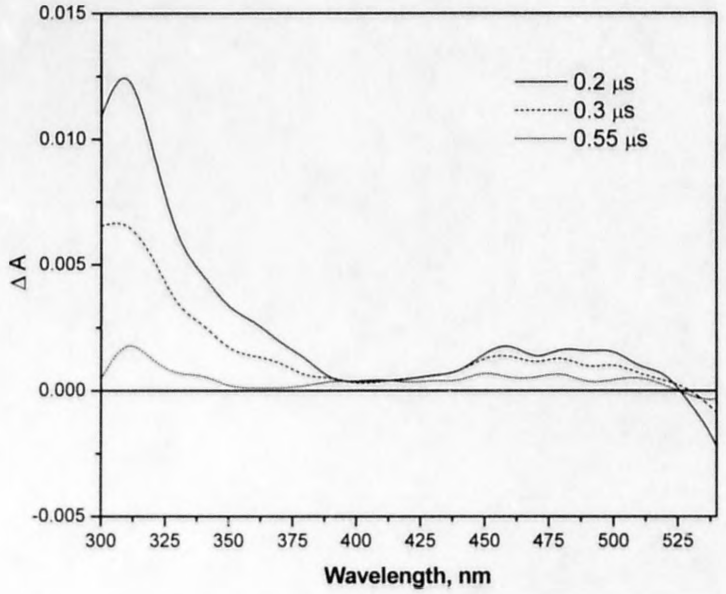

Figure 4.10. Excited state absorption difference spectra of **20** in MTHF followed by 355 nm excitation at 7 mJ/pulse. The delay times are specified on the graph.

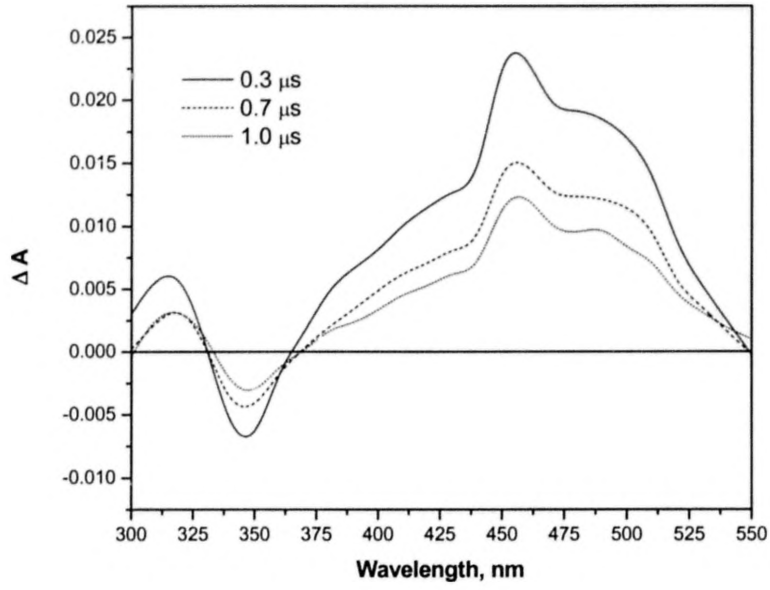

Figure 4.11. Excited state absorption difference spectra of **21** in MTHF followed by 355 nm excitation at 4 mJ/pulse. The delay times are specified on the graph.

The absorption spectrum of phen$^{\cdot-}$ possesses strong features in the 520-650 nm region as well in the UV.[50,51] While we can not evaluate the long wavelength segment and the MLCT bleach interferes with the 375-450 nm range, the absorptions below 375 nm and between 450-520 nm are assigned to the reduced phen ligand in complex **18**. Similar excited state spectroscopic features are observed in reference chromophore **20**, except the MLCT bleach is largely obscured by the absorption transients assigned to the reduced phen-C≡CH species, Figure 4.10. Compound **21** on the other hand displays a noticeably different spectrum than **20** and **18**. There is a detectable ground state bleaching near 350 nm in the region where the Au(I)-acetylide chromophore is the predominate absorber and there are transients observed above 370 nm with peaks at ~450 nm and below 330 nm with a maximum at ~320 nm, Figure 4.11. As the luminescence data for

21 are consistent with a Re(I) → phen-R charge transfer excited state, the TA data can be interpreted in the following manner. Upon the formation of the charge transfer excited state several spectroscopic features should be observed. One is the ground state bleaching of the MLCT transition, which in the case of **21** is completely obscured by other transient absorptions, precluding its use as a diagnostic tool. Another is the formation of the diimine ligand radical anion which generally possess strong, highly allowed absorption features in the UV and visible. These would be associated with the Ph_3PAu-C≡C-phen ligand in **21**, and should be distinct from phen (compound **18**) or phen-C≡C-H (compound **20**) which appears to be the case. However, an often neglected spectroscopic feature are the π-π* transitions localized on the diimine ligand framework. In most MLCT complexes, these strong absorption features occur in the deep UV and are therefore not amenable to TA measurements. Compound **21** happens to possess low energy π-π* transitions centered near 350 nm because of the Au-acetylide linkage in strong electronic contact with the phenanthroline ligand.[43] It stands to reason that upon formation of the MLCT excited state, the spectral features associated with the Ph_3PAu-C≡C-phen ligand would bleach and simultaneously yield strong diimine ligand radical anion transients. The excited state difference spectrum measured for **21** is consistent with these expectations and may signal that the electron delocalizes into the Au-acetylide region of the molecule in the excited state. Alternatively, similar spectroscopic features may be observed if a ligand-localized triplet state were produced.

Table 4.1. Measured and Calculated Photophysical Parameters in MTHF.

Compound	$\lambda_{abs\ max}$, nm	$\lambda_{em\ max}$, nm RT	$\lambda_{em\ max}$, nm 77 K	τ, ns RT	τ, μs 77 K	Φ [a]	k_r, s^{-1} [b]	k_{nr}, s^{-1} [b]
21	347 400	598	527 570 620	960 930 TA [c]	456	0.018	1.9×10^4	1.02×10^6
20	400	615	504 543 585	163 156 TA [c]	30 (0.53)[d] 410 (0.47)[d]	0.008	4.9×10^4	6.08×10^6
18	386	606	535	227 214 TA [c]	7.6	--	--	--

[a] Photoluminescence quantum yield measured relative to $Re(bpy)(CO)_3Cl$, $\Phi_{DCM} = 0.005$.[2]

[b] Radiative (k_r) and nonradiative (k_{nr}) rate constants calculated by $k_r = \Phi / \tau$ and $k_{nr} = (1 - \Phi) / \tau$.

[c] Excited state lifetime determined by transient absorption spectroscopy using 355 nm excitation.

[d] Relative amplitudes of each intensity decay component determined from a biexponential fit.

Conclusions

The tethering of a Au(I)-acetylide linkage to a Re(I) complex through the diimine ligand yields a new molecule (**21**) with a lowest MLCT excited state at room temperature and a lowest ^{3}IL excited state at 77 K in a MTHF glass. While the Au(I)-acetylide chromophore acts as a near-visible light harvesting moiety, sensitizing the lowest ^{3}MLCT state, its low-lying triplet state unfortunately does not appear to influence excited state decay. The photoluminescence and time-resolved absorption data in **21** suggest that in the charge transfer excited state, the electron is delocalized into the Au-acetylide fragment which aids in extending the lifetime of the excited state.

References

(1) Wrighton, M. S.; Morse, D. L. *J. Am. Chem. Soc.* **1974**, *96*, 998-1003.

(2) Caspar, J. V.; Meyer, T. J. *J. Phys. Chem.* **1983**, *87*, 952-957.

(3) Worl, L. A.; Duesing, R.; Chen, P.; Della Ciana, L.; Meyer, T. J. *J. Chem. Soc. Dalton Trans.* **1991**, 849-858.

(4) Luong, J. C.; Nadjo, L.; Wrighton, M. S. *J. Am. Chem. Soc.* **1978**, *100*, 5790-5795.

(5) Giordano, P. J.; Wrighton, M. S. *J. Am. Chem. Soc.* **1979**, *101*, 2888-2897.

(6) Fredericks, S. M.; Luong, J. C.; Wrighton, M. S. *J. Am. Chem. Soc.* **1979**, *101*, 7415-7417.

(7) Smothers, W. K.; Wrighton, M. S. *J. Am. Chem. Soc.* **1983**, *105*, 1067-1069.

(8) Chen, P.; Westmoreland, T. D.; Danielson, E.; Schanze, K. S.; Anthon, D.; Neveux Jr., P. E.; Meyer, T. J. *Inorg. Chem.* **1987**, *26*, 1116-1126.

(9) Mabrouk, P. A.; Wrighton, M. S. *Inorg. Chem.* **1986**, *25*, 526-531.

(10) Kalyanasundaram, K. *J. Chem. Soc. Faraday Trans. 2* **1986**, 2401-2415.

(11) Juris, A.; Campagna, S.; Bidd, I.; Lehn, J.-M.; Ziessel, R. *Inorg. Chem.* **1988**, *27*, 4007-4011.

(12) Sacksteder, L.; Zipp, A. P.; Brown, E. A.; Streich, J.; Demas, J. N.; DeGraff, B. A. *Inorg. Chem.* **1990**, *29*, 4335-4340.

(13) Perkins, T. A.; Hauser, B. T.; Eyler, J. R.; Schanze, K. S. *J. Phys. Chem.* **1990**, *94*, 8745-8748.

(14) Shaw, J. R.; Schmehl, R. H. *J. Am. Chem. Soc.* **1991**, *113*, 389-394.

(15) Leasure, R. M.; Sacksteder, L.; Nesselrodt, D.; Reitz, G. A.; Demas, J. N.; DeGraff, B. A. *Inorg. Chem.* **1991**, *30*, 3722-3728.

(16) MacQueen, D. B.; Eyler, J. R.; Schanze, K. S. *J. Am. Chem. Soc.* **1992**, *114*, 1897-1898.

(17) Kotch, T. G.; Lees, A. J.; Fuerniss, S. J.; Papathomas, K. I. *Chem. Mater.* **1992**, *4*, 675-683.

(18) Sacksteder, L.; Lee, M.; Demas, J. N.; DeGraff, B. A. *J. Am. Chem. Soc.* **1993**, *115*, 8230-8232.

(19) Wang, Y.; Schanze, K. S. *Inorg. Chem.* **1994**, *33*, 1354-1362.

(20) Striplin, D. R.; Crosby, G. A. *Chem. Phys. Lett.* **1994**, *221*, 426-430.

(21) Paolucci, F.; Marcaccio, M.; Paradisi, C.; Roffia, S.; Bignozzi, C. A.; Amatore, C. *J. Phys. Chem. B* **1998**, *102*, 4759-4769.

(22) Schanze, K. S.; Lucia, L. A.; Cooper, M.; Walters, K. A.; Ji, H.-F.; Sabina, O. *J. Phys. Chem. A* **1998**, *102*, 5577-5584.

(23) Yam, V. W.-W.; Lau, V. C.-Y.; Wu, L.-X. *J. Chem. Soc. Dalton Trans.* **1998**, 1461-1468.

(24) Guo, X.-Q.; Castellano, F. N.; Li, L.; Lakowicz, J. R. *Anal. Chem.* **1998**, *70*, 632-637.

(25) Ley, K. D.; Schanze, K. S. *Coord. Chem. Rev.* **1998**, *171*, 287-307.

(26) Ley, K. D.; Li, Y.; Johnson, J. V.; Powell, D. H.; Schanze, K. S. *Chem. Commun.* **1999**, 1749-1750.

(27) Walters, K. A.; Ley, K. D.; Cavalaheiro, C. S. P.; Miller, S. E.; Gosztola, D.; Wasielewski, M. R.; Bussandri, A. P.; van Willigen, H.; Schanze, K. S. *J. Am. Chem. Soc.* **2001**, *123*, 8329-8342.

(28) Walters, K. A.; Dattelbaum, D. M.; Ley, K. D.; Schoonover, J. R.; Meyer, T. J.; Schanze, K. S. *Chem Commun.* **2001**, 1834-1835.

(29) Yam, V. W.-W.; Lau, V. C.-Y.; Cheung, K.-K. *Organometallics* **1995**, *14*, 2749-2753.

(30) Yam, V. W.-W.; Lau, V. C.-Y.; Cheung, K.-K. *Organometallics* **1996**, *15*, 1740-1744.

(31) Yam, V. W.-W.; Chong, S. H.-F.; Cheung, K.-K. *Chem. Commun.* **1998**, 2121-2122.

(32) Yam, V. W.-W. *Chem. Commun.* **2001**, 789-796.

(33) Tyson, D. S.; Henbest, K. B.; Bialecki, J.; Castellano, F. N. *J. Phys. Chem. A* **2001**, *105*, 8154-8161.

(34) Ziessel, R.; Suffert, J.; Youinou, M.-T. *J. Org. Chem.* **1996**, *61*, 6535-6546.

(35) Cordaro, J. G.; McCusker, J. K.; Bergman, R. G. *Chem. Commun.* **2002**, 1496-1497.

(36) Lin, R.; Fu, Y.; Brock, C. P.; Guarr, T. F. *Inorg. Chem.* **1992**, *31*, 4346-4353.

(37) Su, D.; Menger, F. M. *Tett. Lett.* **1997**, *38-42*.

(38) Mongin, O.; Gossauer, A. *Tetrahedron* **1997**, *53*, 6835-6846.

(39) Pabst, G. R.; Pfuller, O. C.; Sauer, J. *Tetrahedron* **1999**, *55*, 8045-8064.

(40) Aspley, C. J.; Williams, J. A. G. *New. J. Chem.* **2001**, *25*, 1136-1147.

(41) Goze, C.; Kozlov, D. V.; Castellano, F. N.; Suffert, J.; Ziessel, R. *Tetrahedron Lett.* **2003**, *44*, 8713-8716.

(42) Goze, C.; Kozlov, D. V.; Tyson, D. S.; Ziessel, R.; Castellano, F. N. *New. J. Chem.* **2003**, *27*, 1679-1683.

(43) Shiotsuka, M.; Yamamoto, Y.; Okuno, S.; Kitou, M.; Nozaki, K.; Onaka, S. *Chem. Commun.* **2002**, 590-591.

(44) Irwin, M. J.; Vittal, J. J.; Puddephatt, R. J. *Organometallics* **1997**, *16*, 3541-3547.

(45) Che, C.-M.; Chao, H.-Y.; Miskowski, V. M.; Li, Y.; Cheung, K.-K. *J. Am. Chem. Soc.* **2001**, *123*, 4985-4991.

(46) Boyde, S.; Strouse, G. F.; Jones Jr., W. E.; Meyer, T. J. *J. Am. Chem. Soc.* **1990**, *112*, 7395-7396.

(47) Strouse, G. F.; Schoonover, J. R.; Duesing, R.; Boyde, S.; Jones Jr., W. E.; Meyer, T. J. *Inorg. Chem.* **1995**, *34*, 473-487.

(48) Whittle, C. E.; Weinstein, J. A.; George, M. W.; Schanze, K. S. *Inorg. Chem.* **2001**, *40*, 4053-4062.

(49) Chen, P.; Meyer, T. J. *Chem. Rev.* **1998**, *98*, 1439-1477.

(50) Kato, T.; Shida, T. *J. Am. Chem. Soc.* **1979**, *101*, 6869-6876.

(51) Turro, C.; Chung, Y. C.; Leventis, N.; Kuchenmeister, M. E.; Wagner, P. J.; Leroi, G. E. *Inorg. Chem.* **1996**, *35*, 5104-5106.